DEVELOPMENT OF NOVEL ANALYTICAL METHODS TO ELUCIDATE THE ROLES OF

ACTIVE XENOBIOTICS AND ENDOGENOUS MOLECULES IN TOXICITY,

METABOLISM AND POST-TRANSLATIONAL MODIFICATION

by

XIANGKUN YANG

(Under the Direction of Michael G. Bartlett)

ABSTRACT

Bioanalysis of active xenobiotics, including drugs, chemicals and toxicants, as well as endogenous compounds, is important not only for pharmacokinetics/toxicokinetic studies, but also for understanding their mechanisms of actions including toxicity, metabolism and protein post-translational modifications. However, these molecules are challenging to analyze, mainly due to their chemical instability and/or biological activity, and lack of blank matrices for endogenous molecules. In this dissertation, a series of novel, sensitive and specific analytical methods were developed, validated and applied to quantitate these molecules and their metabolites in complex biological matrices to investigate their mechanisms of actions. Chapter 1 is the introduction and describes the layout of the dissertation. Chapter 2 is a literature review of xenobiotic toxicity studies by liquid chromatography tandem mass spectrometry (LC-MS/MS), particularly from the perspective of protein adducts. Chapter 3 describes method development and validation for the determination of chlorpyrifos and its metabolites in cells and culture media

by LC-MS/MS. Chapter 4 describes the determination of Lys-40 acetylated α-tubulin in rat brain tissue by immunoprecipitation–mass spectrometry, a key post-translational modification hypothesized to be disrupted by exposure to organophosphates. Chapter 5 describes the development of a method for the quantitative profiling of cellular acyl-Coenzyme As (acyl-CoAs) compounds by LC-MS/MS to probe the metabolism of fatty acids. In Chapter 6, a method for the simultaneous quantitation of quetiapine and its active metabolite norquetiapine in rat plasma and brain tissue by LC-MS/MS is presented.

INDEX WORDS:

LC-MS/MS, Quantitation, Bioanalysis, Toxicity, Metabolism, Post-translational Modification, Organophosphates, Chlorpyrifos, Tubulin, Acetylation, Acyl-CoAs and Quetiapine

DEVELOPMENT OF NOVEL ANALYTICAL METHODS TO ELUCIDATE THE ROLES OF

ACTIVE XENOBIOTICS AND ENDOGENOUS MOLECULES IN TOXICITY,

METABOLISM AND POST-TRANSLATIONAL MODIFICATION

by

XIANGKUN YANG

B.S., Sichuan University, China, 2011

A Dissertation Submitted to the Graduate Faculty of The University of Georgia in Partial

Fulfillment of the Requirements for the Degree

DOCTOR OF PHILOSOPHY

ATHENS, GEORGIA

2017

DEVELOPMENT OF NOVEL ANALYTICAL METHODS TO ELUCIDATE THE ROLES OF

ACTIVE XENOBIOTICS AND ENDOGENOUS MOLECULES IN TOXICITY,

METABOLISM AND POST-TRANSLATIONAL MODIFICATION

by

XIANGKUN YANG

Major Professor:	Michael G. Bartlett
Committee:	Alvin V. Terry, Jr.
	Y. George Zheng
	Arthur Roberts
	Ron Orlando

Electronic Version Approved:

Suzanne Barbour
Dean of the Graduate School
The University of Georgia
August 2017

DEDICATION

I would like to thank my parents, my mother Xiuzhen Fan and my father Yangcheng Yang, who always give me strength and courage, and have confidence in me even when I doubt myself.

ACKNOWLEDGEMENTS

TABLE OF CONTENTS

CHAPTER 1

INTRODUCTION

Bioanalysis of active small molecules, including xenobiotics and endogenous molecules, can provide important information to elucidate their mechanisms of actions. However, their special chemical and biological characteristics, including chemical instability, protein-adduct formation and rapid metabolism, impose a great challenge on sample preparation and analyte detection. The lack of blank matrices is an additional challenge for endogenous molecules. In this dissertation, three classes of molecules: an organophosphate insecticide (chlorpyrifos), acyl-coenzyme As (acyl-CoAs) and an atypical antipsychotic (quetiapine) were incorporated for investigation using liquid chromatography tandem mass spectrometry (LC-MS/MS). In this dissertation, novel analytical methods were developed and validated to quantitate these compounds and their metabolites in biological samples to support pharmacokinetic/toxicokinetic studies, to interrogate their metabolic processes, and to illustrate the impact on protein post-translational modifications.

In this dissertation, Chapter 2 is a literature review covering toxicity and biomarker studies of xenobiotics including organophosphates, polycyclic aromatic hydrocarbons, acetaminophen, alkylating agents and other related compounds. General mass spectrometry strategies for protein adduct characterization were summarized. Toxicological target proteins for each class of xenobiotics, and the application of protein adducts as potential biomarkers of exposure or toxic response were discussed. Chapter 3 describes a LC-MS/MS method developed and validated for the determination of chlorpyrifos and its metabolites in cells and culture media.

This method has been successfully applied to study the neurotoxicity and metabolism of chlorpyrifos in a human neuronal model. Chapter 4 describes an immunoprecipitation-mass spectrometry (IP-MS) method developed for the quantitation α-tubulin acetylation at Lys-40 in rat brain tissue. This key post-translational modification was found to be inhibited by exposure to organophosphates. In Chapter 5, cellular acyl-CoAs were quantitatively profiled under the challenge of various dietary fatty acids. Hierarchical clustering in the remodeling of acyl-CoA profiles revealed a fatty-acid-specific pattern. Individual acyl-CoAs were identified as potential biomarkers which were altered differently in divergent tumorigenicity states of cells. In Chapter 6, an LC-MS/MS assay was developed and validated to simultaneously quantitate quetiapine and its active metabolite norquetiapine in rat plasma and brain tissue. This method has been applied to investigate the pharmacokinetics and impact of quetiapine and norquetiapine on cognition.

CHAPTER 2

LITERATURE REVIEW:

A REVIEW OF XENOBIOIC TOXICITY STUDIES BY LIQUID CHROMATOGRAPHY

TANDEM MASS SPECTROMETRY (LC-MS/MS)

Abstract

The determination of protein-xenobiotic adducts using mass spectrometry is an emerging area which allows detailed understanding of the underlying mechanisms involved in toxicity. These approaches can also be used to reveal potential biomarkers of exposure or toxic response. The following review covers studies of protein adducts resulting from exposure to a wide variety of xenobiotics including organophosphates, polycyclic aromatic hydrocarbons, acetaminophen, alkylating agents and other related compounds.

Key words

Protein adduct, covalent modification, post-translational modification, mass spectrometry, toxicity, biomarker, organophosphate, polycyclic aromatic hydrocarbon, acetaminophen and alkylating agent.

1. Introduction

Proteins can be covalently modified by xenobiotics (drugs, toxicants and/or their metabolites) at active amino acid residues, resulting in protein adduction. Protein adducts are important players in the initiation of toxicity but are poorly understood for many compounds. It has been demonstrated that toxicity occurs when adduct formation impairs important protein structures and/or functions, such as catalytic activity, ion translocation, or protein-protein interactions. A well-known example is acute toxicity involving organophosphates, which is attributed to covalent binding at serine residues and irreversible inhibition of acetylcholinesterase (AChE) in nerve cells. A common scenario for protein adduct-induced toxicity is[1]: 1) Protein adducts are formed at (a) key amino acid(s) of one or more proteins important for the function of a biological pathway; 2) The adduct(s) lead to changes in protein structure(s) and/or function(s); 3) Protein changes accumulate and reach a level sufficient for pathway failure; and 4) Pathway failure leads to cell damage and toxicity. Because a xenobiotic compound can react with multiple proteins at multiple sites, it is a challenge to identify the mechanistically important protein adduct(s) and covalently modified site(s).

A biomarker indicates the state of biological conditions based on a molecular or process change. Protein adducts are good candidates for biomarkers, to diagnose chemical poisoning, examine exposure to toxicants, clinically monitor drugs and evaluate pharmacological responses to a therapy. Adducts with serum albumin and hemoglobin are most commonly studied as biomarkers, because these two proteins are abundant in the blood, have multiple modifiable amino acids, and at least serum albumin has a highly conserved sequence among species[2] which facilitates the translation of protein adduct studies from animals to humans. Protein adducts have some advantages over other types of biomarkers. Protein adducts are usually stable. They are

formed via nucleophilic substitution, in which reactive xenobiotics are often metabolized to electrophilic agents, which attack nucleophilic atoms (especially O, N and S) at side chains of amino acid residues[3]. Protein adducts are generally long-lived and accumulative, compared to small molecules and their metabolites, because protein adducts have the same lifetime as the protein, e.g. 3-4 weeks for human serum albumin and 17 weeks for hemoglobin in erythrocytes[4,5]. Protein adducts also have a longer lifetime than DNA adducts, because they are not actively repaired[6]. Biomarkers from adducts with plasma proteins usually allow a higher sensitivity for detection, compared to biomarkers based on inhibition of specific enzymes. For example, mice treated with a nontoxic dose of chlorpyrifos oxon had MS-detectable protein adducts in blood up to 4 days post exposure, after the established biomarker (AChE assay) turned uninformative[4].

Currently, mass spectrometric and immunological methods [e.g. Western blot and enzyme-linked immunosorbent assay (ELISA)] are two common methods for determining the covalent modification of proteins by xenobiotics. Immunological strategies are based on specific antigen-antibody interactions providing good sensitivity. However, the cross-reactivity of antibodies may lead to false positives and incorrect results[3]. In addition, immunoassays rely on antibody availability, therefore make the discovery of new covalent modifications difficult. Even when the modification sites are known and antibodies are available, simultaneous determination of different modifications will be labor-intensive, and epitope masking effects will make it difficult to identify modifications when they are in close proximity. In comparison, mass spectrometry can simultaneously identify and characterize many different modifications in multiple proteins, and the detection is independent of antibodies.

This paper aims to review MS-identified protein adducts generated from different classes of xenobiotics. The roles of the protein adducts will be discussed, from the perspective of mediating toxicity and their application as biomarkers. Most research data in this article are based on in vivo and in vitro cell culture studies which mimic actual conditions of toxicant poisoning or drug treatment. Studies of protein treatment with xenobiotics are selected with caution to exclude those applying clinically irrelevantly high concentrations of testing agents. Other adducts from xenobiotics, such as xenobiotic-DNA adducts and indirect modifications by xenobiotics through lipid peroxides and free radicals, will not be discussed in this review.

2. General MS strategies for protein adducts characterization

Different types of MS instrumentation have been applied to study protein adducts. Their capabilities, including strengths and weaknesses, have been discussed in other reviews[7,8,9]. Although MS-based approaches are different for particular modifications of interest, there is one general working procedure for characterizing protein adducts: 1) The target proteins are isolated from the matrix, such as cell lysate, serum or tissue homogenate, based on the properties of proteins (e.g. assembly-disassembles cycles of tubulin[10]), or with immunoaffinity methods; 2) The proteins are denatured, reduced, alkylated (and digested with specific enzymes for bottom-up approaches); 3) Protein adducts are analyzed with mass spectrometry, either using the bottom-up or top-down approaches as shown in Figure 1, discussed below; and 4) Data are analyzed using databases, to characterize the protein adducts, including identification of the modified proteins/protein isoforms, localization of modification, and quantitation of covalent modification.
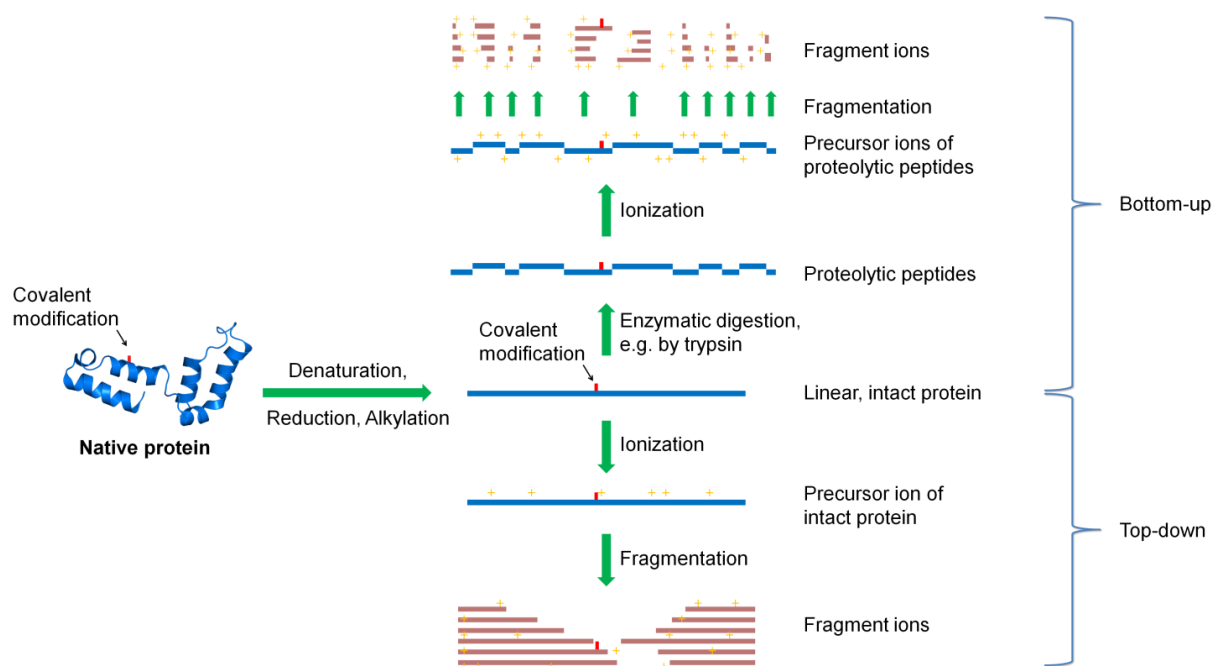
Figure 1. Bottom-up and top-down mass spectrometric approaches for characterization of a protein adduct, developed from[11].

The top-down approach provides a full sequence and post-translational modification (PTM) coverage, permits assessment of protein isoforms and validation of N- and C-terminal sequences[8]. Since this approach studies intact proteins, even native proteins[12,13], no enzymatic digestion is required, and denaturation, reduction and alkylation can be eliminated in some cases. This simplified procedure minimizes the loss of labile covalent modifications and the generation of artificial modifications in sample preparation, allowing the characterization of labile post-translational modifications or even noncovalent modifications. For example, the study of metallodrug-protein adducts using a top-down approach is preferred because they are prone to metallodrug cleavage during enzymatic digestion[14]. The top-down approach can determine covalent binding sites of metallodrugs by fragmenting the protein, and recognizing the modified

fragments based on their characteristic isotopic pattern and *m/z* values. However, because fragment ions from an intact protein usually have long sequences, and a full spectrum covering all theoretical ions is difficult to achieve in experiments, occasionally tandem mass spectrometry alone cannot determine the site of modification, and a combination with multiple-stage tandem mass spectrometry (e.g. MS^3 and MS^4) is necessary in the top-down approach[15]. In comparison, tandem mass spectrum is usually sufficient to identify the modification sites in the bottom-up approach, because short to middle-length peptides are analyzed. In addition, it is more challenging to identify modification with the top-down approach when the modified fragment is an isobaric mixture with different binding sites. It is less a problem for bottom-up, because of its ready compatibility with chromatographic techniques which allows separation of isobaric peptides before MS analysis. The bottom-up approach has also been applied to study labile covalent modification. In an insulin-cisplatin case study, platinum-protein bonds were demonstrated to survive the whole enzymatic digestion process after simple modification (Tris buffer instead of ammonium bicarbonate buffer, high intensity focused ultrasound for accelerating digestions, etc), and new binding sites were identified on insulin with the bottom-up approach compared to the ones found with the top-down approach[16].

Currently, the majority of published data utilized the bottom-up approach to characterize covalent modifications of proteins. One important reason is that top-down approaches require the highest mass accuracy, mass resolving power and sensitivity generally only permitted by expensive Fourier transform ion cyclotron resonance (FTICR) and Orbitrap instruments, while bottom-up approaches utilize triple quadrupole (QQQ), Quadrupole Time-of-Flight (Q-TOF) and Quadrupole ion trap (Q-TRAP) instrumentations, which are more generally available. Also, the

9

application of the top-down approach is generally restricted to small proteins, due to the highly complex mass spectra generated for interpretation.

Fragmentation allows identification of fragment ions with a signature of the xenobiotic, thus is necessary for localization of covalent modifications. Traditionally, CID (Collision-Induced Dissociation) has been the most commonly used mechanism for fragmenting peptides or proteins, by colliding with neutral molecules (helium, nitrogen or argon), giving rise to b/y-type series of fragment ions. CID is widely performed with FTICR, QQQ, Q-TRAP and Q-TOF instruments. In a tag-free approach, detection of drug-adducted proteins was achieved by relying solely on the characteristic CID product ions of xenobiotics, generated under appropriate collision energy conditions during tandem mass spectrometry. Electron Capture Dissociation (ECD) is an effective method for fragmenting larger multiply charged intact proteins. ECD directly introduces low energy electrons to trapped ions, primarily producing c- and z-type fragments. Another difference is that ECD promotes retention of labile covalent modifications after backbone bond dissociation[17,18], thus facilitating the generation of fragment ions with covalent modifications to provide more valuable information for characterizing protein adducts. However, ECD applications are primarily limited to FTICR mass spectrometry. ETD (Electron Transfer Dissociation) induces fragmentation in a similar mechanism as ECD, but the electrons are transferred by radical anions. ETD also generates c- and z-type ions, results in softer and more random protein backbone cleavages than CID, and retain PTMs to a large extent[19], but it's mainly advantageous over ECD in its compatibility with more common instrumentation[20]. ETD has emerged as a better fragmentation technique than others when investigating metallodrug–protein adducts with a top–down approach, with respect to fragment numbers and localization of modification sites[21]. However, ETD was observed to perform worse in generating low charge

peptide ions (<3+) and low-molecular weight fragment ions versus CID in a bottom-up approach. Charge loss of short peptide ions by electron capture during fragmentation may be the reason, which gives rise to neutral fragments absent from the MS/MS spectrum[16,22]. In addition, optimal experimental conditions for ETD seem to be dependent on the peptide fragmented, thus ETD needs more optimization work than CID in some cases[16]. In conclusion, a combination of different fragmentation mechanisms may increase the information derived from protein or peptide fragmentation, and facilitate a more accurate identification of chemical modifications[9].

3. MS-identified protein adducts

3.1 Organophosphate-protein adducts

3.1.1 Organophosphate adducts and toxicity

Organophosphates (OPs) are a class of chemicals that are widely used as insecticides in agriculture, public hygiene, homes and veterinary practice. In addition, OPs were historically used as chemical warfare agents, and continue to pose a nonnegligible threat to society. Exposure to OPs can lead to acute or chronic poisoning, depending on the route of administration, dose and duration of time. Acute toxicity of OPs has been intensively studied: the cholinergic syndrome associated with OP poisoning is caused by covalent inhibition of AChE at serine residues. However, cholinesterase inhibition alone fails to explain the wide range of OP toxicities, especially when exposure to OPs is prolonged and at doses which are too low to alter cholinesterase activity. OP-induced neurotoxicity is a major type of OP noncholinesterase toxicity, and includes deficits in cognition, learning, information processing, memory, depression and psychotic symptoms[23]. These symptoms known as OP-induced neuropsychiatric disorders (COPIND) are independent of AChE inhibition, and are observed in subjects who have experienced acute OP poisoning or chronic OP exposure. The underlying mechanisms for OP

11
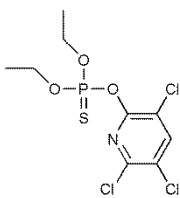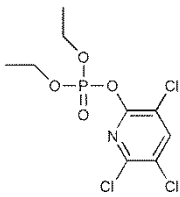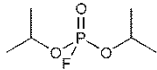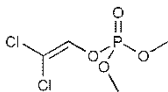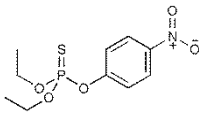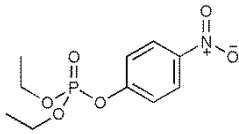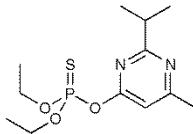
neurotoxicity, as well as the target proteins, are still unclear. It has been demonstrated that OPs can covalently modify specific amino acid residues (an example in Figure 2), including serine, tyrosine, lysine and histidine in various proteins. Organophosphorylation at amino acid residues is dose- and site-dependent, and most identified modifications occurred at tyrosine and lysine residues on protein surface regions in the vicinity of positively charged amino acids[24,25,29].
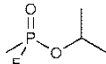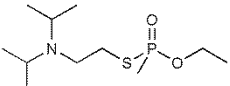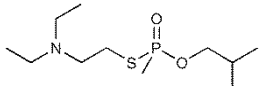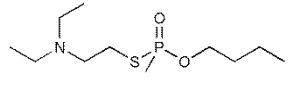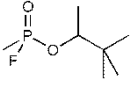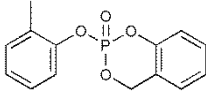
Each OP molecule makes a particular added mass when adducted to an amino acid residue (see Table 1) and can be identified by MS, mostly via bottom-up approaches. Using mass spectrometry, multiple covalent modifications have been identified in various proteins, and MS/MS has determined the modification sites for albumin, tubulin, actin, keratin, transferrin, ubiquitin, and glyceraldehyde-3-phosphate dehydrogenase (GAPDH), mostly at tyrosine, lysine and serine residues[27,28,30,33]. Dozens of other proteins have been identified using a biotin-linked organophosphorus ester (10-fluoroethoxyphosphinyl-N-biotinamidopentyldecanamide, FP-biotin) pull-down assay. However, the modification sites are yet to be identified.
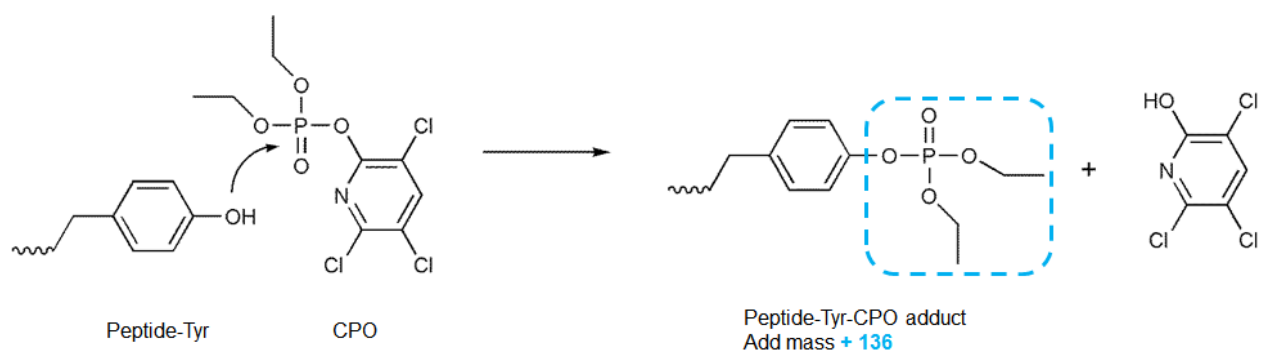
Figure 2. An example of an OP compound (chlorpyrifos oxon, CPO) reacting with a tyrosine residue.

Table 1. Chemical structures of OPs and the respective added mass when adducted to an amino acid residue (no aging)

OPs and molar mass (g/mol)	Structure	Added Mass	Ref
OP insecticides			
Chlorpyrifos (CPF) 350.59		152	[26]
Chlorpyrifos oxon (CPO) Active metabolite of CPF 334.52		136	[4] [27] [28] [29]
Diisopropyl fluorophosphates (DFP) 184.15		164	[27] [29] [34]
Dichlorvos (DDVP) 220.98		108	[29] [30]
Parathion 291.26		152	[31] [34]
Paraoxon Active metabolite of parathion 275.20		136	[34] [54]
Diazinon 304.34		152	[34]

OP nerve agents			
Sarin 140.09		120	[29] [32]
VX 267.37		106	[33] [34]
Russian VX (RVX) 267.37		106	[33]
CVX (Chinese VX) 267.37		106	[33]
Soman 182.18		162	[35]
Others			
Cresyl saligenin phosphate 276.23		170 (Y) 106 (H, K)	[36]

A potential toxicological target of OPs is the axonal transport system. Axonal transport is a neuronal process responsible for the transport of organelles, proteins, mRNA, and signaling molecules by motor proteins (dynein and kinesin), to and from a neuron's cell body through its axon along tubulin-assembled microtubules[38]. OP-induced neurotoxicity is accompanied by decreased activity of axonal transport[37]. Defects in many axonal transport-involved proteins have been confirmed to cause cognitive deficits and neurodegenerative disease, such as Alzheimer's and Huntington's diseases, with which chronic OP poisoning shares similar symptoms[38].

Tubulin, kinesin and dynein are key proteins in the axonal transport system. Of them, tubulin provides the structural basis for motor proteins (kinesin and dynein) to transport along. Tubulin was identified as the major protein extracted with avidin beads from the brains of mice dosed with FP-biotin, in the absence of AChE inhibition[28]. Mass spectrometry has identified multiple organophosphorylated sites on tryptic peptides of CPO or DFP-treated bovine tubulin, including Tyr-83, 103, 108, 161, 224, 262, 272, 357, 399 and Lys-60, 336, 163, 394, 401 in the α-tubulin subunit; and Tyr-50, 51, 59, 106, 159, 281, 310, 340 and Lys-58 in the β-tubulin subunit[27,28]. Aging, loss of an alkoxy side chain from the adducted OP, which was observed in OP-cholinesterase adducts, was not detected in OP-labeled tubulin. These OP-labeled amino acids are conserved, therefore are also likely to be modified in humans and other species. Tyr-83 in α-tubulin was identified as the most reactive tyrosine, which was labeled (12%) with an equimolar concentration of CPO (0.01mM) after 24h incubation, and had 61% labeling with 0.5 mM CPO. Tyr-281 was the most reactive tyrosine in β tubulin (34% labeling at 0.5 mM CPO). Other tyrosines were significantly less reactive than these two tyrosines, exhibiting 5%-22% labeling under the same conditions[28]. From the brains of mice chronically dosed with CPO or CPF at an AChE inhibition-free dose, OP labeling at Tyr-281 and Ser-338 of β-tubulin was identified[10]. Aberrant phosphorylation of tubulin has been demonstrated to disrupt tubulin function and stability[39], considering that organophosphorylation and phosphorylation share many tyrosine residues[28], it is possible that organophosphorylation may play a similar role as aberrant phosphorylation.

Tubulin polymerization is essential for the life of a neuron and function of the axonal transport system. Tubulin polymerization inhibitors have been validated to initiate cell apoptosis[40]. Confirmed by nanoimaging and mass spectrometry, in vitro and in vivo studies

demonstrated that OPs (CPF or CPO) treatment and CPO adduction disrupted tubulin polymerization and decreased the binding between microtubules and associated proteins[10,41]. In addition to neurotoxicity, OPs have negative effects on the liver[42], kidney[43] and reproductive systems[44,45], suggesting other protein adducts contribute to the toxicity. DDVP is reported to induce hepatocellular vacuoles and cell swelling[46]. A proteomic study identified that, after direct incubation with lysed human hepatocyte-like cells (HepaRG) or competitive binding with FP-biotin, DDVP formed adducts with dozens of proteins covering different biological pathways, including apoptosis and survival, cell adhesion and remodeling, cell differentiation, energy regulation, stress response and transport[30]. A protein forming abundant adducts with DDVP is glyceraldehyde -3-phosphate dehydrogenase (GAPDH). GAPDH is traditionally known as an enzyme in glycolysis, but has been recently recognized as a multifunctional protein, working as a transcription factor, a microtubule formation catalyst, a modulator for stress response molecules (i.e., glutathione, nitric oxide, and p53) and a trigger for apoptosis[47,51]. GAPDH activity is regulated by phosphorylation, and OP (DDVP) treatment and adduct formation has been shown to impair its function[48]. DDVP has been reported to covalently modify GAPDH at Ser-312, Tyr-255, Tyr-314, and Tyr-320, among which Tyr-255 is the most reactive where modification was identified at 50 μM DDVP. Tyr-255 is known to be involved in GAPDH intranuclear accumulation and nuclear export, and a change in the sequence containing Tyr-255 resulted in a GAPDH nuclear accumulation[49]. DDVP adduction at Tyr-255 may affect the GAPDH tetrameric structure and trafficking between the nucleus and cytoplasm, leading to GAPDH accumulation in the nucleus, an event known to induce apoptosis[30,50]. In addition, Tyr-314 is also recognized as an important amino acid responsible for binding between the NAD+ nicotinamide moiety and GAPDH, and therefore is key for catalytic activity[51]. Similar to Tyr-

255, the organophosphorylation on this site may also impair GAPDH function and induce toxicity.

3.1.2 OPs adducts as biomarkers

Cholinesterase activity inhibition is established as the major indicator for exposure to OPs. However, it may be uninformative in cases of chronic OP poisoning, when exposure to OPs is at a relatively low dose and over a long period of time. Butyrylcholinesterase (BChE) is a non-specific cholinesterase in plasma and liver. In the cases of OP poisoning, BChE protects AChE by covalently binding with OPs at Ser-198 to deactivate the OPs[52]. Different from other proteins, BChE organophosphorylation at Ser-198 usually undergoes a dealkylation process called aging, catalyzed by the neighboring amino acid residues His-438 and Gly-197[53]. Therefore, there are two different added masses at Ser-198, one is the unaged adduct and the other is the aged adduct[53]. OP-BChE adducts are good biomarkers for monitoring OP exposure, because BChE reacts with a wide range of OPs, even when the doses are too low to modify other proteins. The aged OP-BChE adduct is more stable than the unaged adduct, thus is usually monitored as the biomarker. However, because BChE is not an abundant plasma protein, purification methods are always required to increase the recovery, to ensure the assay monitoring OP-labeled BChE has sufficient sensitivity. For example, biotinylated anti-BChE polyclonal antibodies conjugated to streptavidin magnetic beads were validated to extract BChE from paraoxon-treated human plasma[54], confirmed using Western blot and mass spectrometry. An LTQ Orbitrap method identified the tryptic peptide containing Ser-198, either in unmodified or modified form (aged, added mass = 108 Da), using LC–MS and MS/MS. Quantitation of Ser-198 labeling was achieved using precursor ions mass spectra, enabled by high resolution mass spectrometry. Some other methods to purify OP-BChE include: titanium oxide (TiO_2) for OP-

modified BChE peptides[52], ion exchange chromatography and procainamide affinity chromatography for intact BChE[55].

Despite extensive research advances, OP-BChE adducts have their intrinsic disadvantages as biomarkers: the aging process of OP-labeled Ser-198 diminishes the differences in adducted groups from different OP compounds[52], making it difficult to determine the OP compound originally exposed to testing subjects. In addition, OP-Ser adduction on BChE is unstable, and can be reversed by oxime therapies, or even spontaneously[56]. Moreover, active serine sites are less common than other modifiable amino acids such as tyrosine and lysine, making serine-based biomarkers less sensitive for detection. Albumin is the most abundant protein in plasma, thus can be a good substrate for OPs and provide sensitive biomarkers. MS has identified organophosphorylation on Tyr-411, Tyr-435 and Lys-438[4,35]. Diethoxyphosphate–tyrosine (CPO-tyrosine) from plasma proteins (mostly albumin) has been validated as a biomarker for monitoring exposure to CPO[5]. CPO-tyrosine was released from labelled proteins by pronase, a proteases mixture capable of digesting proteins into individual amino acids. CPO-tyrosine was isolated using HPLC and detected with MS by selectively monitoring the precursor ion at m/z 318 (CPO-tyrosine, 318 Da), after confirming its identity with MS/MS. The limit of detection for CPO-tyrosine was 0.1% labeling of albumin. For mice treated with a nontoxic dose of CPO (3 mg/kg), CPO-tyrosine was detectable in blood up to 5 days after dosing, while AChE and BChE activity returned to normal after 2 days. Similar results were shown for human self-poisoned by CPF. More importantly, the adducts on tyrosine residues were not affected by oxime treatment[26]. In addition, proteolytic peptides with CPO labeling at Tyr-411 of albumin were also studied as biomarkers, but showed poorer sensitivity: the limit of detection was 10% labeling of albumin, which is over 10 times higher than the labeling ratio at

lethal OP doses. Babakov et al. (personal communication) discovered that OP-labeled albumin and peptides containing unlabeled Tyr-411 bind to Fe^{3+} affinity beads at pH 11 and elute at pH 2.6. These PHOS-selective iron affinity beads were applied to enrich CPO-labelled and unlabeled peptides ($VRY_{411}TKKVPQVST$ and $LVRY_{411}TKKVPQVST$) identified using MALDI-TOF/TOF, from pepsin digestion of albumin and human plasma, and increased the limit of detection to 0.2% of organophosphorylated albumin from 0.43 µL of plasma[35]. In addition, a polyclonal antibody to soman-tyrosine was developed, which can be applied in affinity purification of this biomarker[57].

3.2 Reactive metabolites of polycyclic aromatic hydrocarbons (PAHs)

3.2.1 PAH-protein adducts and toxicity

Polycyclic aromatic hydrocarbons (PAHs) are compounds containing multiple fused aromatic rings and only carbon and hydrogen. PAHs have been identified as major carcinogenic/mutagenic agents associated with an increased risk of respiratory, blood and neoplastic diseases[58]. PAHs are found in fossil fuels (petroleum and coal) and produced by incomplete combustion of organic matter, such as in automotive engines, coke ovens and forest fires. PAHs are important components of particulate matter in polluted air, with human exposure by inhalation[59]. Oral exposure can arise following dietary consumption of overcooked meat and repeatedly heated cooking oil[60]. PAHs themselves are inert compounds, but they are metabolized by monooxygenases CYPs into multiple reactive compounds (e.g. Figure 3) which generate electrophiles and cause cytotoxicity[61], especially at sites of metabolism, such as pulmonary epithelial Clara cells and hepatic cells. Active metabolites of PAHs form DNA-adducts and oxidize DNA with reactive oxygen species, ultimately resulting in genotoxicity[58]. Protein adducts also induce toxicity, however, until recently, the specific proteins adducted by

reactive metabolites of PAHs have been difficult to identify. A clearer understanding of PAH protein targets and functional consequences will provide insights into the mechanisms for toxicity, and allow for the development of biomarkers to monitor both exposure to PAHs and toxicity.
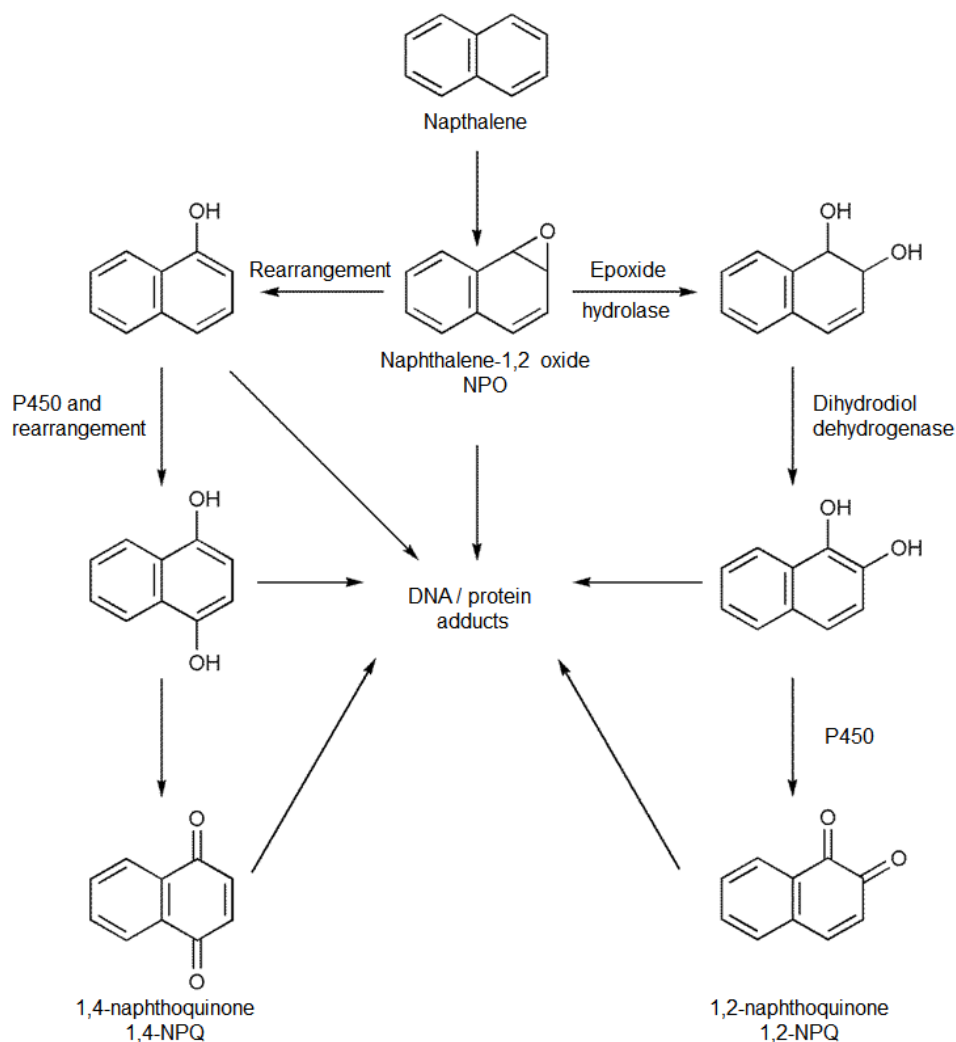
Figure 3. Metabolic activation of naphthalene.

Naphthalene has two fused aromatic rings and is the simplest PAH compound. Naphthalene is abundant in air pollution, and is naturally derivatized into 1-nitronaphthalene and methylnitronaphthalene in particulate matter[62]. After metabolic activation, naphthalene and 1-nitronaphthalene were found to covalently bind to tissue proteins, and the level of adduction was correlated with the extent of cytotoxic injury in the airway epithelium[63]. Dissected airways from rodents and rhesus macaques were observed to metabolize naphthalene and 1-nitronaphthalene, generate active metabolites and form similar amounts of protein adducts between the two species[64]. To identify the adducted proteins, distal bronchioles and parenchyma from rhesus monkeys were incubated with 100 μM [^{14}C]naphthalene or [^{14}C]1-nitronaphthalene (either specific activity = 52 mCi/mmol), and adducted (^{14}C-labeled) proteins were visualized by storage phosphor imaging, after separation with two-dimensional gel electrophoresis (2-DE). Labeled proteins were digested in-gel with trypsin and analyzed using a Q-TOF for identification. The identified adducted proteins include: eight cytoskeletal proteins [tropomyosin, tubulin β-1, β/γ actin, α-tubulin, actin cytoplasmic 1 (β-actin), myosin light chain alkali, actin and desmin], two chaperone proteins (heat shock protein 60 kDa, mitochondrial and heat shock 70 kDa protein 9B, mitochondrial), seven metabolic enzymes (aldehyde dehydrogenase, aldehyde dehydrogenase 1A1, protein-glutamine gamma-glutamyltransferase, 15-hydroxyprostaglandin dehydrogenase, glutathione S-transferase Pi, monoamine or phenol-sulfating phenol sulfotransferase and α-enolase), one redox protein (thiol-specific antioxidant protein/peroxiredoxin 2), two proteins involved in ion balance and cell signaling (chloride intracellular channel protein 1 and annexin VI) and three extracellular proteins (selenium-binding protein, β globin and serum albumin) [62]. Most proteins were covalently bound with both naphthalene and 1-nitronaphthalene. The same methodology was applied to identify *in vivo* proteins adducted by [^{14}C]1-nitronaphthalene in the

airway epithelium of rats with a single (50 mg/kg) interperitoneal injection. MALDI TOF/TOF and ESI LC-MS/MS identified 8 adducted proteins whose functions cover splicing regulation, transport, ethanol oxidation, glycolysis and oxidation stress[61]. Most in vivo adducted proteins in airways were the same proteins adducted in vitro (dissected airways[62]) and in situ (structurally intact lung model[65]) with naphthalene and 1-nitronaphthalene. Since PAHs are also orally exposed to humans, adduction to hepatic proteins is anticipated to occur. A total of 18 proteins from mouse liver microsomes formed adduction with [^{14}C]naphthalene in vitro: protein disulfide isomerase precursor, ER-60 protease, α-actin, mouse urinary proteins, and cytochrome b5 reductase in pellet fractions and protein disulfide isomerase, heat shock protein 70, and α-actin in supernatant fractions[66]. The modification sites by active metabolites on actin and protein disulfide isomerase have been identified in vitro[67].

Naphthalene-1,2-oxide (NPO), 1,2-naphthoquinone (1,2-NPQ) and 1,4-naphthoquinone (1,4-NPQ) are reactive metabolites of naphthalene, which can covalently modify functional proteins to induce toxic effects[67,68]. The adducts of 1,4-NPQ and 1,2-NPQ on apomyoglobin and human hemoglobin were characterized using LC-MS and MS/MS[67]. Each adducted amino acid has an added mass of 156 from 1,4-NPQ or 1,2-NPQ (see Figure 4). Four 1,4-NPQ labeled lysine residues (Lys-45, Lys-62, Lys-77 and Lys-98) and one 1,2-NPQ labeled lysine residue (Lys-62) were identified on apomyoglobin. Two N-terminal valine residues of the α and β chains of human hemoglobin were labeled by both 1,4-NPQ and 1,2-NPQ. No protein adducts were formed with 2-methyl-1,4-naphthoquinone, suggesting loss of reactivity of 1, 4-NPQ after 2-methylation.

Figure 4. 1,4-NPQ covalently modifies a lysine residue, adding a mass of 156.

3.2.2 PAHs-protein adducts as biomarkers

Hemoglobin and albumin form stable adducts with PAH metabolites in blood, and have been studied extensively as biomarkers of human PAH exposure[69]. Early methods indirectly measured adducts with benzene metabolites (benzene oxide) and major naphthalene metabolites (NPO, 1,2-NPQ and 1,4-NPQ) by measuring adducts on cysteine residues[70,71]. Cys-adducts with different metabolites of naphthalene were cleaved and derivatized into different trifluoroacetylated derivatives for detection with GC-MS. The limit of detection was 50 pmol adduct/g protein for NPO, 1,2-NPQ and 1,4-NPQ. After administration of 100 mg/kg naphthalene to F344 rats, the three adducts in hemoglobin and albumin were measured at 0.861-16.4 nmol/g. 1,2-NPQ-hemoglobin and -albumin were detected at much higher levels than 1,4-NPQ adducts, suggesting a greater metabolism into 1,2-NPQ than 1,4-NPQ from naphthalene. Another GC/MS based method to evaluate PAH quinone adducts is tetramethylammonium hydroxide (TMAH) thermochemolysis, which permitted detection of all thiol and amine adducts[72].

In addition to naphthalene, benzo(a)pyrene (BP) is another well-researched PAH compound. Active metabolites of BP include (±)-syn- and (±)-anti-BP-7,8-diol-9,10-epoxides

(syn- and anti-BPDE), with anti-BPDE being the predominant isomer. BPDE has been demonstrated to form carboxylic ester bulky adducts with aspartate, glutamate and the C-terminus in hemoglobin or serum albumin[73,74], but the ester adducts are prone to hydrolysis both in vitro and in vivo, and therefore are not good biomarkers. BPDE is able to form stable adducts at histidine, contributing to 70% and 10% of the total BPDE adduction in hemoglobin and albumin, respectively[75]. The labeling of human serum albumin was identified at His-146[76]. The conditions for sample preparation and quantitation with LC-MS/MS were optimized for three bulky adducts from PAH diolepoxides (PAHDE) [BPDE, DE of dibenzo[a,l]pyrene (DBPDE) and dibenzo[a,h]anthracene (DBADE)][77]. Briefly, PAHDE-treated serum albumin (1:0.45 molar ratio) was digested with pronase, labeled peptides (PAHDE-His-Pro, PAHDE-His-Pro-Tyr and PAHDE-Lys) were enriched (LC-UV or SPE), identified with LC-MS/MS and quantitated using MRM mode. The analytical assay demonstrated very high sensitivity, the limit of detection was 1 fmol adduct/mg SA extract from 5 mg SA. The method was applied to measure BPDE-His from mice dosed with 100 mg/ kg BP, which showed the highest level (13 fmol/mg) 3 days after exposure. However, the level of BPDE-His in serum albumin was 400 times lower than that of BPDE-adduct to deoxyguanosine (BPDE-dG) in liver DNA from the same mice. This observation suggested a lower reactivity of BPDE with histidine in albumin than with dG in DNA. Considerable improvement will be needed before this method can be applicable to monitor human exposure to BP[78].

3. 3 Protein adducts with active metabolites of acetaminophen

Acetaminophen (abbreviated as APAP, also known as paracetamol) is a common over-the-counter (OTC) analgesic/antipyretic used worldwide. Metabolism of APAP occurs in the liver. Its main pathway (up to 90%) is phase II-conjugation, with sulfate or glucuronide, which

deactivates the compound and facilitates its excretion. Another minor pathway is phase I-oxidation, via which a toxic metabolite N-acetyl-p-benzoquinone imine (NAPQI) is generated. At a normal dose and physiological conditions, NAPQI is generated in small amounts and is immediately detoxified by binding with glutathione (GSH) at the thiol group. Hepatotoxicity occurs when excessive NAPQI saturates conjugation and accumulates, such as in the cases of APAP overdose[79].

It is thought that NAPQI induces hepatotoxicity through a few possible mechanisms, including adduct formation of functional proteins[80, 81]. NAPQI has strong reactivity with cysteine, adding a mass of 149 after adduction[87], and its adduction with proteins has excellent correlation with APAP toxicity[82]. NAPQI covalently binds with mitochondrial proteins, the protein adducts induce peroxynitrite generation and mitochondrial permeability, ultimately promoting oxidative stress[83]. In a data-dependent acquisition (DDA) measurement of APAP-treated liver microtissues, NAPQI adducts with four mitochondrial proteins related to oxidation stress (glycine amidinotransferase, Parkinson disease protein 7, peroxiredoxin-6 and voltage-dependent anion-selective channel protein 2) and two other proteins (annexin A2 and formimidoyltransferase-cyclodeaminase) were identified. The modification of the signal peptides were detectable at a subtoxic concentration of 13.7 μM APAP[84]. The activity of some other proteins was observed to be inhibited by APAP in vivo, including glutamine synthase, glutamate dehydrogenase, Ca^{2+}/Mg^{2+}-ATPase and glutamate cysteine ligase[80].

Glutathione S-transferases (GST) catalyze the conjugation of GSH with xenobiotics, thus are important for the detoxification of APAP. A member of human GST family, GST pi (GSTP) was observed as a target protein for NAPQI in vivo[85]. The covalent modification was identified at Cys-41 in vitro, in a dose-dependent pattern identified using isobaric tags for relative and

absolute quantitation (iTRAQ) labeling and MRM LC-MS/MS quantitation of the Cys-containing peptides. The modification was correlated with inhibition of GSH conjugating activity, and one modification on a GSTP subunit seemed to be sufficient to inhibit the functional GSTP dimer as a whole[86]. NAPQI adduct formation was also identified in human liver microsome GST (mGST) at Cys-50 with mass spectrometry, in a time-dependent manner during microsomal incubations with APAP[87,88].

Like albumin adducts with many other xenobiotics, NAPQI-albumin adducts have been studied as biomarkers to assess APAP exposure, metabolism and adverse effects. Cys-43 in human and mouse serum albumin, and Cys-579 in mouse serum albumin were identified to be adducted by NAPQI. In an analytical method for low-level detection of NAPQI-albumin adducts in serum samples, albumin was extracted with albumin affinity chromatography and cleaned with gel-filtration chromatography. A tryptic peptide containing Cys-43 was identified using LC-MS/MS and the ratio of adduction was calculated with the peak areas ratio of NAPQI-modified Cys-43 peptides to total Cys-43 peptides. In mice dosed with a maximum tolerable dose of APAP (300 mg/kg), signs of hepatotoxicity were observed in liver histology combined with an increase of alanine aminotransferase (ALT) levels. However, aspartate aminotransferase (AST) was not effected. It was determined that 0.2% of the total mouse serum albumin was adducted by NAPQI[89]. Some other methods have utilized pronase to digest human albumin to release APAP-Cys as the biomarker[90,91] and quantitated the biomarker using MRM LC-MS/MS. The most sensitive method in this strategy was validated with an limit of detection of 0.5 ng/mL and an LLOQ of 1.0 ng/mL[91].

3.4 Protein adducts with alkylating agents

Alkylating agents are a big class of compounds that transfer alkyl carbon groups to biomolecules. A notorious member of this class is mustard gas, which have historically been deployed as chemical warfare agents. Clinically, alkylating agents (e.g. nitrogen mustards) are important antineoplastics, and their therapeutic action relies on the formation of stable DNA adducts, which cause DNA damage and cell death. Nevertheless, DNA is not the only target of alkylating antineoplastic agents, proteins also contain potential reactive sites for adduct formation. More than being helpful in understanding the toxicity to be alleviated, protein adduct-induced cytotoxicity can be exploited to further improve alkylating agents as anticancer drugs.

Reactive aziridinium ion   Nu: nucleophilic moiety
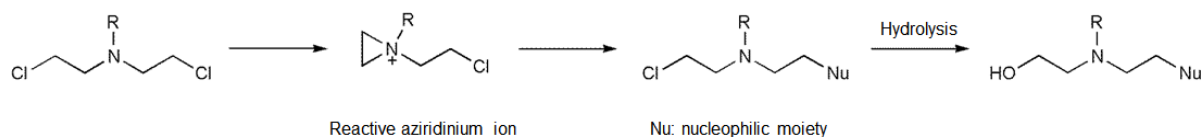
Figure 5. Nitrogen mustards covalently bind with nucleophilic moiety[92].

Alkylating agents were observed to form stable adducts with cysteine, lysine and histidine residues[92]. One example of representative alkylating agents nitrogen mustards covalently binding with a nucleophilic moiety is shown in Figure 5. The covalent binding depends on the electrophilic aziridinium cation, which is formed without metabolic activation[92]. Adducts by alkylating agents, mostly nitrogen mustards, have been characterized for multiple model proteins, including hemoglobin[93], human serum albumin[94], metallothionein[95], O6-alkylguanine DNA alkyltransferase[96] and cytochrome c[97]. In order to determine the selectivity

of nitrogen mustards towards different amino acids, and their adduct structures, three Cys-, Lys- and His-containing heptapeptides (AcPAACAA, AcPAAKAA, and AcPAAHAA) were incubated with mechloroethamine and tris-(2-chlorethyl)amine. Reaction with the Cys-containing peptides was much more favorable than others under the same conditions. It was identified that, despite having at least 2 reactive groups, one nitrogen mustard molecule only formed adduction with one reactive amino acid residue, even at a molar excess (50:1-200:1) and lengthy incubation times. Mechloroethamine yielded a mass increase of 120 Da, and tris-(2-chlorethyl)amine resulted in a mass increase of 150 Da, due to the loss of the second chlorine during adduction. For all peptide adducts, stable hydrolysis (replacement of Cl with OH) products were observed within 24 h of formation, and tris-(2-chlorethyl)amine adducts were more prone to hydrolysis, the ratio reaching 50% in less than 24h.

Mass spectrometry showed that the raloxifene metabolite diquinone methide, alkylated P450 3A4 at Cys-239, and inactivated the enzyme likely by unfolding the protein to an inactive conformation[98]. Glutathione reductase (GR) is a critical enzyme in cellular thiol-based redox regulation, which catalyzes the reduction of oxidized glutathione (GSSG) to GSH with NADPH, defending against oxidative stress[99]. In vitro experiments found that 6-hydroxymethylacylfulvene (HMAF), an antitumor agent and an analogue of illudin S (a natural mushroom sesquiterpenoid toxin), covalently modified purified yeast GR at Cys-42 and Cys-46 ($+ 2{\times}246$ Da) and irreversibly inhibited the enzymatic activity ($IC_{50} = 216$ μM). A drug binding-induced conformational change in GR was probed following a significant decrease in intrinsic GR fluorescence, which was complete at μM levels of HMAF. In Hela cells exposed to 4μM HMAF, cytotoxicity was accompanied with a significant inhibition of cellular GR activity and without a change in cellular GR concentration, suggesting protein adduct-induced inhibition of

the cellular enzyme[100]. Another target protein for developing antineoplastic alkylating agents is Trx2, an antioxidant and antiapoptotic protein overexpressed in imexon-resistant myeloma cells. Activity of Trx2, both in vitro and in cells (143B osteosarcoma cells), exhibited potent and persistent inhibition after alkylation at Cys-93 by N-ethylmaleimide, by inhibiting dissociation of Trx from its substrate and interfering with mitochondrial redox regulation[101].

Covalent binding to Cys-34 of human serum albumin and the stable adducted peptides have been demonstrated for many clinically important nitrogen mustards (mechlorethamine, chlorambucil, melphalan, cyclophosphamide and nornitrogen mustard) and sulfur mustards, both in vitro and in vivo[94, 102]. A biomarker for sulfur mustard, an adducted tripeptide [sulfur-hydroxyethylthioethyl (S-HETE) Cys-Pro-Phe for human serum albumin and (S-HETE) Cys-Pro-Tyr for rat serum albumin] has been validated with LC-MS/MS in multiple reports. For example, (S-HETE)-Cys-Pro-Phe was reliably produced with proteinase K from sulfur mustard-exposed human blood samples, it was purified with solid phase extraction and analyzed with isotope dilution UHPLC-MS/MS. The method has been validated over a concentration range of 3 to 250 ng/mL with a calculated limit of detection of 1.74 ng/mL[103]. In an in vivo study, the (S-HETE) Cys-Pro-Tyr peptide was detectable via LC-MS/MS up to 7 days after exposure of rats to sulfur mustard (i.v dose, 0.3 mg/kg = 0.1 LDs)[102]. The N-terminal valine of hemoglobin is also commonly adducted by alkylating agents[103]. A method has been developed for the quantitation of alkylated (methylated) hemoglobin from rats exposed to methane sulfonate (MMS). In the assay, hemoglobin was isolated from rat red blood cells, digested with trypsin and the methylated hemoglobin β chain N-terminal peptide (MeVHLTDAEK) was selected as the signature peptide for alkylation. The peptide was quantitated with LC-MS/MS using MRM mode. Negative ion ESI was applied due to the two acidic amino acid residues within the peptide. The limit of

quantitation for MeVHLTDAEK was 1.95 ng/mL (5.9 pmol/mg hemoglobin) and the linear range was 1.95-625 ng/mL. For rats orally dosed with 0.5 mg MMS/kg (n = 5) for 4 days, the mean concentration of alkylated hemoglobin was 10.02 pmol/mg[104].

3.5 Protein adducts with other xenobiotics

Important findings have been achieved with mass spectrometry towards the identification/characterization of protein adducts by other xenobiotics, such as amoxicillin[108], withaferin[109], diclofenac[110], fipexide[105], mycophenolic acid[113] and monocrotaline pyrrole[106]. Such findings give deeper insights into different pathways for toxicity initiation and development. However, these compounds are difficult to classify, and corresponding reports are sporadic for each compound. A shared pattern among analogs for target proteins and modification sites is missing. Considering the above, a concise combined summary about some representative compounds are provided.

Covalent binding of β-lactam to proteins, in the process known as haptenation, is essential in eliciting an immunological and allergic reaction[107]. Human serum albumin is the major target of amoxicillin, and haptenation at Lys-190 was identified in ex vivo samples from healthy subjects dosed with amoxicillin[108], which is helpful in delineating the mechanisms and developing new diagnostic tools for the allergic effects. Withaferin, a steroidal lactone, was demonstrated to covalently modify NF-κB Essential Modulator (NEMO), a key polyubiquitin chain-binding protein in canonical NF-κB signaling[109]. The modification occurred at Cys-397 in the C-terminal zinc finger (ZF) domain of NEMO. This modification led to an alteration in NEMO's interaction with polyubiquitin chains both in vitro and in vivo, directing the binding to long Lys-48-linked polyubiquitin chains but not tetra-ubiquitin species, thereby shedding light on the design of novel drugs to modulate ubiquitin-based cellular processes. Diclofenac, a

nonsteroidal anti-inflammatory drug, is involved with idiosyncratic hepatotoxicity and hypersensitivity. Protein adducts with its reactive metabolites, including 5-hydroxydiclofenac, diclofenac o-imine methide and diclofenac acyl glucuronide, have been identified in vivo and are considered to initiate the adverse effects[110,111,112]. The covalent modification on human glutathione-S-transferase P1-1 and human serum albumin have been characterized[111,112], but more target proteins need to be characterized in vivo, to clarify the relationship between protein adduction and the adverse effects. The hepatotoxicity of the immunosuppressant mycophenolic acid is considered to result from the covalent modification of its acyl glucuronide metabolite by proteins. Multiple potential target proteins have been identified in kidney tissue from rats treated with mycophenolate mofetil[113], but the impact of these protein modifications on protein functions and physiological pathways remain to be demonstrated.

4. Conclusion

Protein-xenobiotic adducts are attracting increasing research interest, for the elucidation of their roles in toxicity initiation and/or development, as well as applications as biomarkers. Mass spectrometry is an ideal technique to qualitatively and quantitatively characterize protein adducts, with good sensitivity, high efficiency and reliable methodologies. However, significant work remains to be made in the field of protein adduction. Most current research focuses on the identification of covalent modifications on target proteins. There are fewer reports about the effects of modification on protein function, and reports about the consequences on biological processes and pathways are very scarce. In vivo studies of protein adducts are also lacking, and the relationships of protein-xenobiotic adduct formation with dose, toxicity and biomarker sensitivity remain to be established for many xenobiotics. Greater efforts need to be devoted to

31

address these limitations, along with the advancements in MS technology, to provide a deeper understanding about the functional consequences of protein adducts.

References

1. R. M. LoPachin, A. P. DeCaprio. Protein adduct formation as a molecular mechanism in neurotoxicity. Toxicol. Sci. 2005, 86, 214.

2. M. Otagiri. A molecular functional study on the interactions of drugs with plasma proteins. Drug Metab. Pharmacokinet. 2005, 20, 309.

3. M. Tornqvist, C. Fred, J. Haglund, H. Helleberg, B. Paulsson, R. Rydberg. Protein adducts: quantitative and qualitative aspects of their formation, analysis and applications. J. Chromatogr. B-Analytical Technol. Biomed. Life Sci. 2002, 778, 279.

4. W. Jiang, E. G. Duysen, O. Lockridge. Mice treated with a nontoxic dose of chlorpyrifos oxon have diethoxyphosphotyrosine labeled proteins in blood up to 4 days post exposure, detected by mass spectrometry. Toxicology 2012, 295, 15.

5. H. U. Kafferlein, B. Marczynski, T. Mensing, T. Bruning. Albumin and hemoglobin adducts of benzo a pyrene in humans-Analytical methods, exposure assessment, and recommendations for future directions. Crit. Rev. Toxicol. 2010, 40, 126.

6. P. Koivisto, K. Peltonen. Analytical methods in DNA and protein adduct analysis. Anal. Bioanal. Chem. 2010, 398, 2563.

7. A. R. Farley, A. J. Link, IDENTIFICATION AND QUANTIFICATION OF PROTEIN POSTTRANSLATIONAL MODIFICATIONS, in Guide to Protein Purification, Second Edition, (Eds: R.R. Burgess, M.P. Deutscher). Elsevier Academic Press Inc, San Diego, 2009, pp. 725–763.

8. C. A. Srebalus Barnes, A. Lim. Applications of mass spectrometry for the structural characterization of recombinant protein pharmaceuticals. Mass Spectrom. Rev. 2007, 26, 370.

9. M. Colzani, G. Aldini, M. Carini. Mass spectrometric approaches for the identification and

quantification of reactive carbonyl species protein adducts. J. Proteomics 2013, 92, 28.

10. W. Jiang, E. G. Duysen, H. Hansen, L. Shlyakhtenko, L. M. Schopfer, O. Lockridge. Mice Treated with Chlorpyrifos or Chlorpyrifos Oxon Have Organophosphorylated Tubulin in the Brain and Disrupted Microtubule Structures, Suggesting a Role for Tubulin in Neurotoxicity Associated with Exposure to Organophosphorus Agents. Toxicol. Sci. 2010, 115, 183.

11. T. Wehr. Top-down versus bottom-up approaches in proteomics. Lc Gc North Am. 2006, 24, 1004.

12. H. Zhang, W. D. Cui, M. L. Gross. Native electrospray ionization and electron-capture dissociation for comparison of protein structure in solution and the gas phase. Int. J. Mass Spectrom. 2013, 354, 288.

13. H. L. Li, J. J. Wolff, S. L. Van Orden, J. A. Loo. Native Top-Down Electrospray Ionization-Mass Spectrometry of 158 kDa Protein Complex by High-Resolution Fourier Transform Ion Cyclotron Resonance Mass Spectrometry. Anal. Chem. 2014, 86, 317.

14. N. B. Zhang, Y. G. Du, M. Cui, Z. Q. Liu, S. Y. Liu. Comprehensive identification of the binding sites of cisplatin in hen egg white lysozyme. Anal. Bioanal. Chem. 2014, 406, 3537.

15. N. B. Zhang, H. Liu, M. Cui, Y . G. Du, Z. Q. Liu, S. Y. Liu. Direct determination of the binding sites of cisplatin on insulin-like growth factor-1 by top-down mass spectrometry. J. Biol. Inorg. Chem. 2015, 20, 1.

16. E. Moreno-Gordaliza, B. Canas, M. A. Palacios, M. M. Gomez-Gomez. Novel insights into the bottom-up mass spectrometry proteomics approach for the characterization of Pt-binding proteins: The insulin-cisplatin case study. Analyst 2010, 135, 1288.

17 . N. Rauniyar, K. Prokai-Tatrai, L. Prokai. Identification of carbonylation sites in apomyoglobin after exposure to 4-hydroxy-2-nonenal by solid-phase enrichment and liquid

chromatography-electrospray ionization tandem mass spectrometry. J. Mass Spectrom. 2010, 45, 398.

18. R. A. Zubarev. Electron-capture dissociation tandem mass spectrometry. Curr. Opin. Biotechnol. 2004, 15, 12.

19. J. E. P. Syka, J. J. Coon, M. J. Schroeder, J. Shabanowitz, D. F. Hunt. Peptide and protein sequence analysis by electron transfer dissociation mass spectrometry. Proc. Natl. Acad. Sci. U. S. A. 2004, 101, 9528.

20. M. S. Kim, A. Pandey. Electron transfer dissociation mass spectrometry in proteomics. Proteomics 2012, 12, 530.

21. S. M. Meier, Y. O. Tsybin, P. J. Dyson, B. K. Keppler, C. G. Hartinger. Fragmentation methods on the balance: unambiguous top-down mass spectrometric characterization of oxaliplatin-ubiquitin binding sites. Anal. Bioanal. Chem. 2012, 402, 2655.

22. C. G. Hartinger, Y. O. Tsybin, J. Fuchser, P. J. Dyson. Characterization of platinum anticancer drug protein-binding sites using a top-down mass spectrometric approach. Inorg. Chem. 2008, 47, 17.

23. A. V Terry. Functional consequences of repeated organophosphate exposure: Potential non-cholinergic mechanisms. Pharmacol. Ther. 2012, 134, 355.

24. O. Tacal, O. Lockridge. Methamidophos, dichlorvos, O-methoate and diazinon pesticides used in Turkey make a covalent bond with butyrylcholinesterase detected by mass spectrometry. J. Appl. Toxicol. 2010, 30, 469.

25. B. Li, L. M. Schopfer, H. Grigoryan, C. M. Thompson, S. H. Hinrichs, P. Masson, O. Lockridge. Tyrosines of Human and Mouse Transferrin Covalently Labeled by Organophosphorus Agents: A New Motif for Binding to Proteins that Have No Active Site

Serine. Toxicol. Sci. 2009, 107, 144.

26. B. Li, P. Eyer, M. Eddleston, W. Jiang, L. M. Schopfer, O. Lockridge. Protein tyrosine adduct in humans self-poisoned by chlorpyrifos. Toxicol. Appl. Pharmacol. 2013, 269, 215.

27. H. Grigoryan, B. Li, W. H. Xue, M. Grigoryan, L. M. Schopfer, O. Lockridge. Mass spectral characterization of organophosphate-labeled lysine in peptides. Anal. Biochem. 2009, 394, 92.

28. H. Grigoryan, L. M. Schopfer, E. S. Peeples, E. G. Duysen, M. Grigoryan, C. M. Thompson, O. Lockridge. Mass spectrometry identifies multiple organophosphorylated sites on tubulin. Toxicol. Appl. Pharmacol. 2009, 240, 149.

29. B. Li, L. M. Schopfer, S. H. Hinrichs, P. Masson, O. Lockridge. Matrix-assisted laser desorption/ionization time-of-flight mass spectrometry assay for organophosphorus toxicants bound to human albumin at Tyr411. Anal. Biochem. 2007, 361, 263.

30. T. M. Bui-Nguyen, W. E. Dennis, D. A. Jackson, J. D. Stallings, J. A. Lewis. Detection of Dichlorvos Adducts in a Hepatocyte Cell Line. J. Proteome Res. 2014, 13, 3583.

31. D. Noort, A. G. Hulst, A. van Zuylen, E. van Rijssel, M. J. van der Schans. Covalent binding of organophosphorothioates to albumin: a new perspective for OP-pesticide biomonitoring? Arch. Toxicol. 2009, 83, 1031.

32. Y. Bao, Q. Liu, J. Chen, Y. Lin, B. D. Wu, J. W. Xie. Quantification of nerve agent adducts with albumin in rat plasma using liquid chromatography-isotope dilution tandem mass spectrometry. J. Chromatogr. A 2012, 1229, 164.

33. C. Schmidt, F. Breyer, M. M. Blum, H. Thiermann, F. Worek, H. John. V-type nerve agents phosphonylate ubiquitin at biologically relevant lysine residues and induce intramolecular cyclization by an isopeptide bond. Anal. Bioanal. Chem. 2014, 406, 5171.

34. D. R. W. Verstappen, A. G. Hulst, A. Fidder, N. P. E. Vermeulen, D. Noort. Interactions of

organophosphates with keratins in the cornified epithelium of human skin. Chem. Biol. Interact. 2012, 197, 93.

35. W. Jiang, Y. A. Dubrovskii, E. P. Podolskaya, E. A. Murashko, V. Babakov, F. Nachon, P. Masson, L. M. Schopfer, O. Lockridge. PHOS-Select Iron Affinity Beads Enrich Peptides for the Detection of Organophosphorus Adducts on Albumin. Chem. Res. Toxicol. 2013, 26, 1917.

36 . M. S. Liyasova, L. M. Schopfer, O. Lockridge. Cresyl Saligenin Phosphate, an Organophosphorus Toxicant, Makes Covalent Adducts with Histidine, Lysine, and Tyrosine Residues of Human Serum Albumin. Chem. Res. Toxicol. 2012, 25, 1752.

37. C. M. Hernandez, W. D. Beck, S. X. Naughton, I. Poddar, B. L. Adam, N. Yanasak, C. Middleton, A. V Terry. Repeated exposure to chlorpyrifos leads to prolonged impairments of axonal transport in the living rodent brain. Neurotoxicology 2015, 47, 17.

38. G. B. Stokin, L. S. B. Goldstein, Axonal transport and Alzheimer's disease, in Annual Review of Biochemistry. Annual Reviews, Palo Alto, 2006, pp. 607–627.

39. M. B. Abou-Donia. Organophosphorus ester-induced chronic neurotoxicity. Arch. Environ. Health 2003, 58, 484.

40. M. Yeste-Velasco, D. Alvira, F. X. Sureda, V. Rimbau, A. Forsby, M. Pallas, A. Carnins, J. Folch. DNA low-density array analysis of colchicine neurotoxicity in rat cerebellar granular neurons. Neurotoxicology 2008, 29, 309.

41. H. Grigoryan, O. Lockridge. Nanoimages show disruption of tubulin polymerization by chlorpyrifos oxon: Implications for neurotoxicity. Toxicol. Appl. Pharmacol. 2009, 240, 143.

42. J. E. Loeffler, J. C. Potter, S. L. Scordelis, H. R. Hendrickson, C. K. Huston, A. C. Page. LONG-TERM EXPOSURE OF SWINE TO A DICHLORVOS C-14 ATMOSPHERE. J. Agric. Food Chem. 1976, 24, 367.

43. S. Li, X. Q. Ran, L. Xu, J. F. Wang. microRNA and mRNA Expression Profiling Analysis of Dichlorvos Cytotoxicity in Porcine Kidney Epithelial PK15 Cells. DNA Cell Biol. 2011, 30, 1073.

44. S. Sarin, K. D. Gill. Dichlorvos induced alterations in glucose homeostasis: Possible implications on the state of neuronal function in rats. Mol. Cell. Biochem. 1999, 199, 87.

45. M. Abdollahi, M. Donyavi, S. Pournourmohammadi, M. Saadat. Hyperglycemia associated with increased hepatic glycogen phosphorylase and phosphoenolpyruvate carboxykinase in rats following subchronic exposure to malathion. Comp. Biochem. Physiol. C-Toxicology Pharmacol. 2004, 137, 343.

46. Dichlorvos (DDVP): Risk Characterization Document; California Environmental Protection Agency: Sacramento, CA, 1996.

47. C. Nicholls, H. Li, J. P. Liu. GAPDH: A common enzyme with uncommon functions. Clin. Exp. Pharmacol. Physiol. 2012, 39, 674.

48. M. T. Ryzlak, R. Pietruszko. HETEROGENEITY OF GLYCERALDEHYDE-3-PHOSPHATE DEHYDROGENASE FROM HUMAN-BRAIN. Biochim Biophys Acta 1988, 954, 309.

49. V. M. Brown, E. Y. Krynetski, N. F. Krynetskaia, D. Grieger, S. T. Mukatira, K. G. Murti, C. A. Slaughter, H. W. Park, W. E. Evans. A novel CRM1-mediated nuclear export signal governs nuclear accumulation of glyceraldehyde-3-phosphate dehydrogenase following genotoxic stress. J. Biol. Chem. 2004, 279, 5984.

50. R. Ishitani, M. Tanaka, K. Sunaga, N. Katsube, D. M. Chuang. Nuclear localization of overexpressed glyceraldehyde-3-phosphate dehydrogenase in cultured cerebellar neurons undergoing apoptosis. Mol. Pharmacol. 1998, 53, 701.

51. D. A. Butterfield, S. S. Hardas, M. L. B. Lange. Oxidatively Modified Glyceraldehyde-3-Phosphate Dehydrogenase (GAPDH) and Alzheimer's Disease: Many Pathways to Neurodegeneration. J. Alzheimers Dis. 2010, 20, 369.

52. W. Jiang, E. A. Murashko, Y. A. Dubrovskii, E. P. Podolskaya, V. N. Babakov, J. Mikler, F. Nachon, P. Masson, L. M. Schopfer, O. Lockridge. Matrix-assisted laser desorption/ionization time-of-flight mass spectrometry of titanium oxide-enriched peptides for detection of aged organophosphorus adducts on human butyrylcholinesterase. Anal. Biochem. 2013, 439, 132.

53. F. Nachon, O. A. Asojo, G. E. O. Borgstahl, P. Masson, O. Lockridge. Role of water in aging of human butyrylcholinesterase inhibited by echothiophate: The crystal structure suggests two alternative mechanisms of aging. Biochemistry 2005, 44, 1154.

54. U. K. Aryal, C. T. Lin, J. S. Kim, T. H. Heibeck, J. Wang, W. J. Qian, Y. H. Lin. Identification of phosphorylated butyrylcholinesterase in human plasma using immunoaffinity purification and mass spectrometry. Anal. Chim. Acta 2012, 723, 68.

55. B. Li, I. Ricordel, L. M. Schopfer, F. Baud, B. Megarbane, P. Masson, O. Lockridge. Dichlorvos, chlorpyrifos oxon and Aldicarb adducts of butyrylcholinesterase, detected by mass spectrometry in human plasma following deliberate overdose. J. Appl. Toxicol. 2010, 30, 559.

56. T. Matsubara, I. Horikoshi. SPONTANEOUS REACTIVATION OF MOUSE PLASMA CHOLINESTERASE AFTER INHIBITION BY VARIOUS ORGANO-PHOSPHORUS COMPOUNDS. J. Pharmacobiodyn. 1984, 7, 322.

57. B. Li, E. G. Duysen, M. T. Froment, P. Masson, F. Nachon, W. Jiang, L. M. Schopfer, G. M. Thiele, L. W. Klassen, J. Cashman, G. R. Williams, O. Lockridge. Polyclonal Antibody to Soman-Tyrosine. Chem. Res. Toxicol. 2013, 26, 584.

58. L. Ayi-Fanou, P. H. Avogbe, B. Fayomi, G. Keith, C. Hountondji, E. E. Creppy, H. Autrup,

B. H. Rihn, A. Sanni. DNA-Adducts in Subjects Exposed to Urban Air Pollution by Benzene and Polycyclic Aromatic Hydrocarbons (PAHs) in Cotonou, Benin. Environ. Toxicol. 2011, 26, 93.

59. R. Atkinson, J. Arey. ATMOSPHERIC CHEMISTRY OF GAS-PHASE POLYCYCLIC AROMATIC-HYDROCARBONS - FORMATION OF ATMOSPHERIC MUTAGENS. Environ. Health Perspect. 1994, 102, 117.

60. S. Srivastava, M. Singh, J. George, K. Bhui, A. M. Saxena, Y. Shukla. Genotoxic and carcinogenic risks associated with the dietary consumption of repeatedly heated coconut oil. Br. J. Nutr. 2010, 104, 1343.

61. A. M. Wheelock, B. C. Boland, M. Isbell, D. Morin, T. C. Wegesser, C. G. Plopper, A. R. Buckpitt. In vivo effects of ozone exposure on protein adduct formation by 1-nitronaphthalene in rat lung. Am. J. Respir. Cell Mol. Biol. 2005, 33, 130.

62. C. Y. Lin, B. C. Boland, Y. J. Lee, M. R. Salemi, D. Morin, L. A. Miller, C. G. Plopper, A. R. Buckpitt. Identification of proteins adducted by reactive metabolites of naphthalene and 1-nitronaphthalene in dissected airways of rhesus macaques. Proteomics 2006, 6, 972.

63. M. Cho, C. Chichester, D. Morin, C. Plopper, A. Buckpitt. COVALENT INTERACTIONS OF REACTIVE NAPHTHALENE METABOLITES WITH PROTEINS. J. Pharmacol. Exp. Ther. 1994, 269, 881.

64. B. Boland, C. Y. Lin, D. Morin, L. Miller, C. Plopper, A. Buckpitt. Site-specific metabolism of naphthalene and 1-nitronaphthalene in dissected airways of rhesus macaques. J. Pharmacol. Exp. Ther. 2004, 310, 546.

65. C. Y. Lin, M. A. Isbell, D. Morin, B. C. Boland, M. R. Salemi, W. T. Jewell, A. J. Weir, M. V Fanucchi, G. L. Baker, C. G. Plopper, A. R. Buckpittt. Characterization of a structurally intact in situ lung model and comparison of naphthalene protein adducts generated in this model vs

lung microsomes. Chem. Res. Toxicol. 2005, 18, 802.

66. M. A. Isbell, D. Morin, B. Boland, A. Buckpitt, M. Salemi, J. Presley. Identification of proteins adducted by reactive naphthalene metabolites in vitro. Proteomics 2005, 5, 4197.

67. N. T. Pham, W. T. Jewell, D. Morin, A. R. Buckpitt. Analysis of naphthalene adduct binding sites in model proteins by tandem mass spectrometry. Chem. Biol. Interact. 2012, 199, 120.

68. F. G. Zhang, M. J. Bartels. Structural analysis of naphthoquinone protein adducts with liquid chromatography/tandem mass spectrometry and the scoring algorithm for spectral analysis (SALSA). Rapid Commun. Mass Spectrom. 2004, 18, 1809.

69. N. Verma, M. Pink, A. W. Rettenmeier, S. Schmitz-Spanke. Review on proteomic analyses of benzo a pyrene toxicity. Proteomics 2012, 12, 1731.

70. K. YeowellOconnell, T. A. McDonald, S. M. Rappaport. Analysis of hemoglobin adducts of benzene oxide by gas chromatography mass spectrometry. Anal. Biochem. 1996, 237, 49.

71. S. Waidyanatha, M. A. Troester, A. B. Lindstrom, S. M. Rappaport. Measurement of hemoglobin and albumin adducts of naphthalene-1,2-oxide, 1,2-naphthoquinone and 1,4-naphthoquinone after administration of naphthalene to F344 rats. Chem. Biol. Interact. 2002, 141, 189.

72. M. K. Briggs, E. Desavis, P. A. Mazzer, R. B. Sunoj, S. A. Hatcher, C. M. Hadad, P. G. Hatcher. A new approach to evaluating the extent of Michael adduct formation to PAH quinones: Tetramethylammonium hydroxide (TMAH) thermochemolysis with GC/MS. Chem. Res. Toxicol. 2003, 16, 1484.

73. B. W. Day, P. L. Skipper, R. H. Rich, S. Naylor, S. R. Tannenbaum. CONVERSION OF A HEMOGLOBIN ALPHA-CHAIN ASPARTATE(47) ESTER TO N-(2,3-DIHYDROXYPROPYL)ASPARAGINE AS A METHOD FOR IDENTIFICATION OF THE

PRINCIPAL BINDING-SITE FOR BENZO A PYRENE ANTI-DIOL EPOXIDE. Chem. Res. Toxicol. 1991, 4, 359.

74. B. W. Day, P. L. Skipper, J. Zaia, K. Singh, S. R. Tannenbaum. ENANTIOSPECIFICITY OF COVALENT ADDUCT FORMATION BY BENZO A PYRENE ANTI-DIOL EPOXIDE WITH HUMAN SERUM-ALBUMIN. Chem. Res. Toxicol. 1994, 7, 829.

75. H. Helleberg, M. Tornqvist. A new approach for measuring protein adducts from benzo a pyrene diolepoxide by high performance liquid chromatography/tandem mass spectrometry. Rapid Commun. Mass Spectrom. 2000, 14, 1644.

76. B. W. Day, P. L. Skipper, J. Zaia, S. R. Tannenbaum. BENZO A PYRENE ANTI-DIOL EPOXIDE COVALENTLY MODIFIES HUMAN SERUM-ALBUMIN CARBOXYLATE SIDE-CHAINS AND IMIDAZOLE SIDE-CHAIN OF HISTIDINE(146). J. Am. Chem. Soc. 1991, 113, 8505.

77. E. Westberg, U. Hedebrant, J. Haglund, T. Alsberg, J. Eriksson, A. Seidel, M. Tornqvist. Conditions for sample preparation and quantitative HPLC/MS-MS analysis of bulky adducts to serum albumin with diolepoxides of polycyclic aromatic hydrocarbons as models. Anal. Bioanal. Chem. 2014, 406, 1519.

78. E. A. C. Westberg, R. Singh, U. Hedebrant, G. Koukouves, V. L. Souliotis, P. B. Farmer, D. Segerback, S. Kyrtopoulos, M. A. Tornqvist. Adduct levels from benzo a pyrenediol epoxide: Relative formation to histidine in serum albumin and to deoxyguanosine in DNA in vitro and in vivo in mice measured by LC/MS-MS methods. Toxicol. Lett. 2015, 232, 28.

79 . L. F. Prescott. KINETICS AND METABOLISM OF PARACETAMOL AND PHENACETIN. Br. J. Clin. Pharmacol. 1980, 10, S291.

80. B. K. Park, N. R. Kitteringham, J. L. Maggs, M. Pirmohamed, D. P. Williams, The role of

metabolic activation in drug-induced hepatotoxicity, in Annual Review of Pharmacology and Toxicology. Annual Reviews, Palo Alto, 2005, pp. 177–202.

81. D. C. Evans, A. P. Watt, D. A. Nicoll-Griffith, T. A. Baillie. Drug-protein adducts: An industry perspective on minimizing the potential for drug bioactivation in drug discovery and development. Chem. Res. Toxicol. 2004, 17, 3.

82. L. P. James, P. R. Mayeux, J. A. Hinson. Acetaminophen-induced hepatotoxicity. Drug Metab. Dispos. 2003, 31, 1499.

83. H. Jaeschke, M. R. McGill, C. D. Williams, A. Ramachandran. Current issues with acetaminophen hepatotoxicity-A clinically relevant model to test the efficacy of natural products. Life Sci. 2011, 88, 737.

84. R. Bruderer, O. M. Bernhardt, T. Gandhi, S. M. Miladinovic, L. Y. Cheng, S. Messner, T. Ehrenberger, V. Zanotelli, Y. Butscheid, C. Escher, O. Vitek, O. Rinner, L. Reiter. Extending the Limits of Quantitative Proteome Profiling with Data-Independent Acquisition and Application to Acetaminophen-Treated Three-Dimensional Liver Microtissues. Mol. Cell. Proteomics 2015, 14, 1400.

85. Y. C. Qiu, L. Z. Benet, A. L. Burlingame. Identification of the hepatic protein targets of reactive metabolites of acetaminophen in vivo in mice using two-dimensional gel electrophoresis and mass spectrometry. J. Biol. Chem. 1998, 273, 17940.

86. R. E. Jenkins, N. R. Kitteringham, C. E. P. Goldring, S. M. J. Dowdall, J. Hamlett, C. S. Lane, J. S. Boerma, N. P. E. Vermeulen, B. K. Park. Glutathione-S-transferase pi as a model protein for the characterisation of chemically reactive metabolites. Proteomics 2008, 8, 301.

87. N. Y. Shin, Q. F. Liu, S. L. Stamer, D. C. Liebler. Protein targets of reactive electrophiles in human liver microsomes. Chem. Res. Toxicol. 2007, 20, 859.

88. H. Y. Zhang, J. P. Gan, Y. Z. Shu, W. G. Humphreys. High-Resolution Mass Spectrometry-Based Background Subtraction for Identifying Protein Modifications in a Complex Biological System: Detection of Acetaminophen-Bound Microsomal Proteins Including Argininosuccinate Synthetase. Chem. Res. Toxicol. 2015, 28, 775.

89. L. Switzar, L. M. Kwast, H. Lingeman, M. Giera, R. H. H. Pieters, W. M. A. Niessen. Identification and quantification of drug-albumin adducts in serum samples from a drug exposure study in mice. J. Chromatogr. B-Analytical Technol. Biomed. Life Sci. 2013, 917, 53.

90. S. F. Cook, A. D. King, Y. Chang, G. J. Murray, H. R. K. Norris, R. C. Dart, J. L. Green, S. C. Curry, D. E. Rollins, D. G. Wilkins. Quantification of a biomarker of acetaminophen protein adducts in human serum by high-performance liquid chromatography-electrospray ionization-tandem mass spectrometry: Clinical and animal model applications. J. Chromatogr. B-Analytical Technol. Biomed. Life Sci. 2015, 985, 131.

91. T. Hairin, A. R. Marzilawati, E. M. H. Didi, S. Mahadeva, Y. K. Lee, N. Abd Rahman, A. M. Mustafa, Z. Chik. Quantitative LC/MS/MS analysis of acetaminophen-cysteine adducts (APAP-CYS) and its application in acetaminophen overdose patients. Anal. Methods 2013, 5, 1955.

92. V. R. Thompson, A. P. DeCaprio. Covalent Adduction of Nitrogen Mustards to Model Protein Nucleophiles. Chem. Res. Toxicol. 2013, 26, 1263.

93. H. Thulin, V. Zorcec, D. Segerback, A. Sundwall, M. Tornqvist. Oxazolidonylethyl adducts to hemoglobin and DNA following nornitrogen mustard exposure. Chem. Biol. Interact. 1996, 99, 263.

94. D. Noort, A. G. Hulst, R. Jansen. Covalent binding of nitrogen mustards to the cysteine-34 residue in human serum albumin. Arch. Toxicol. 2002, 76, 83.

95. M. Antoine, D. Fabris, C. Fenselau. Covalent sequestration of the nitrogen mustard

mechlorethamine by metallothionein. Drug Metab. Dispos. 1998, 26, 921.

96. R. Loeber, E. Michaelson, Q. Fang, C. Campbell, A. E. Pegg, N. Tretyakova. Cross-linking of the DNA repair protein O-6-alkylguanine DNA alkyltransferase to DNA in the presence of antitumor nitrogen mustards. Chem. Res. Toxicol. 2008, 21, 787.

97. M. D. Person, D. E. Mason, D. C. Liebler, T. J. Monks, S. S. Lau. Alkylation of cytochrome c by (glutathion-S-yl)-1,4-benzoquinone and iodoacetamide demonstrates compound-dependent site specificity. Chem. Res. Toxicol. 2005, 18, 41.

98. B. R. Baer, L. C. Wienkers, D. A. Rock. Time-dependent inactivation of P450 3A4 by raloxifene: Identification of Cys239 as the site of apoprotein Alkylation. Chem. Res. Toxicol. 2007, 20, 954.

99. W. L. Sweet, J. S. Blanchard. HUMAN ERYTHROCYTE GLUTATHIONE-REDUCTASE - CHEMICAL MECHANISM AND STRUCTURE OF THE TRANSITION-STATE FOR HYDRIDE TRANSFER. Biochemistry 1991, 30, 8702.

100. X. D. Liu, S. J. Sturla. Profiling patterns of glutathione reductase inhibition by the natural product illudin S and its acylfulvene analogues. Mol. Biosyst. 2009, 5, 1013.

101. Y. Chen, Y. M. Go, J. Pohl, M. Reed, J. Y. Cai, D. P. Jones. Increased mitochondrial thioredoxin 2 potentiates N-ethylmaleimide-induced cytotoxicity. Chem. Res. Toxicol. 2008, 21, 1205.

102. D. Noort, A. Fidder, C. Degenhardt-Langelaan, A. G. Hulst. Retrospective detection of sulfur mustard exposure by mass spectrometric analysis of adducts to albumin and hemoglobin: An in vivo study. J. Anal. Toxicol. 2008, 32, 25.

103. B. G. Pantazides, B. S. Crow, J. W. Garton, J. A. Quinones-Gonzalez, T. A. Blake, J. D. Thomas, R. C. Johnson. Simplified Method for Quantifying Sulfur Mustard Adducts to Blood

Proteins by Ultrahigh Pressure Liquid Chromatography Isotope Dilution Tandem Mass Spectrometry. Chem. Res. Toxicol. 2015, 28, 256.

104. F. G. Zhang, M. J. Bartels, L. H. Pottenger, M. R. Schisler, J. J. Grundy, B. B. Gollapudi. Quantitation of methylated hemoglobin adducts in a signature peptide from rat blood by liquid chromatography/negative electrospray ionization tandem mass spectrometry. Rapid Commun. Mass Spectrom. 2008, 22, 1455.

105. L. Sleno, E. Varesio, G. Hopfgartner. Determining protein adducts of fipexide: mass spectrometry based assay for confirming the involvement of its reactive metabolite in covalent binding. Rapid Commun. Mass Spectrom. 2007, 21, 4149.

106. M. W. Lame, A. D. Jones, D. W. Wilson, S. K. Dunston, H. J. Segall. Protein targets of monocrotaline pyrrole in pulmonary artery endothelial cells. J. Biol. Chem. 2000, 275, 29091.

107. A. Ariza, D. Garzon, D. R. Abanades, V. de los Rios, G. Vistoli, M. J. Torres, M. Carini, G. Aldini, D. Perez-Sala. Protein haptenation by amoxicillin: High resolution mass spectrometry analysis and identification of target proteins in serum. J. Proteomics 2012, 77, 504.

108. D. Garzon, A. Ariza, L. Regazzoni, R. Clerici, A. Altomare, F. R. Sirtori, M. Carini, M. J. Torres, D. Perez-Sala, G. Aldini. Mass Spectrometric Strategies for the Identification and Characterization of Human Serum Albumin Covalently Adducted by Amoxicillin: Ex Vivo Studies. Chem. Res. Toxicol. 2014, 27, 1566.

109. C. Hooper, S. S. Jackson, E. E. Coughlin, J. J. Coon, S. Miyamoto. Covalent Modification of the NF-kappa B Essential Modulator (NEMO) by a Chemical Compound Can Regulate Its Ubiquitin Binding Properties in Vitro. J. Biol. Chem. 2014, 289, 33161.

110. J. A. Jones, L. Kaphalia, M. Treinen-Moslen, D. C. Liebler. Proteomic characterization of metabolites, protein adducts, and biliary proteins in rats exposed to 1,1-dichloroethylene or

diclofenac. Chem. Res. Toxicol. 2003, 16, 1306.

111. J. S. Boerma, S. Dragovic, N. P. E. Vermeulen, J. N. M. Commandeur. Mass Spectrometric Characterization of Protein Adducts of Multiple P450-Dependent Reactive Intermediates of Diclofenac to Human Glutathione-S-transferase P1-1. Chem. Res. Toxicol. 2012, 25, 2532.

112. T. G. Hammond, X. L. Meng, R. E. Jenkins, J. L. Maggs, A. S. Castelazo, S. L. Regan, S. N. L. Bennett, C. J. Earnshaw, G. P. Aithal, I. Pande, J. G. Kenna, A. V Stachulski, B. K. Park, D. P. Williams. Mass Spectrometric Characterization of Circulating Covalent Protein Adducts Derived from a Drug Acyl Glucuronide Metabolite: Multiple Albumin Adductions in Diclofenac Patients. J. Pharmacol. Exp. Ther. 2014, 350, 387.

113. A. R. Asif, V. W. Armstrong, A. Voland, E. Wieland, M. Oellerich, M. Shipkova. Proteins identified as targets of the acyl glucuronide metabolite of mycophenolic acid in kidney tissue from mycophenolate mofetil treated rats. Biochimie 2007, 89, 393.

CHAPTER 3

DETERMINATION OF CHLORPYRIFOS AND ITS METABOLITES IN CELLS AND

CULTURE MEDIA BY LIQUID CHROMATOGRAPHY-ELECTROSPRAY IONIZATION

TANDEM MASS SPECTROMETRY (LC-MS/MS)

Xiangkun Yang, Xian Wu, Kyle A. Brown, Thao Le, Steven L. Stice and Michael G. Bartlett
Submitted to *Journal of Chromatography B*, March 14, 2017

Abstract

A sensitive method to simultaneously quantitate chlorpyrifos, chlorpyrifos oxon and the detoxified product 3,5,6-trichloro-2-pyridinol (TCP) was developed using either liquid-liquid extraction for culture media samples, or protein precipitation for cell samples. Multiple reaction monitoring in positive ion mode was applied for the detection of chlorpyrifos and chlorpyrifos oxon, and selected ion recording in negative mode was applied to detect TCP. The method provided linear ranges from 5-500, 0.2-20 and 20-2000 ng/mL for media samples and from 0.5-50, 0.02-2 and 2-200 ng/million cells for CPF, CPO and TCP, respectively. The method was validated using selectivity, linearity, precision, accuracy, recovery, stability and dilution tests. This method has been successfully applied to study the neurotoxicity and metabolism of chlorpyrifos in a human neuronal model.

Keywords

Chlorpyrifos, chlorpyrifos oxon, TCP, neuron, metabolism, neurotoxicity, culture media, LC-MS/MS

1. Introduction

Chlorpyrifos (O,O-diethyl O-[3,5,6,-trichloro-2-pyridyl] phosphorothionate, CPF) is a common organophosphate insecticide, acaracide and miticide. It has been widely used in both agricultural and non-agricultural areas since 1965. Like other organophosphate pesticides, exposure to high doses of chlorpyrifos can lead to acute poisoning, by covalently inhibiting acetylcholinesterase (AChE), overstimulating the nervous system causing neuromuscular symptoms and at very high exposures initiates seizures, respiratory paralysis and death. In addition, there are human epidemiological studies demonstrating that long-term, low-level exposure to chlorpyrifos can lead to chronic neurotoxicity in the absence of cholinesterase inhibition, including deficits in cognition, memory, emotional state and syntactic reasoning[1,2]. The underlying mechanism is minimally understood. There is evidence in animal experiments that the axonal transport system is a potential toxicological target, which was found to be negatively affected by repeated, low-level chlorpyrifos exposures that were not associated with acute cholinergic symptoms[3,4,5].

CPF is metabolically activated to a potent phosphorylating agent, chlorpyrifos oxon (CPO). It's found that the desulfuration of CPF in human liver microsomes is mediated by CYP2B6 at low concentrations[6], and by CYP3A4 at high concentrations[7]. Extreme variability was observed in the formation of CPO in patients poisoned by CPF, possibly due to interindividual variability in its metabolism[8]. CPF and CPO are detoxified to TCP (3,5,6-trichloro-2-pyridinol) by CYP2C19 which has the highest intrinsic clearance for CPF detoxification[9]. In the environment, CPF is mainly hydrolyzed to TCP, when applied to plants or soil. The degradation rate is dependent on factors including pH, temperature, chemicals, ultraviolet light and microbial activity[10]. Urinary TCP is a biomarker to assess chlorpyrifos

exposure in risk groups, and significant differences were observed between exposed subjects and reference subjects[11].

Accurate determination of CPF and its metabolites is challenging due to their chemical instability. In addition, CPF and CPO can covalently modify various proteins at serine, tyrosine, lysine and histidine residues, making their bioanalysis more challenging[12]. Multiple LC-MS/MS methods have been developed and validated to determine CPF and its metabolites in human or animal blood[13], serum[14], urine[14,15] and brain tissue[16]. However, few methods were validated for the quantitation of CPO; for methods validated for CPO, CPO escaped detection in the application to real samples[13,16]. An enzyme-based assay was developed to address this concern[17]. The method utilized the fast covalent binding of CPO to butyrylcholinesterase (BChE), inhibiting BChE activity in a concentration-dependent manner. However, the sample preparation is more complex than conventional methods: titration with equine BChE is required after extracting CPO from human plasma. In addition, the linear range of this assay was narrow (2 nM - 20 nM CPO), making it necessary to dilute high concentrations and reduce the BChE amount for low concentrations.

Human pluripotent stem cell derived cell models are important in studies of the cellular metabolism of chlorpyrifos, and the molecular and cellular processes involved in its chronic neurotoxicity. Until now, no methods have been reported to quantitate chlorpyrifos and its metabolites in cells and culture media. In this paper, we have established and validated a method, with protein precipitation for cell sample preparation and liquid-liquid extraction for media sample preparation using LC-MS/MS for detection, which simultaneously quantitates CPF, CPO and TCP. After validation, this method was applied to analyze neurons treated with CPF to study the neurotoxicity. This method also facilitates investigations into the neuroprotective role of

astrocytic cytochrome P450s against chlorpyrifos exposure in an astrocyte-neuron co-culture system.
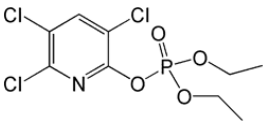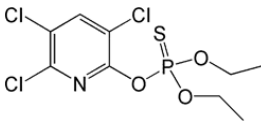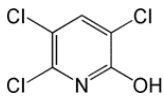
2. Experimental

2.1. Chemicals and reagents

Chlorpyrifos (CPF, 99.5% pure), chlorpyrifos oxon (CPO, 98.5% pure), and 3,5,6-trichloro-2-pyridinol (TCP, 99% pure) were all purchased from Chem Service (West Chester, PA). The chemical structures are shown in Fig. 1. Ammonium acetate, isopropyl ether, LC-MS grade methanol, acetonitrile, water and formic acid were purchased from Sigma-Aldrich (St. Louis, MO). Human pluripotent stem cell derived NeuroNet™ pure human neurons (DIV 28 neurons) and culture media (AB2™ basal media supplemented with ANS™ neural supplement) were acquired from ArunA Biomedical (Athens, GA).

Fig. 1. Chemical structures and physicochemical properties of CPF, CPO and TCP. XLogP3 values were obtained from PubChem database.

	CPF	CPO	TCP
Mass	350.58	334.51	198.43
XLogP3	5.3	3.5	3.7

2.2. Instrumentation

An Agilent 1100 binary pump HPLC system (Santa Clara, CA) coupled to a Waters Micromass Quattro Micro triple quadrupole mass spectrometer with an ESI source (Milford, MA) was applied for LC–MS/MS analysis. Masslynx 4.0 software by Waters (Beverly, MA) was used

for instrument control and data processing. A Labconco CentriVap Complete Vacuum Concentrator (Kansas City, MO) was utilized for sample evaporation.

2.3. LC-MS/MS conditions

A Zorbax Eclipse XDB-C8 (2.1×150 mm, 5 μm) column coupled with a Phenomenex SecurityGuard C-8 guard column (4.0 mm×2.0 mm) was used for the separation. The column temperature was kept at 32 ℃. The mobile phase A was 0.025% formic acid in water and mobile phase B was acetonitrile. The injection volume was 15 μL. The analytes were separated using a gradient method, with a 0.3 mL/min flow rate, (time/minute, % mobile phase B): (0, 60), (2, 80), (2.01, 80), (5, 80), (6, 60), (10, 60). The autosampler injection needle was rinsed with methanol after each injection. Nitrogen was used as the desolvation gas at a flow rate of 500 L/h. The desolvation temperature was 500 ℃ and the source temperature was 120 ℃. Argon was used as the collision gas, and the collision cell pressure was set at 3.5×10^{-3} mbar. Samples were analyzed by the mass spectrometer in positive ion mode for CPF and CPO, and in negative ion mode for TCP. In MS tune setting, the capillary voltage was 3.5 kV and the cone voltage was 28 V for the determination of CPF and CPO. The tune parameters were 4 kV and -22 V for TCP. The collision energy was 22 eV for CPF and 15 eV for CPO. Multiple reaction monitoring (MRM) functions were applied for detecting CPF and CPO, and the monitored ion transitions were 352 →200 and 336→280, respectively. A selected ion recording (SIR) function for m/z = 198 was applied for the detection of TCP.

2.4. Standards and QCs

The primary stocks were prepared at 0.5 mg/mL in acetonitrile for all analytes, and stored in the refrigerator (+4 ℃) when not in use. All dilutions were made with acetonitrile. Standard working solutions containing all three analytes were prepared fresh before use. The

concentrations for all standard and quality control (QC) working solutions are listed in Table 1. 10 μL of a standard or QC working solution was spiked with cell pellet (1×10^6 cells) or 90 μL blank cell culture media to make the corresponding standard or QC samples.

2.5. Sample preparation

Media sample preparation: 1.7 mL of diisopropyl ether was added to each 100 μL of culture media. The mixture was vortexed for 10 min before centrifuged at 20000×g, 5 ℃ for 10 min. 1.5 mL of organic supernatant was collected and evaporated to complete dryness in the vacuum concentrator at 55 ℃ for 10 min. The sample was reconstituted with 100 μL of acetonitrile.

Cell sample preparation: 1 mL of methanol was added to the cell pellet (1×10^6 cells). The mixture was briefly vortexed and stored at -80 ℃ for 15 min. The cell lysate was centrifuged at 20000×g, 5 ℃ for 10 min, and 0.9 mL of supernatant was transferred to a glass tube. Another 1 mL of acetonitrile was added to the extract and evaporated to dryness. The residue was reconstituted with 100 μL of acetonitrile. The following procedures are the same as in media sample preparation: reconstituted samples were sonicated, vortexed, and centrifuged at 15,000×g, 5 ℃ for 10 min. 80 μL of supernatant was transferred into an autosampler vial for analysis using LC-MS/MS.

2.6. Method validation

Selectivity, linearity, intra- and inter-day precision and accuracy, recovery, stability and dilution tests were conducted for method validation. Selectivity (n = 6) was tested by comparing the chromatograms of blank samples with those at the LLOQ. For media samples, the linearity was validated using calibration standard samples over the concentration ranges of 5-500, 0.2-20 and 20-2000 ng/mL for CPF, CPO and TCP, respectively. The linearity ranges were 0.5-50,

0.02-2 and 2-200 ng/million cells for CPF, CPO and TCP in cell samples. Calibration curves were made using the peak area over the concentration (ng/mL) or amount (ng/million cells), with 1/x weighted linear regression. The intra-day (n = 5) and inter-day (n = 15) precision and accuracy were tested with QC samples at the LLOQ, low, middle and high QC (LQC, MQC and HQC) concentrations. Recovery (n = 3), including matrix effect, relative recovery and absolute recovery in culture media and cells, were tested by calculating from peak areas of spiked samples, post-preparation spiked samples and standard solutions at the LQC, MQC and HQC concentrations.

Autosampler stability (25 ℃, 10 h) and bench-top stability (25 ℃, 2 h) of the analytes were tested at the LQC and HQC points. Dilution tests (n = 5) were conducted by diluting spiked media samples to the ULOQ with blank media, and by diluting post-preparation spiked cell samples with post-prepared blank matrix.

2.7. Application

NeuroNet™ pure human neurons (DIV 28 neurons) were thawed and maintained according to manufacturer's instructions. DIV 28 neurons (1×10^6 cells/well in the 6 well culture plate) were exposed to CPF (10 μM) for 48 h before sample collection. All biological samples were stored at −80 °C until use. Fresh calibration standard samples were prepared each day for quantitation.

3. Results and discussion

3.1. Method development

The MS parameters were optimized on the tune page accompanied by a direct infusion of the standard solution (10 μg/mL of each analyte). Positive ion mode was applied for the detection of CPF and CPO, and negative ion mode was applied for TCP, based on the intensities

of analytes under each ion mode. In addition, CPO presented significantly higher ionization efficiency than CPF (> 10 folds) under the same MS parameters, possibly due to the feasibility of charge retention on the P=O group compared to the P=S group. Product ion mass spectra for CPF and CPO were acquired using injections of the same standard solution. The most abundant fragment ion for each analyte was included to the MRM function, and the monitored ion transitions were 352→200 for CPF and 336→280 for CPO. We failed to detect fragment ions for TCP, likely because of the stable aromatic ring. A selected ion recording (SIR) function of m/z=198 was applied to detect TCP.

Liquid-liquid extraction was applied to prepare media samples. A variety of organic solvents, including isopropyl ether, dichloromethane and ethyl acetate, were tested. Tested solvents provided similar recoveries of CPO,. Isopropyl ether allowed the highest recovery of CPF (1-fold and 20% higher than ethyl acetate and dichloromethane, respectively), and dichloromethane failed to extract TCP. In addition, the least time evaporation was required was for the isopropyl ether extract. Based on above, isopropyl ether was selected as the solvent. TCP is a weak acidic compound, thus a more acidic pH facilitates its neutralization in the aqueous phase and extraction by the organic phase. The recovery of TCP from cell culture media significantly increased (by 1-fold) when the neutral pH was adjusted to 4 with formic acid. Therefore, cell culture media was adjusted to pH 4, and cell pellet samples were mixed with 1 μL of 10% formic acid before sample preparation.

3.2. Selectivity

Selectivity (n = 6) was validated by analyzing blank culture media, spiked media samples (5.0, 0.2 and 20 ng/mL CPF, CPO and TCP, respectively), blank cells, and spiked cell samples (0.5, 0.02 and 2 ng CPF, CPO and TCP). Chromatograms of the same matrix were compared

between blank and spiked samples (Fig. 2). No significant interferences from blank matrices were observed, demonstrating that the LC-MS/MS method has the necessary selectivity to differentiate and quantitate analytes in cells and culture media in the presence of matrix components.

(A) Blank cell culture media

(B) Cell culture media at the LLOQ

(C) Blank cells
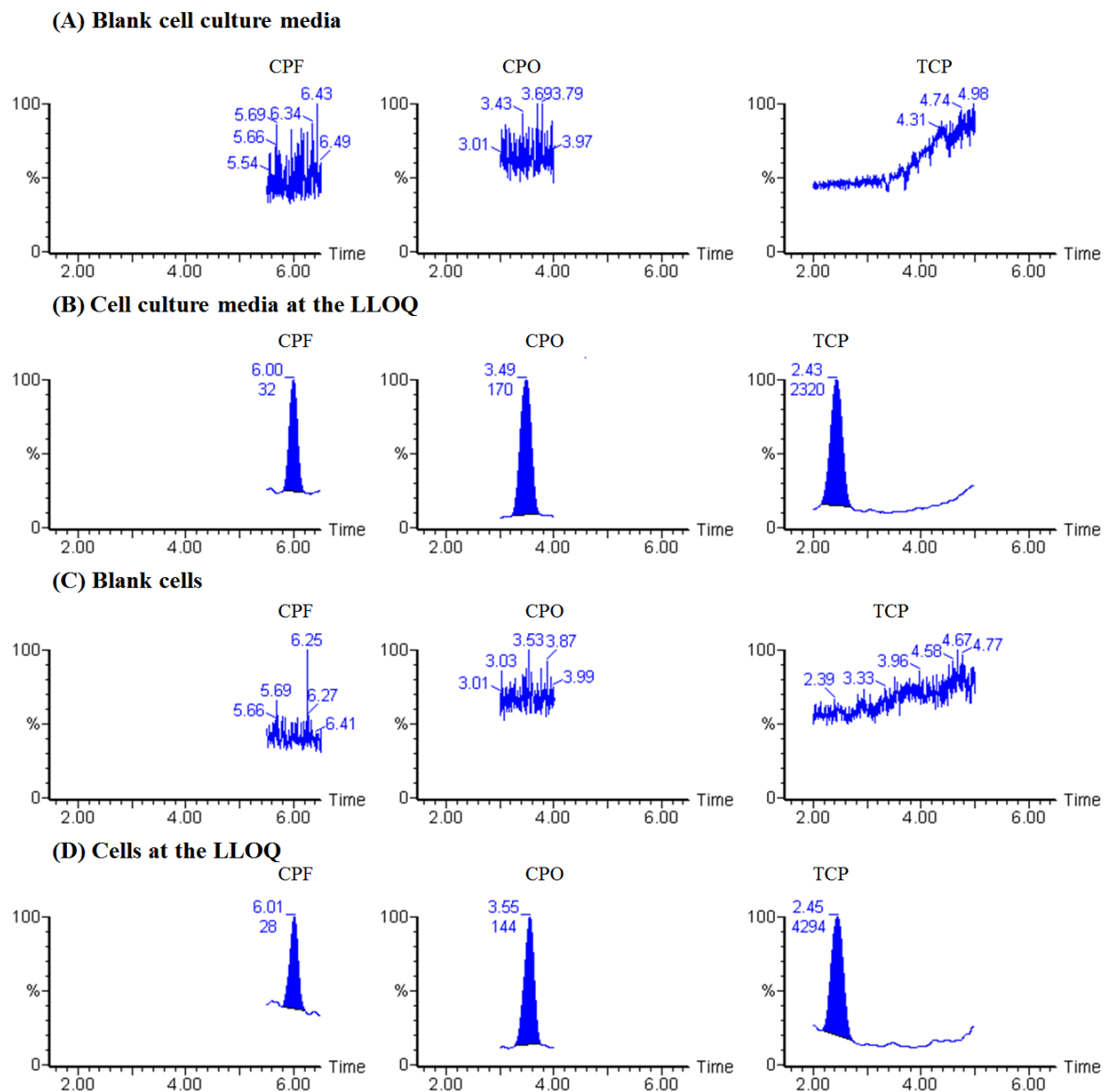
(D) Cells at the LLOQ

Fig. 2. Representative chromatograms of CPF, CPO and TCP in blank cell culture media (A), cell culture media at the LLOQ (B), blank cells (C) and cells at the LLOQ (D). Retention times for analytes are shown in minutes.

3.3. Linearity

The linear concentration ranges to be validated were: 5-500, 0.2-20 and 20-2000 ng/mL for media samples and 0.5-50, 0.02-2 and 2-200 ng/million cells for CPF, CPO and TCP, respectively. Calibration curves were made from peak areas of analytes, using 1/x weighted linear regressions. Slopes, intercepts and R^2 values from the calibration curves are shown in Table 2. The method allows for good linearity ($R^2 > 0.99$) for all analytes in either matrix within the tested range.

3.4. Precision and accuracy

The intra-day (n = 5) and inter-day (n = 15) precision and accuracy for all analytes were tested using the LLQC, LQC, MQC and HQC samples. For cell culture media samples, the LLOQ contains 5.0 ng/mL, 0.2 ng/mL, 20.0 ng/mL CPF, CPO and TCP; the LQC contains 15.0 ng/mL, 0.6 ng/mL, 60.0 ng/mL CPF, CPO and TCP; the MQC contains 150.0, 6.0 ng/mL, 600.0 ng/mL CPF, CPO and TCP; and the HQC contains 375.0 ng/mL, 15.0 ng/mL, 1500.0 ng/mL CPF, CPO and TCP. The amounts of analytes are the same in QCs from cell samples, but are in units of ng/million cells. The LLOQ contains 0.5, 0.02, 2.0 ng/million cells CPF, CPO and TCP; the LQC contains 1.5, 0.06 ng and 6.0 ng/million cells CPF, CPO and TCP; the MQC contains 15.0, 0.6 and 60.0 ng/million cells CPF, CPO and TCP; and the HQC contains 37.5, 1.5 and 150.0 ng/million cells CPF, CPO and TCP. Relative standard deviations (RSD) were calculated to evaluate method precision. Relative errors (RE) were calculated to evaluate method accuracy.

Table 3 shows the quantitation, RSD and RE values of all analytes in QC culture media and cell samples. All RSD and RE values are within 15% (except for the LLOQ, within 20%) and meet the requirements from Guidance for Industry (Bioanalytical Method Validation) by the FDA. In addition, according to the requirements of the same guidance, we have also validated the LLOQ for culture media (5.0 ng/mL, 0.2 ng/mL, 20.0 ng/mL CPF, CPO and TCP) and for cells (0.5, 0.02, 2.0 ng CPF, CPO and TCP per million cells). The LLOQ was determined because the RSD and RE for either analyte in either matrix are within 20%, and the response at the LLOQ is over five times the response from blank samples.

3.5. Recovery

Absolute recovery, relative recovery and matrix effects (n = 3) were tested in culture media and cells, with spiked samples, post-preparation spiked samples and standard solutions at the LQC, MQC and HQC in triplicate. The absolute recovery was demonstrated by the ratio of peak areas between spiked samples and the average of standard solutions. Relative recovery was demonstrated by the ratio of peak areas between spiked samples and the average of post-preparation spiked samples. Matrix effects were demonstrated by the ratio of peak areas between post-preparation spiked samples and the average of standard solutions. A ratio over 100% represents an enhancing matrix effect, a ratio below 100% represents a suppressing matrix effect, and the percentage of enhancement or suppression is calculated as the deviation from 100%. Table 4 shows the absolute recovery (AR), relative recovery (RR), matrix effect and the type in both matrices at 3 QC values. The absolute and relative recoveries are consistent for the same analyte in the same matrix. There is weak to medium suppressive matrix effect for CPF and CPO in both matrices, possibly resulting from co-eluting matrix components competing for ionization. In the contrast, weak to medium enhancing matrix effects were observed for TCP in both

matrices, suggesting that the matrix components facilitated the ionization of TCP in the negative ion mode.

3.6. Stability

To validate autosampler stability (25 ℃, 10 h) and bench-top stability (25 ℃, 2 h), two sets (n = 3) of spiked culture media and cell samples at the LQC and HQC were prepared. One set was analyzed immediately, and the data were applied as the time zero control. The same samples were injected after 10 h to test autosampler stability. The other set was analyzed after being placed on the bench for 2 h. For each stability test, the ratio to the time-zero control was calculated. The data are shown in Table 5. No significant degradation was observed, validating the stability of analytes in both matrices during sample handling and preparation.

3.7. Dilution

Concentrations of CPF, CPO and TCP in real samples are dependent on the treatment dose, time, cellular metabolism, compound degradation and other factors. The dilution test (n = 5) was conducted to validate sample dilution when analyte concentrations in real samples are higher than the upper limit of quantitation (ULOQ). Spiked culture media samples at 5-fold the ULOQ were diluted to the ULOQ using blank culture media prior to sample preparation. Due to the difficulty of transferring blank cell pellets, cell samples at 5-fold the ULOQ were prepared, and dilution was done to the ULOQ with blank post-prepared cell matrix before LC-MS analysis. Quantitative results, precision and accuracy (n = 5) are shown in Table 6. The RSD and RE values for each analyte in either matrix are within 15%, validating the dilution test.

3.8. Application

The validated method was applied to simultaneously quantitate CPF and its metabolites (CPO and TCP) in human neurons (DIV 28 neurons) and culture media. Each million neurons (n

= 3) were continuously exposed to 10 μM CPF for 48 h before sample collection. To compare, blank media (n = 3) were incubated with 10 μM CPF under the same conditions. Cell and culture media samples were analyzed with the validated method. Because the amount of CPF in cells was over the upper limit of the validated range, cells samples were diluted 20 fold with blank post-prepared matrix before injection. All analytes were detected in both matrices, and the determined levels were over the LLOQ (data shown in Table 7).

Significant degradation of CPF was observed in culture media, and abundant degradation products (mostly TCP) were observed in either group, demonstrating the instability of CPF under cell culture conditions. Concentrations of CPF and CPO in culture media, especially CPO, declined in the presence of neurons, possibly due to the formation of protein adducts[12]. The high level of CPF in cells can be explained by the lipophilicity of CPF, which facilitated its trans-membrane distribution. The low cellular levels of TCP are correlated with its relatively high polarity, which tends to facilitate secretion out of cells once formed. The concentration of TCP in cell culture media was similar between groups, suggesting that drug metabolizing enzymes in neurons were unable to make a significant contribution to the detoxification of CPF [18].

4. Conclusion

A sensitive LC-MS/MS method to quantitate CPF and its main metabolites CPO and TCP in human pluripotent stem cell derived neuron cells and culture media has been developed for the first time. Good selectivity, sensitivity, linearity of calibration curve, accuracy, precision, recovery and stability were validated according to the FDA Guidance for Industry (Bioanalytical Method Validation). The validated method has been successfully applied to study the metabolism of CPF by neuronal cells.

References

1. S.M. Ross, I.C. McManus, V. Harrison, O. Mason, Crit. Rev. Toxicol. 43 (2013) 21-44.

2. D.S. Rohlman, W.K. Anger, P.J. Lein, Neurotoxicology 32 (2011) 268-276.

3. C.M. Hernandez, W.D. Beck, S.X. Naughton, I. Poddar, B.L. Adam, N. Yanasak, C. Middleton, A. V Terry, Neurotoxicology 47 (2015) 17-26.

4. A. V Terry, D.A. Gearhart, W.D. Beck, J.N. Truan, M.L. Middlemore, L.N. Williamson, M.G. Bartlett, M.A. Prendergast, D.W. Sickles, J.J. Buccafusco, J. Pharmacol. Exp. Ther. 322 (2007) 1117-1128.

5. A. V Terry, J.D. Stone, J.J. Buccafusco, D.W. Sickles, A. Sood, M.A. Prendergast, J. Pharmacol. Exp. Ther. 305 (2003) 375-384.

6. R.J. Foxenberg, B.P. McGarrigle, J.B. Knaak, P.J. Kostyniak, J.R. Olson, Drug Metab. Dispos. 35 (2007) 189-193.

7. F.M. Buratti, M.T. Volpe, A. Meneguz, L. Vittozzi, E. Testai, Toxicol. Appl. Pharmacol. 186 (2003) 143-154.

8. F. Eyer, D.M. Roberts, N.A. Buckley, M. Eddleston, H. Thiermann, F. Worek, P. Eyer, Biochem. Pharmacol. 78 (2009) 531-537.

9. A.L. Crane, K. Klein, U.M. Zanger, J.R. Olson, Toxicology 293 (2012) 115-122.

10. S. Das, T.K. Adhya, J. Environ. Manage. 152 (2015) 36-42.

11. J.W. Albers, S. Berent, D.H. Garabrant, B. Giordani, S.J. Schweitzer, R.P. Garrison, R.J. Richardson, J. Occup. Environ. Med. 46 (2004) 367-378.

12. X.K. Yang, M.G. Bartlett, Rapid Commun. Mass Spectrom. 30 (2016) 652-664.

13. L.N. Williamson, M.G. Bartlett, A. V Terry, J. Liq. Chromatogr. Relat. Technol. 30 (2007) 273-285.

14. J. V Sancho, O.J. Pozo, F. Hernandez, Rapid Commun. Mass Spectrom. 14 (2000) 1485-1490.

15. W. Bicker, M. Lammerhofer, W. Lindner, J. Chromatogr. B-Analytical Technol. Biomed. Life Sci. 822 (2005) 160-169.

16. L.N. Williamson, A. V Terry, M.G. Bartlett, Rapid Commun. Mass Spectrom. 20 (2006) 2689-2695.

17. R. Heilmair, F. Eyer, P. Eyer, Toxicol. Lett. 181 (2008) 19-28.

18. S.L. Miksys, R.F. Tyndale, J. Psychiatry Neurosci. 27 (2002) 406-415.

Table 1. Concentrations (ng/mL) of analytes in standard and QC working solutions.

Standard working solution	CPF	CPO	TCP
A	5000	200	20000
B	2500	100	10000
C	1250	50	5000
D	500	20	2000
E	250	10	1000
F	125	5	500
G	50	2	200
LLOQ	50	2	200
LQC	150	6	600
MQC	1500	60	6000
HQC	3750	150	15000

Table 2. Calibration curves for CPF, CPO and TCP in cell culture media and cells (n = 3). Quantitation units: cell culture media: ng/mL; cells: ng/million cells.

Analyte	Cell culture media			Cells		
	Slope	Intercept	R^2	Slope	Intercept	R^2
CPF	10.1070 ±1.0505	-7.8342 ±14.4258	0.9957 ±0.0029	22.4304±2.0033	-4.6608 ±3.3870	0.9900±0.0044
CPO	332.9817 ±30.2517	-5.5474 ±3.4559	0.9972 ±0.0016	6585.40±834.33	-7.6712±13.2846	0.9943±0.0051
TCP	62.2681 ±0.1355	-100.9538 ±32.0791	0.9989 ±0.0005	1615.55±171.09	329.22±1276.01	0.9944±0.0023

Table 3. The intra-day (n = 5) and inter-day (n = 15) precision (RSD) and accuracy (RE) of the LC–MS/MS method used to quantitate CPF, CPO and TCP in culture media and cells. Units for nominal and measured levels: concentration in culture media: ng/mL, cells: ng/million cells.

Matrix	Analyte	Nominal level	Intra-day			Inter-day		
			Measured level	RSD (%)	RE (%)	Measured level	RSD (%)	RE (%)
Culture media (ng/mL)	CPF	5	5.50±0.41	7.51%	10.00%	5.05±0.68	13.47%	1.00%
		15	14.95±1.21	8.09%	-0.33%	14.22±1.07	7.52%	-5.20%
		150	134.25±7.35	5.48%	-10.50%	128.45±7.35	5.72%	-14.37%
		375	349.25±42.09	12.05%	-6.87%	336.10±37.36	11.12%	-10.37%
	CPO	0.2	0.21±0.03	12.28%	5.00%	0.22±0.04	18.18%	10.00%
		0.6	0.64±0.02	3.56%	6.67%	0.58±0.08	13.79%	-3.33%
		6	5.19±0.07	1.29%	-13.50%	5.74±0.85	14.81%	-4.33%
		15	13.99±0.76	5.40%	-6.73%	15.37±1.71	11.13%	2.47%
	TCP	20	21.64±1.70	7.84%	8.20%	21.17±1.67	7.88%	5.85%

		60	59.21±7.55	12.75%	-1.32%	62.98±5.70	9.04%	4.97%
		600	596.04±71.79	12.04%	-0.66%	613.78±68.52	11.16%	2.19%
		1500	1427.20±188.04	13.18%	-4.85%	1486.53±222.11	14.94%	-0.90%
Cells (ng/million cells)	CPF	0.5	0.59±0.10	17.46%	17.00%	0.60±0.11	18.33%	20.00%
		1.5	1.58±0.20	12.58%	5.50%	1.54±0.17	11.04%	2.67%
		15	13.96±1.26	9.03%	-6.93%	13.90±1.92	13.81%	-7.33%
		37.5	36.00±2.05	5.69%	-3.99%	35.74±2.81	7.86%	-4.69%
	CPO	0.02	0.020±0.001	5.00%	0.00%	0.021±0.004	16.64%	5.88%
		0.06	0.067±0.010	14.93%	11.67%	0.070±0.009	13.23%	14.29%
		0.6	0.658±0.039	5.93%	9.67%	0.658±0.030	4.58%	5.70%
		1.5	1.668±0.112	6.71%	11.20%	1.745±0.112	6.43%	14.04%
	TCP	2	1.62±0.06	3.98%	-19.25%	1.90±0.37	19.64%	-5.00%
		6	5.13±0.40	7.77%	-14.58%	5.76±0.84	14.57%	-4.00%
		60	57.57±1.21	2.10%	-4.05%	58.72±5.12	8.73%	-2.13%
		150	143.53±20.84	14.52%	-4.31%	139.79±18.28	13.08%	-6.81%

Table 4. Absolute recovery (%AR, n = 3), relative recovery (%RR, n = 3) and matrix effect (%ME, n = 3) of the method. Units for nominal levels: concentration in culture media: ng/mL, cells: ng/million cells.

Matrix	Analyte	Nominal level	AR (%)	RR (%)	ME (%)		Type
Culture media (ng/mL)	CPF	15	50.75±4.54	72.39±6.57	70.10%	29.90%	Suppression
		150	52.31±2.13	81.87±3.19	63.90%	36.10%	Suppression
		375	46.40±4.93	79.04±6.02	58.71%	41.29%	Suppression
	CPO	0.6	59.96±6.40	61.25±5.54	97.89%	2.11%	Suppression
		6	58.73±2.57	59.23±1.37	99.16%	0.84%	Suppression
		15	66.33±4.67	57.78±8.54	114.79%	14.79%	Enhancement
	TCP	60	45.92±1.27	44.45±1.23	103.32%	3.32%	Enhancement
		600	46.61±4.39	45.81±1.18	101.74%	1.74%	Enhancement
		1500	46.63±1.14	46.33±1.13	100.64%	0.64%	Enhancement
Cells (ng/million cells)	CPF	1.5	59.29 ± 11.44	73.17 ± 14.11	81.03%	18.97%	Suppression
		15	64.39 ±7.27	72.56 ± 11.58	88.74%	11.26%	Suppression
		37.5	61.77 ±6.51	77.82 ± 10.17	79.38%	20.62%	Suppression

CPO	0.06	55.32 $\pm$ 8.70	79.63 $\pm$ 12.84	69.47%	30.53%	Suppression
	0.6	55.54 $\pm$ 3.91	75.12 $\pm$ 5.29	73.94%	26.06%	Suppression
	1.5	60.64 $\pm$ 4.47	77.94 $\pm$ 5.75	77.80%	22.20%	Suppression
TCP	6	103.64 $\pm$ 8.27	87.28 $\pm$ 7.71	118.74%	18.74%	Enhancement
	60	110.81 $\pm$ 14.59	92.23 $\pm$ 12.14	120.14%	20.14%	Enhancement
	150	111.23 $\pm$ 14.31	85.25 $\pm$ 10.32	130.48%	30.48%	Enhancement

Table 5. Autosampler stability (n = 3) and bench-top stability (n = 3) of CPF, CPO and TCP at the LQC and HQC in culture media and cells. Stabilities are shown as percentages of relative concentration when compared to the time zero control (mean ± SD). Units for nominal levels: concentration in culture media: ng/mL, cells: ng/million cells.

Matrix	Analyte	Nominal level	Autosampler stability (%)	Bench-top stability (%)
Culture	CPF	15	91.23 ±2.44	101.60 ±8.29
media		375	97.19 ±3.07	96.25 ±1.98
(ng/mL)	CPO	0.6	98.52 ±5.77	96.93 ±1.84
		15	92.53 ±2.11	94.01 ±0.62
	TCP	60	97.77 ±0.66	89.32 ±2.95
		1500	99.92 ±3.47	97.91 ±3.24
Cells	CPF	1.5	96.01 ±5.88	87.76 ±1.22
(ng/million		37.5	95.24 ±2.77	95.75 ±1.30
cells)	CPO	0.06	96.71 ±7.11	98.49 ±0.77
		1.5	98.54 ±2.44	97.76 ±1.21
	TCP	6	100.17 ±5.61	97.92 ±2.24
		150	97.99 ±2.99	101.14 ±3.01

Table 6. Precision (RSD) and accuracy (RE) of spiked samples (n = 5) at 5-fold the ULOQ in culture media and cells diluted to the ULOQ.

Matrix	Analyte	Nominal level	Measured level	RSD (%)	RE (%)
Culture	CPF	2500	2426.07 $\pm$ 140.81	5.80%	-2.96%
media	CPO	100	95.49 $\pm$ 7.00	7.33%	-4.51%
(ng/mL)	TCP	10000	9951.33 $\pm$ 1067.47	10.73%	-0.49%
Cells	CPF	250	246.33 $\pm$ 16.50	6.70%	-1.47%
(ng/million	CPO	10	10.27 $\pm$ 0.75	7.31%	2.70%
cells)	TCP	1000	949.33 $\pm$ 31.00	3.27%	-5.07%

Table 7. Quantitation of CPF, CPO and TCP in culture media and cells, obtained from culture media incubated with 10 µM CPF for 48 h (Blank media + CPF) and DIV 28 neurons treated with 10 µM CPF under the same conditions (Neurons + CPF) and. N/A: not applicable.

Treatments	Analyte	Conc. in culture media (ng/mL)	Levels in cells (ng/million cells)
Blank media + CPF	CPF	140.07 ± 15.76	N/A
	CPO	0.78 ± 0.01	N/A
	TCP	84.23 ± 10.87	N/A
Neurons + CPF	CPF	105.80 ± 13.10	725.76 ± 180.17
	CPO	0.18 ± 0.03	0.19 ± 0.03
	TCP	74.72 ± 9.00	2.52 ± 0.15

CHAPTER 4

DETERMINATION OF LYS-40 ACETYLATED ALPHA-TUBULIN IN RAT BRAIN TISSUE

BY IMMUNOPRECIPITATION-MASS SPECTROMETRY (IP-MS)

Xiangkun Yang and Michael G. Bartlett
To be submitted to *Analytical Chemistry*

Abstract

Acetylation at α-tubulin Lys-40 is a key post-translational modification (PTM) in the nervous system, and is a potential biomarker for neurodegenerative diseases and xenobiotic-induced neurotoxicity. However, the absolute level of this key PTM has not been determined in the brain. Immunoprecipitation-mass spectrometry (IP-MS) combines antibody specificity and mass spectrometry selectivity, and is being widely applied for the targeted quantitation of proteins within complex biomatricies. Lys-40 acetylation has not been previously studied with MS, due to the lack of cleavage sites in the vicinity for trypsin and other common enzymes, making it challenging to identify a surrogate peptide for MS analysis. In this study, we report such a peptide was identified for the first time after pepsin digestion, and an IP-MS based assay was developed to absolutely quantitate Lys-40 acetylated α-tubulin in rat brain tissue. The workflow includes pepsin digestion, immunoaffinity enrichment of the acetylated peptide, and quantitation using a stable isotope labelled peptide. Only a small amount of brain tissue (2 mg) was required for each analysis. The method provided a linear range of 1.0–100.0 pmol/mg brain tissue, and selectivity, precision and accuracy were validated. This method has been successfully applied in a preclinical study of chlorpyrifos neurotoxicity, and we observed a significant decrease of brain tubulin acetylation after chronic exposure to this organophosphate insecticide.

Key words

Tubulin acetylation, immunoprecipitation, mass spectrometry, chlorpyrifos and neurotoxicity

74

1. Introduction

Tubulin is a protein superfamily including α-, β-, γ-, Δ-, δ-, ε- and ζ-tubulins[1]. Heterodimers of α- and β-tubulin polymerize into microtubules accompanying GTP hydrolysis. Microtubules alternate between periods of growth and shrinkage known as "dynamic instability"[2]. This property is essential for cellular activities including cell migration, division and development. In neurons, microtubules are "railways" of the axonal transport system responsible for the transport of organelles, proteins, mRNA, and signaling molecules by motor proteins, of which kinesin delivers from the cell body to the synaptic terminal and dynein delivers in the opposite direction.

Tubulin receives a host of post-translational modifications (PTMs) in the nervous system, including acetylation[3], detyrosination[4], Δ2 modification[5], polyglutamylation[6] and polyglycylation[7]. These PTMs, except for tubulin acetylation, occur at the C-terminal region of α-tubulin or β-tubulin on the outside surface of microtubules [8]. By contrast, tubulin acetylation occurs at Lys-40 on the lumen surface and is preserved in α-tubulin isotypes. It is mediated with α-tubulin acetyltransferase 1 (ATAT1)/MEC-17 from inside out, and its deacetylation is mediated with histone deacetylase 6 (HDAC6) and NAD-dependent deacetylase sirtuin-2 (SIRT2), allowing for a balance of tubulin acetylation[9,10]. Lys-40 acetylation is associated with dendrite growth, microtubule stabilization, and binding with motor proteins[11], and experiments have shown that kinesin-1 can only bind to MTs when Lys-40 of α-tubulin was acetylated[11].

Decreases in tubulin acetylation were observed in multiple neurodegenerative diseases[12,13] and neurotoxicity induced by different toxicants[14,15]. In patients with Huntington's disease (HD), tubulin acetylation reduction was concomitant with the decreased transport of MT-dependent vesicles containing brain-derived neurotrophic factor (BDNF). The transport defects

could be rescued by increasing tubulin acetylation after treatment with the HDAC inhibitor trichostatin A (TSA). This increased acetylation enhanced the recruitment of motor proteins including kinesin-1 and dynein[12]. Similarly, diisopropyl fluorophosphate (DFP), an organophosphate insecticide was associated with a decline in tubulin acetylation. This alternation, coupled with deficits in microtubule dynamics, mitochondrial transport, and dopamine release, were found to be correctable or improved by tubacin, a drug that inhibits HDAC6[14].

Considering tubulin acetylation as a promising biomarker for multiple neuronal deficits, it is necessary to have analytical methods for this key PTM. Western blot is most commonly applied for the detection of tubulin acetylation[16,17]. A method was validated using chemically acetylated tubulin as the standard, and the percentages of acetylated tubulin relative to total tubulin were estimated in three different cell lines (0-7%). However, the potential cross-reactivity of the antibody with other proteins or other acetylated lysines on tubulin[16,18] may complicate the result. Immunoprecipitation-mass spectrometry (IP-MS) has emerged as an important technique for the targeted quantitation of proteins in biological matrices, which reduces matrix complexity with antibody specificity and detects the analyte with mass spectrometry selectivity[19]. It is predominantly based on a surrogate peptide generated from tryptic digestion, but the lack of cleavage sites near Lys-40 makes it difficult to generate a peptide containing Lys-40. In this paper, such a peptide was identified after peptic digestion. We developed and validated the first MS-based assay, using immunoprecipitation for surrogate peptide enrichment, selected ion recording (SIR) mass spectrometry for detection, to absolutely quantitate Lys-40 acetylated α-tubulin in the rat brain tissue. This method has been successfully applied in a chronic neurotoxicity study of an organophosphate insecticide chlorpyrifos, to facilitate the mechanistic study of organophosphate neurotoxicity.

2. Materials and Methods

2.1 Materials

Acetyl-α-tubulin (Lys-40) monoclonal antibodies: mouse monoclonal antibody (mAb) [6-11B-1] was acquired from Novus Biologicals (Littleton, CO) and rabbit mAb [D20G3] was purchased from Cell Signaling Technology (Boston, MA). Protein G magnetic beads were obtained from Bio-rad (Hercules, CA). Whole rat brains (Wistar Hannover) were purchased from Bioreclamation IVT (Westbury, NY). Pure tubulin (bovine) was purchased from Cytoskeleton (Denver, CO). Modified pepsin (porcine) was purchased from Princeton Separations (Adelphia, NJ). Protease inhibitors trichostatin A (TSA), phenylmethylsulfonyl fluoride (PMSF), 1, 10-phenanthroline were purchased from Cayman Chemical (Ann Arbor, MI), Research Products International (Mt Prospect, IL) and Oakwood Chemical (Estill, SC), respectively. Fmoc amino acids and resins for solid phase peptide synthesis, including Fmoc-Leu-OH (13C$_6$,15N) and Fmoc-Lys(Ac)-OH, were purchased from ChemPep (Wellington, FL). 2-(N-morpholino)ethanesulfonic acid (MES) anhydrous was purchased from Amresco (Solon, OH). Glycine, tris(hydroxymethyl)aminomethane, Ethylenediaminetetraacetic acid (EDTA), magnesium chloride, dithiothreitol (DTT), hydrochloric acid, and LC-MS grade solvents including formic acid, trifluoroacetic acid, acetonitrile and water were purchased from Sigma−Aldrich (St. Louis, MO).

2.2 Solid Phase peptide synthesis

Peptides YCLEHGIQPDGQMPSDKTIGGGDDSF (Lys-40 peptide), YCLEHGIQPDGQMPSDK(ac)TIGGGDDSF (surrogate peptide for Lys-40 acetylated α-tubulin, surrogate peptide) and YCL*EHGIQPDGQMPSDK(ac)TIGGGDDSF (L* = 7 Da mass shift, stable isotope labelled peptide, SIL peptide) were synthesized using Fmoc solid-phase peptide

synthesis with the AAPPTec Focus XC automated peptide synthesizer (Louisville, KY). Peptides were purified with an Agilent Polaris 5 C18-A preparative column (150 × 21.2 mm, 5 μm) on the Shimadzu LC-20AT HPLC system with a SPD-20A UV-Vis detector (Kyoto, JP).

2.3 LC-MS/MS conditions

Mobile phase A was water containing 0.01% (v/v) formic acid, and mobile phase B was acetonitrile. A Halo® peptide ES-C18 column (100 × 4.6 mm, 2.7 μm) by Advanced Materials Technology (Wilmington, DE) coupled with a C-18 guard column (4.0 mm × 2.0 mm) by Phenomenex (Torrance, CA) was used to separate the peptides. The injection volume was 20 μL. Different LC-MS instrumentation and parameters were applied for peptide sequencing and quantitation. For peptide sequencing, A Waters UPLC system (Milford, MA) coupled to a Waters SYNAPT G2 Q-TOF mass spectrometry with an ESI source (Milford, MA) was operated for LC−MS/MS analysis. Peptides were separated using a gradient method, with a 0.3 mL/min flow rate, (minute, % mobile phase B): (0, 5), (60, 50), (60.01, 95), (67.50, 95), and the run time for each injection was 75 min. MS setting for the SYNAPT G2 mass spectrometer were: capillary voltage 2.00 kV, sample cone voltage: 35 V, extraction cone voltage 4.0 V, source temperature 120 ℃, desolvation temperature 500 ℃ and desolvation gas 500 L/h. Data were acquired with the data-dependent acquisition (DDA) function: 1s MS survey scan in the mass range of 300–1900 were followed by MS/MS scans of up to 3 ions, when intensity rose above 1500 counts/s. MS/MS scan was acquired over the range of 100-1900, with a 2 s scan rate, and was switched to MS survey scan after 3 scans. Trap collision energy was set using charge state recognition, applying the default files for 1-4 charge states. For peptide quantitation, an Agilent 1100 binary pump HPLC system (Santa Clara, CA) interfaced to a Waters Micromass Quattro Micro triple quadrupole mass spectrometer with an ESI source (Milford, MA) was operated for

LC−MS analysis. The capillary voltage was 3.80 kV, the cone voltage was 32 V, the extractor voltage was 1 and RF lens voltage was 2.0 V. The source temperature was 120 ℃, desolvation gas flow rate was 500 L/h and the desolvation temperature was 500 ℃. Peptides were separated using a gradient method, with a 0.3 mL/min flow rate, (minute, % mobile phase B): (0, 25), (15, 40), (15.01, 95), (22.50, 95), and the run time for each injection was 30 min. The selected ion recording (SIR) function was applied to minitor precursor ions m/z 1406.0 and 1409.5 at the retention time of 7.5 min for the surrogate peptide and and the SIL peptide, respectively. Data were processed with Waters software including ProteinLynx Global Server (PLGS) 2.4 and Masslynx 4.1 (Beverly, MA).

2.4 Tissue Extract

One volume of rat brain tissue was resuspended in 1.5 volume of MES buffer (100 mM MES, 1 mM magnesium chloride, 1 mM EDTA, pH 6.8) supplemented with 1 mM PMSF, 1 mM 1, 10-phenanthroline and 5 μM of the HDAC inhibitor trichostatin A (TSA). Brain homogenate was prepared on ice using a tissue grinder. Brain homogenate was frozen at -80 ℃ for 30 min and thawed at 37 ℃. The homogenate was sonicated 5 times for 10 s with 30 s rest intervals on melted ice. Sample was centrifuged at 30,000×g (Beckman TL 120.2) at 4 ℃ for 15 min to remove cell debris, and the supernatant was centrifuged at 100,000×g (Beckman TL 120.2) at 4 ℃ for 1 h. The final supernatant was collected as brain tissue lysate. Protein concentration was determined with a NanoDrop Lite Spectrophotometer by Thermo Fisher Scientific (Waltham, MA).

2.5 Pepsin Digestion and Immunoprecipitation of the acetylated peptide

Brain tissue lysate was mixed with urea to a concentration of 2 M, and acidified to pH 2 with hydrochloric acid. Proteins were digested with pepsin (enzyme: total protein = 1: 2000) at

37 °C for 18 h. Each 5 µL of peptic digest was neutralized and diluted with 45 µL of phosphate-buffered saline supplemented with 0.1% Tween 20 (PBS-T). 1 uL of antibody and 10 pmol SIL peptide were mixed with diluted brain tissue lysate and incubated overnight while rotating at 4 °C. 100 µL of the suspension of protein G magnetic beads were washed with 500 µL of PBS-T three times before incubation with the antibody-antigen mixture for 2 h while rotating at 4 °C. The magnetic beads were washed with ice-cold buffers: PBST twice, PBS once and last with 50 mM ammonium acetate (pH 7). Enriched peptides were eluted with 25 µL of 100 mM glycine-TFA (pH 2.0) at room temperature.

2.6 Method Validation

The same protocol for the preparation of brain tissue lysate was used to prepare a blank matrix for acetylated tubulin, except that TSA, an HDAC6 inhibitor was absent. Selectivity, linearity, precision and accuracy tests were conducted to validate the method. Each test was conducted with 50 µL of 10-fold diluted brain tissue lysate, equal to 2 mg of brain tissue. Selectivity (n = 3) was tested by comparing the chromatograms of analytes in blank brain tissue lysate, with analytes in the same matrix at 1 pmol/mg brain tissue. Linearity was validated with calibration standard samples over the range of 1.0–100 pmol/mg. Calibration curves were made from peak area ratios between analytes and the SIL peptide. The specificity and accurary (n=3) were tested by QC samples at low (3 pmol/mg), middle (30 pmol/mg) and high (75 pmol/mg) concentrations.

2.7 Animal study

Wistar Hannover rats were orally dosed with 18 mg/kg chlorpyrifos in peanut oil every other day for 30 days with a 45 day washout period. Vehicle was peanut oil with 3% DMSO. All procedures employed in this study were reviewed and approved by the Augusta University

Institutional Animal Care and Use Committee and are consistent with AAALAC guidelines. Measures were taken to minimize pain and discomfort in accordance with the National Institutes of Health Guide for the Care and Use of Laboratory Animals (NIH Publications No. 80-23) revised in 1996. Rats were anesthetized with isoflurane. Whole brains were taken after the washout period, washed in PBS, and kept frozen at −80 °C until analysis.

3. Results and discussion

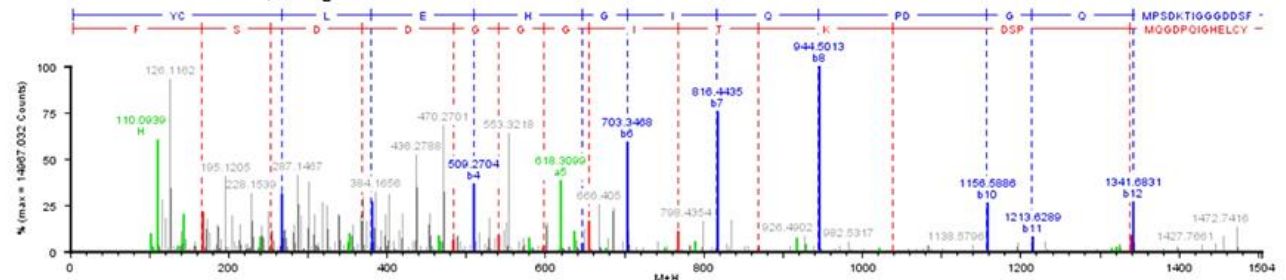### 3.1 Identification of the surrogate peptide

Trypsin is the most commonly used digestive enzyme in proteomics studies, known for its specificity, reproducibility and efficiency. However, in the vicinity of Lys-40, there is only Arg-2 and Lys-60, and a very long peptide would be generated by trypsin in the presence of acetylated Lys-40, beyond the fragmentation and sequencing capability of common mass spectrometry instrumentation. Various other enzymes and cleavage reagents, including formic acid, proteinase K, endoproteinase Asp-N and pepsin were tested to digest purified tubulin (bovine) to identify a peptide sequence containing Lys-40. After pepsin digestion, a peptide sequence Y_{24}CLEHGIQPDGQMPSDKTIGGGDDSF$_{49}$ was identified and a surrogate peptide for acetylated tubulin Y_{24}CLEHGIQPDGQMPSDK(ac)TIGGGDDSF$_{49}$ was identified after immunoprecipitation enrichment. (Figure 1). This sequence is conserved in all α-tubulin chains expressed in human, rat and bovine brain including α1A-, α1B-, α1C- and α4A-tubulin[20], but not in α8-tubulin whose sequence is divergent and lacks Lys-40. In this study, the advantages of pepsin over other enzymes include: 1) Pepsin is an aspartic acid protease, and its digestive activity is not affected by common protease inhibitors supplemented in the lysis buffer, including serine protease inhibitors, cysteine protease inhibitors and metalloprotease inhibitors; 2) The sequence contains Cys and Met which are prone to oxidation, and the oxidation is accelerated at

m/z	Charge	Peak mW	Peptide mw	Delta (Da)	Delta (ppm)	Log likelihood	Sequence	Modification	RT (min)
923.131	3	2766.369	2766.190	0.179	64.870	52.315	Y24CLEHGIQPDGQMPSDKTIGGGDDSF49		26.93
1405.213	2	2808.410	2808.200	0.210	74.680	28.776	Y24CLEHGIQPDGQMPSDKTIGGGDDSF49	Acetyl K40	28.80
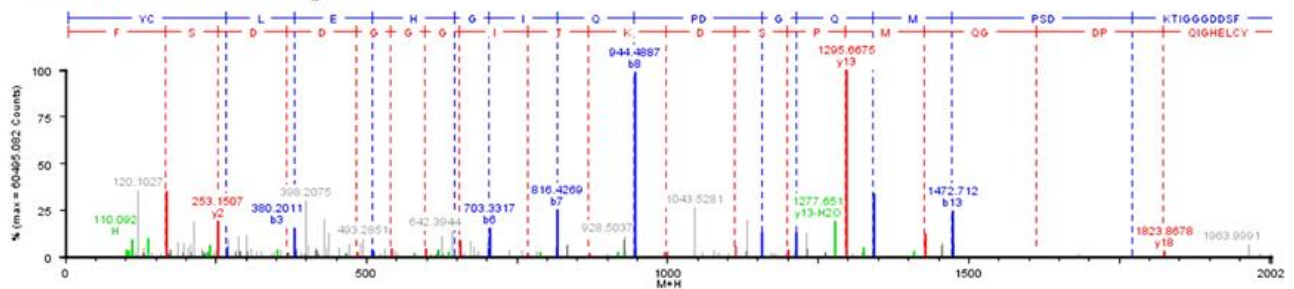
Figure 1. Identification of the peptides containing Lys-40 (Lys-40 peptide, m/z 923.131) and acetylated Lys-40 (surrogate peptide, m/z 1405.213) by ProteinLynx Global Server (PLGS) 2.4.

an alkaline pH, therefore the acidic pH of the peptic digestion prevents the degradation of the peptide; 3) Pepsin demonstrated a high efficiency and reproducibility for the generation of a peptide containing Lys-40. Assuming the ratio of α-tubulin to β-tubulin is 1:1 in purified bovine tubulin, and α8-tubulin and other tubulin isotypes are negligible in the brain[21], pepsin digest efficiency was calculated with ratios of peak areas for the Lys-40 peptide, between the synthetic source and the pepsin digest of 1, 10 and 100 μg/mL total bovine tubulin diluted with 1 mg/mL lysozyme. The digestion efficiency was close to 50% across all tested concentrations (Table 1).

Table 1. Pepsin digestion efficiency (%, n = 3) for the generation of the Lys-40 peptide (YCLEHGIQPDGQMPSDKTIGGGDDSF).

	1 µg/mL	10 µg/mL	100 µg/mL
Digest Efficiency	45.4 ±1.9	53.2 ±5.2	48.9 ±2.4

3.2 Method Development

Immunoprecipitation was tested with two commercially available antibodies for Lys-40 acetylated α-tubulin: mouse mAb 6-11B-1 and rabbit mAb D20G3. The epitope for 6-11B-1 is located on the α3 isoform of Chlamydomonas axonemal α-tubulin, within four residues of acetylated Lys-40[22,23], but the epitope for D20G3 is unreported. The affinity of these two antibodies with protein A and G magnetic beads were tested, by measuring the recovery of the synthetic surrogate peptide from bovine serum albumin in PBS-T. 6-11B-1 mouse mAb and protein G allowed the highest recovery of the acetylated tubulin peptide and were selected for immunoprecipitation.

Table 2. Comparison of the recovery[a] of 36 pmol acetylated peptide from 100 µL of 1 mg/mL bovine serum albumin in PBS-T.

	Protein A		Protein G	
6-11B-1	42%	44%	47%	51%
D20G3	20%	21%	19%	17%

[a] Recovery (%) was calculated according to the following formula: (peak area measured after IP/peak area measured before IP) $\times 100\%$.

The immunoprecipitation protocol was adapted for mass spectrometry analysis. The last washing buffer (PBS buffer) was replaced with 50 mM ammonium acetate (pH 7.0) and the elution buffer (100mM glycine-HCl, pH 2.0) was replaced with 100 mM glycine-TFA (pH 2.0), and did not affect the recovery of the immunoprecipitation. Multiple elution up to three volumes was tested and didn't increase the recovery, either (data not shown). The final optimized protocol is shown in Figure 2.
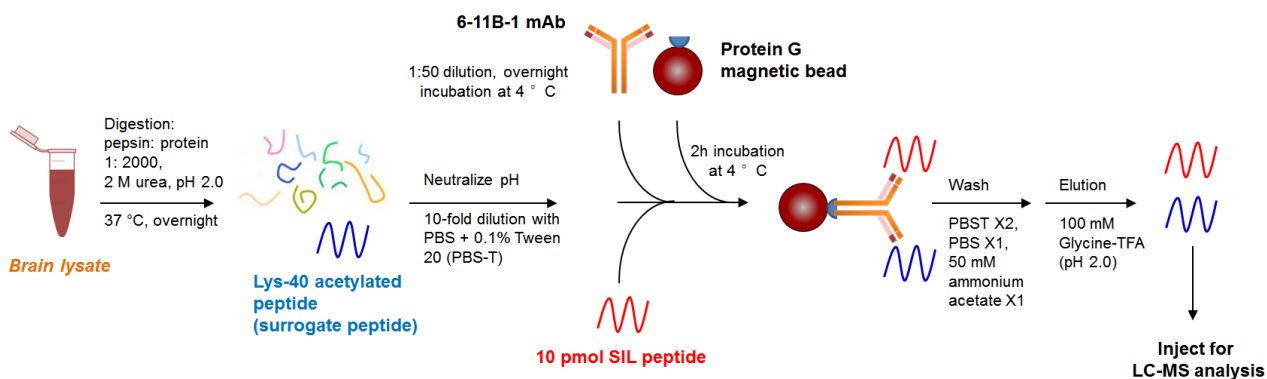
Figure 2. The workflow for the immunoprecipitation of Lys-40 acetylated peptide (surrogate peptide).

3.3 Method Validation

The method was validated with selectivity, linearity, precision and accuracy. Selectivity (n = 3) was validated by analyzing blank samples and spiked samples (1 pmol/mg surrogate peptide and SIL peptide), and chromatograms were compared (Figure 3). No significant interferences from blank matrices were observed, demonstrating that the sample preparation and LC-MS method has the necessary selectivity to differentiate and quantitate analytes in the brain

tissue lysate. LLOQ of the method was determined as 1 pmol/mg brain tissue, with a signal-to-noise (S/N) of 10.
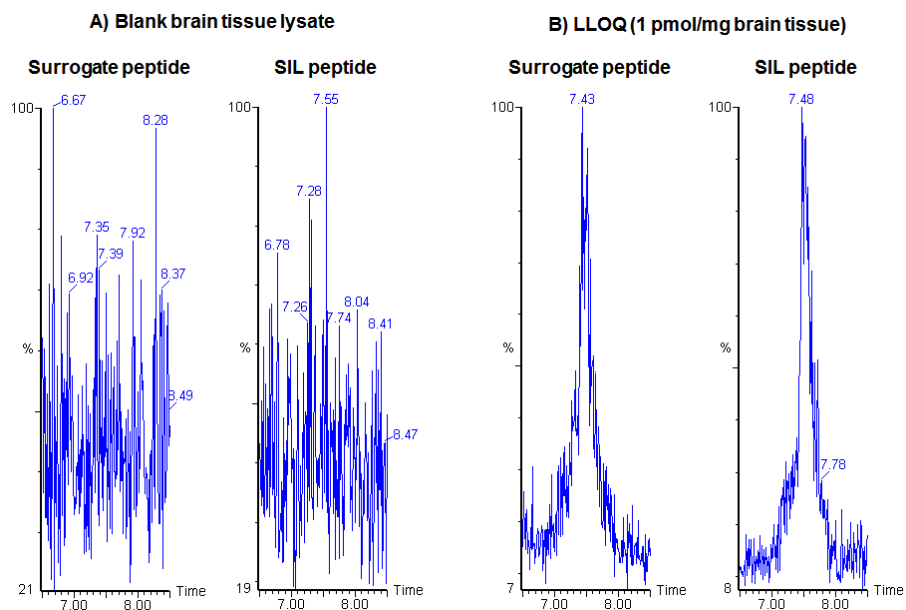
Figure 3. Representative chromatograms of the surrogate and SIL peptide in the blank brain tissue lysate depleted with acetylated tubulin (A), and brain tissue lysate with 1 pmol surrogate and SIL peptide/mg brain tissue (B). Retention times for analytes are shown in minutes.

The linearity was tested over the range of 1.0-100 pmol/mg brain tissue. A calibration curve was made from peak areas of surrogate peptide/SIL peptide, using 1/x weighted linear regressions. The calibration curve, slope, intercept and R^2 value are shown in Figure 4. The method allows
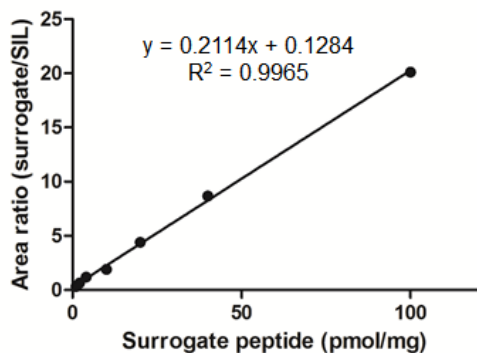
Figure 4. Calibration curve for the surrogate peptide ranging from 1 to 100 pmol/mg brain tissue.

for good linearity ($R^2 > 0.99$) within the tested range and the intercept on the y-axis was close to 0, therefore, we use the formula to calculate the concentration of acetylated tubulin in the brain tissue:

Protein conc (pmol/mg) = SIL amount (pmol) × Response ratio × (1/Digestion efficiency) / 2 mg

Response ratio = Peak area $_{PTM\ peptide}$/Peak area $_{SIL\ peptid}$, SIL amount (pmol) = 10 pmol

The precision and accuracy (n = 3) for acetylated alpha tubulin were tested at 3.0, 30.0 and 75 pmol/mg brain tissue. Precision describes the closeness of a series of measurements from multiple samplings, and was represented by relative standard deviation (RSD); accuracy describes the closeness of measured value to the true value, and was represented by relative error (RE). Table 3 shows the measurement of each QC sample, and the average, RSD and RE values for each group. RSD and RE are all below 15% within each QC group and meet the requirements from the Guidance for Industry (Bioanalytical Method Validation) by the US FDA.

Table 3. The precision (RSD) and accuracy (RE) of the analytical method used to quantitate tubulin acetylation from brain tissue lysate.

	QC Low			QC Middle			QC High		
	3 pmol/mg			30 pmol/mg			75 pmol/mg		
Measured (pmol/mg)	2.5	3.3	2.4	23.7	33.5	29.2	80.4	72.7	73.2
AVG[a]	2.7 ±0.4			28.8 ±4.0			75.4 ±3.5		
RE[b]	-12.0%			-4.0%			0.5%		
RSD[c]	14.8%			13.9%			4.6%		

AVG: average, RE: relative error, RSD: relative standard deviation.

3.4 Application

Chronic exposure to organophosphate insecticides was observed to lead to impairments in cognition and axonal transport, independent of acetylcholinesterase inhibition[24,25,26]. The underlying mechanisms for its neurotoxicity and the target proteins, are still unclear. Considering the importance of Lys-40 acetylation in the nervous system, it is important to have a specific and selective method to absolutely quantitate this key PTM in brain tissue as a biomarker, to establish its association with organophosphate exposure conditions including dose, route of administration and duration of time, as well as with cognition defects and alterations in axonal transport.

The validated method was applied to analyze brain tissue collected from rats (n = 3) orally dosed with chlorpyrifos (18 mg/kg/every other day) in peanut oil for 30 days with a 45 day washout period. Brain tissue lysate from each rat was prepared and analyzed, and the concentration was calculated with the formula above. The average concentration within each

group was calculated and a student t-test was conducted to compare the difference between control and the chlorpyrifos treatment group. α-tubulin acetylation at Lys-40 was inhibited significantly ($P = 0.0198 < 0.05$) by 55.2 % after exposure to chlorpyrifos (Table 4). Organophosphates (OPs) have been demonstrated to covalently modify a wide variety of proteins, and organophosphorylation has been identified on multiple amino acid residues on tubulin, including Try and Lys [27,28]. The inhibition of tubulin acetylation may result from these covalent modifications, through steric effects for acetylation from inside[9], disruption of tubulin polymerization[29], changes in intermolecular forces or covalent modification in the PTM site.

Table 4. The concentration of Lys-40 acetylated α-tubulin in the rat brain tissue obtained from rats in the control and chlorpyrifos treatment group (n = 3).

	Control	Chlorpyrifos treatment
Lys-40 acetylated α-tubulin	33.5 ±6.6	15.0 ±1.9

4. Conclusion

Pepsin digestion allowed for the first-time mass spectrometry-based identification of a surrogate peptide for Lys-40 acetylated α-tubulin. An immunoprecipitation-mass spectrometry assay was developed for the first time to quantitate this key PTM in rat brain tissue, and only a small amount of tissue (2 mg) was required. The method was validated with selectivity, specificity, accuracy and linearity within the range of 1-100 pmol/mg brain tissue. An analytical method for this potential cognition relevant biomarker should facilitate studies of neurodegenerative diseases and neurotoxicity, including the evaluation of pathological

progression, the investigation of the mechanisms of actions, and the observation of therapeutic effects.

References:

1. Turk E, Wills AA, Kwon T, Sedzinski J, Wallingford JB, Stearns T. Zeta-Tubulin Is a Member of a Conserved Tubulin Module and Is a Component of the Centriolar Basal Foot in Multiciliated Cells. Curr. Biol. 2015;25(16):2177-2183.

2 . Mitchison T, Kirschner M. Dynamic Instability of Microtubule Growth. Nature. 1984;312(5991):237-242.

3. Palazzo A, Ackerman B, Gundersen GG. Cell biology - Tubulin acetylation and cell motility. Nature. 2003;421(6920):230-230.

4. Kreitzer G, Liao GJ, Gundersen GG. Detyrosination of tubulin regulates the interaction of intermediate filaments with microtubules in vivo via a kinesin-dependent mechanism. Mol. Biol. Cell. 1999;10(4):1105-1118.

5. Paturlelafanechere L, Edde B, Denoulet P, et al. CHARACTERIZATION OF A MAJOR BRAIN TUBULIN VARIANT WHICH CANNOT BE TYROSINATED. Biochemistry. 1991;30(43):10523-10528.

6. van Dijk J, Rogowski K, Miro J, Lacroix B, Edde B, Janke C. A targeted multienzyme mechanism for selective microtubule polyglutamylation. Mol. Cell. 2007;26(3):437-448.

7. Redeker V, Levilliers N, Schmitter JM, et al. POLYGLYCYLATION OF TUBULIN - A POSTTRANSLATIONAL MODIFICATION IN AXONEMAL MICROTUBULES. Science. 1994;266(5191):1688-1691.

8. Hammond JW, Cai DW, Verhey KJ. Tubulin modifications and their cellular functions. Curr. Opin. Cell Biol. 2008;20(1):71-76.

9. Al-Bassam J, Corbett KD. alpha-Tubulin acetylation from the inside out. Proc. Natl. Acad. Sci. U. S. A. 2012;109(48):19515-19516.

10. Castro-Castro A, Janke C, Montagnac G, Paul-Gilloteaux P, Chavrier P. ATAT1/MEC-17 acetyltransferase and HDAC6 deacetylase control a balance of acetylation of alpha-tubulin and cortactin and regulate MT1-MMP trafficking and breast tumor cell invasion. Eur. J. Cell Biol. 2012;91(11-12):950-960.

11. Reed NA, Cai DW, Blasius TL, et al. Microtubule acetylation promotes kinesin-1 binding and transport. Curr. Biol. 2006;16(21):2166-2172

12. Dompierre JP, Godin JD, Charrin BC, et al. Histone deacetylase 6 inhibition compensates for the transport deficit in Huntington's disease by increasing tubulin acetylation. J. Neurosci. 2007;27(13):3571-3583.

13. Outeiro TF, Kontopoulos E, Altmann SM, et al. Sirtuin 2 inhibitors rescue alpha-synuclein-mediated toxicity in models of Parkinson's disease. Science. 2007;317(5837):516-519.

14. Rao AN, Patil A, Brodnik ZD, et al. Pharmacologically increasing microtubule acetylation corrects stress-exacerbated effects of organophosphates on neurons. Traffic. 2017;18(7):433-441.

15. Avdoshina V, Caragher SP, Wenzel ED, Taraballi F, Mocchetti I, Harry GJ. The viral protein gp120 decreases the acetylation of neuronal tubulin: potential mechanism of neurotoxicity. J. Neurochem. 2017;141(4):606-613.

16. Chesta ME, Carbajal A, Bisig CG, Arce CA. Quantification of acetylated tubulin. Cytoskeleton. 2013;70(6):297-303.

17. Reddy ND, Shoja MH, Biswas S, Nayak PG, Kumar N, Rao CM. An appraisal of cinnamyl sulfonamide hydroxamate derivatives (HDAC inhibitors) for anti-cancer, anti-angiogenic and anti-metastatic activities in human cancer cells. Chem.-Biol. Interact. 2016;253:112-124.

18. Han Z, Chou C-W, Yang X, Bartlett MG, Zheng YG. Profiling Cellular Substrates of Lysine Acetyltransferases GCN5 and p300 with Orthogonal Labeling and Click Chemistry. ACS

chemical biology. 2017.

19 . Becker J, Hoofnagle AN. Replacing immunoassays with tryptic digestion-peptide immunoaffinity enrichment and LC-MS/MS. Bioanalysis. 2012;4(3):281-290.

20. Fukushima N, Furuta D, Hidaka Y, Moriyama R, Tsujiuchi T. Post-translational modifications of tubulin in the nervous system. J. Neurochem. 2009;109(3):683-693.

21. Braun A, Breuss M, Salzer MC, Flint J, Cowan NJ, Keays DA. Tuba8 Is Expressed at Low Levels in the Developing Mouse and Human Brain. Am. J. Hum. Genet. 2010;86(5):819-822.

22 . Ledizet M, Piperno G. IDENTIFICATION OF AN ACETYLATION SITE OF CHLAMYDOMONAS ALPHA-TUBULIN. Proc. Natl. Acad. Sci. U. S. A. 1987;84(16):5720-5724.

23 . Piperno G, Fuller MT. MONOCLONAL-ANTIBODIES SPECIFIC FOR AN ACETYLATED FORM OF ALPHA-TUBULIN RECOGNIZE THE ANTIGEN IN CILIA AND FLAGELLA FROM A VARIETY OF ORGANISMS. J. Cell Biol. 1985;101(6):2085-2094.

24. Hernandez CM, Beck WD, Naughton SX, et al. Repeated exposure to chlorpyrifos leads to prolonged impairments of axonal transport in the living rodent brain. Neurotoxicology. 2015;47:17-26.

25 . Gao J, Naughton SX, Beck WD, et al. Chlorpyrifos and chlorpyrifos oxon impair the transport of membrane bound organelles in rat cortical axons. Neurotoxicology. 2017.

26. Yang XK, Bartlett MG. Identification of protein adduction using mass spectrometry: Protein adducts as biomarkers and predictors of toxicity mechanisms. Rapid Commun. Mass Spectrom. 2016;30(5):652-664.

27. Grigoryan H, Li B, Xue WH, Grigoryan M, Schopfer LM, Lockridge O. Mass spectral characterization of organophosphate-labeled lysine in peptides. Anal. Biochem. 2009;394(1):92-

100.

28 . Grigoryan H, Schopfer LM, Peeples ES, et al. Mass spectrometry identifies multiple organophosphorylated sites on tubulin. Toxicol. Appl. Pharmacol. 2009;240(2):149-158.

29 . Grigoryan H, Lockridge O. Nanoimages show disruption of tubulin polymerization by chlorpyrifos oxon: Implications for neurotoxicity. Toxicol. Appl. Pharmacol. 2009;240(2):143-148.

CHAPTER 5

DEVELOPMENT OF A METHOD FOR THE DETERMINATION OF ACYL-COA

COMPOUNDS BY LIQUID CHROMATOGRAPHY MASS SPECTROMETRY TO PROBE

THE METABOLISM OF FATTY ACIDS

Abstract

Acyl-Coenzyme As (acyl-CoAs) are a group of activated fatty acid molecules participating in multiple cellular processes including lipid synthesis, oxidative metabolism of fatty acids to produce ATP, transcriptional regulation and protein post-translational modification. Quantification of cellular acyl-CoAs is challenging due to their instability in aqueous solutions and lack of blank matrices. Here we demonstrate an LC-MS/MS analytical method which allows for absolute quantitation with broad coverage of cellular acyl-CoAs. This assay was applied to profile endogenous acyl-CoAs under the challenge of a variety of dietary fatty acids in prostate and hepatic cells. Additionally, this approach allowed for detection of multiple fatty acid metabolic processes including the biogenesis of acyl-CoAs, and their elongation, degradation, and desaturation. Hierarchical clustering in the remodeling of acyl-CoA profiles revealed a fatty acid-specific pattern across all tested cell lines, which provides a valuable reference for making predictions in other cell models. Individual acyl-CoAs were identified which were altered differentially by exogenous fatty acids in divergent tumorigenicity states of cells. These findings demonstrate the power of acyl-CoA profiling toward understanding the mechanisms for the progression of tumors or other diseases in response to fatty acids.

Key words

Long-chain acyl-CoAs, fatty acids, metabolism, quantitation, remodeling, LC-MS/MS, cancer and tumorigenicity.

1. Introduction

Fatty acids play critical roles in the malignancy of cancer cells, including generating cellular building blocks for proliferation, regulating membrane structures for coordination of signal transduction and motility (e.g. lipid rafts)[1], and synthesizing a variety of protumorigenic signaling molecules. A high-fat diet is a contributing factor in multiple types of cancer due to its central role in obesity[1,2].The major composition of dietary fats, ranging from vegetable to animal fats, are long-chain fatty acids with chain lengths ranging from C13 to C21 (Table 1). In addition to exogenous sources, levels of cellular fatty acids are also susceptible to metabolic abnormalities during cancer pathogenesis. For example, the elevation of monoacylglycerol lipase (MAGL) in aggressive cancers can increase the levels of free fatty acids in cancer cells[3]. The current evidence to support this hypothesis was summarized in a review supporting limiting fatty acid availability as a therapeutic strategy to control cancer cell proliferation[3].

Table 1. Common dietary fatty acids and corresponding acyl-CoAs

Fatty acids	Corresponding acyl-CoA
Decanoic acid, C10:0	Decanoyl CoA, C10:0 CoA
Lauric acid, C12:0	Lauroyl CoA, C12:0 CoA
Myristic acid, C14:0	Myristoyl CoA, C14:0 CoA
Palmitic acid, C16:0	Palmitoyl CoA, C16:0 CoA
Stearic acid, C18:0	Stearoyl CoA, C18:0 CoA
Oleic acid, *cis*-9-C18:1	Oleoyl CoA, *cis*-9-C18:1 CoA
Elaidic acid, *trans*-9-C18:1	Elaidoyl CoA, *trans*-9-C18:1 CoA
Arachidic acid, C20:0	Arachidoyl CoA, C20:0 CoA

Exogenous and endogenous fatty acids require the formation of fatty acyl-coenzyme As (acyl-CoAs) before entry into bioactive lipid networks and participation in various metabolic pathways. Long-chain fatty acids are activated into acyl-CoAs by one of 13 acyl-CoA synthetase

(ACS) isoforms, and are preferred substrates of long-chain acyl CoA synthetases (ACSL) including ACSL 1, 3, 4, 5 and 6. Acyl-CoAs are key transcriptional ligands and regulate critical cellular processes by complex lipid synthesis and post-translational modification of proteins (acylation)[4]. The involvement of various long-chain acyl-CoAs in the development of cancer is increasingly appreciated. For example, myristoyl CoA modifies and activates a variety of oncogenic tyrosine kinases including the Src kinase family, and myristoylation of c-Src is increased in a number of human cancers, in conjunction with an upregulation of N-myristoyltransferase (NMT)[5], Palmitoylation regulates a wide range of cancer-associated proteins involved with sustained proliferative signaling[6,7] ,resistance to cell death[8], invasion and metastasis[9], angiogenesis[10], and induction of inflammation[11].

Considering the important roles of acyl-CoAs and related enzymes in physiological and pathological pathways, especially in cancer, it's necessary to have an analytical method to profile acyl-CoAs in cells. In addition, to elucidate how a high-fat diet or enzyme abnormality-induced elevation of fatty acids correlates with tumorigenesis and progression, it would be meaningful to make a comprehensive assessment of alterations to the acyl-CoA profile following stress from the addition of different fatty acids. Given enzymatic activities including acyl-CoA synthesis, degradation and elongation, we reasoned that remodeling of the acyl-CoA profile would occur under such conditions. High performance liquid chromatography tandem mass spectrometry (LC-MS/MS) proved to be a reliable analytical technology for determining acyl-CoAs. Considerable efforts have been devoted to develop LC-MS/MS methods for acyl-CoAs profiling in bacteria[12], cancer cells[13,14], and animal tissues[14,15]. However, most methods only determined relative levels of acyl-CoAs, and there is no method aimed at absolute determination of long-chain acyl-CoAs. More noteworthy, until now, there are no quantitative data reporting

the alterations of acyl-CoAs in the presence of fatty acids, or a comparison of acyl-CoA synthesis between normal and cancer cells.

In this paper, we therefore established a new method, with protein precipitation for sample preparation, reversed phase chromatography for separation, followed by multiple reaction monitoring (MRM) mass spectrometry to simultaneously quantitate a variety of acyl-CoAs converted from dietary fatty acids in mammalian cells. Hepatic cells are the major element in the liver for fatty acid metabolism. Additionally, increasing evidence suggests an association of dietary fatty acids with prostate cancer initiation and progression[16,17,18,19].This analytical approach reveals a signature of these cells in multiple fatty acid metabolic processes in addition to metabolic modification after tumorigenic alteration.

2. Experimental procedures

2.1 Reagents and Materials

Various acyl coenzyme As, ammonium salts (acyl-CoAs), including C10:0 CoA, C12:0 CoA, C14:0 CoA, C15:0 CoA, C16:0 CoA, C18:0 CoA, C18:1 (n9) CoA, C18:2 (n6) CoA, C18:3 (n3) CoA, C20:0 CoA, C20:4 CoA, were purchased from Avanti Polar Lipids (Alabaster, AL). Ammonium acetate, LC-MS grade acetonitrile, methanol and water were purchased from Sigma–Aldrich (St. Louis, MO).

2.2 Instrumentation

An Agilent 1100 binary pump HPLC system (Santa Clara, CA) interfaced to a Waters Micromass Quattro Micro triple quadrupole mass spectrometer with an ESI source (Milford, MA) was operated for LC–MS/MS analysis. Masslynx 4.0 software by Waters (Beverly, MA) was applied for data processing. A Labconco CentriVap Complete Vacuum Concentrator (Kansas City, MO) was used to evaporate samples.

2.3 LC-MS/MS conditions

A Luna® C18(2) 100 Å LC column (100 $\times$ 2 mm, 3 μm) coupled with a Phenomenex SecurityGuard C-18 guard column (4.0 mm $\times$ 2.0 mm) was used to separate the analytes. The column temperature was controlled at 32 ℃. The mobile phase A was 10 mM ammonium acetate (pH 6.8), and mobile phase B was acetonitrile. The injection volume was 30 μL. Analytes were separated using a gradient method, with a 0.2 mL/min flow rate, (time/minute, % mobile phase B): (0, 20), (15, 100), (22.5, 100), (22.51, 20), and the run time for each injection was 30 min. The LC system was interfaced by a six-port divert valve to the mass spectrometer, introducing eluates from 1 to 15 min to the ion source. The autosampler injection needle was washed with methanol after each injection. Samples were analyzed by the mass spectrometer in positive ion ESI mode. MS parameters were optimized by direct infusion of 5 μM acyl-CoAs dissolved in 50% acetonitrile at 30 μL/min into the instrument. The capillary voltage was 3.20 kV, the cone voltage was 45 V, the extractor voltage was 0 and RF lens voltage was 3.0 V. Nitrogen was used as the desolvation gas at a flow rate of 500 L/h. The desolvation temperature was 500 ℃ and the source temperature was 120 ℃. Argon was used as the collision gas, the collision cell pressure was 3.5 $\times$ 10^{-3} mbar. A multiple reaction monitoring (MRM) function was applied for the simultaneous detection of all analytes. Ion transitions, retention times and collision energies for all acyl-CoAs are listed in Table 2.

Table 2. Acyl-CoAs in this analytical assay. CE: collision energy, RT: retention times, LOD: limit of detection, LOQ: limit of quantitation.

	Q1 (m/z)	Q3 (m/z)	CE (eV)	RT (min)	LOD (pmol)[a]	LOQ (pmol)[a]
C10:0 CoA	922	415	32	7.30	0.14	0.47
C12:0 CoA	950	443	36	8.26	0.11	0.35

C14:0 CoA	978	471	40	9.14	0.12	0.39
C15:0 CoA	992	485	40	9.63	0.09	0.31
C16:0 CoA	1006	499	40	10.07	0.07	0.25
C18:0 CoA	1034	527	42	11.04	0.07	0.24
C18:1 CoA	1032	525	42	10.25	0.11	0.36
C18:2 CoA	1030	523	42	9.69	0.12	0.38
C18:3 CoA	1028	521	42	9.26	0.14	0.46
C20:0 CoA	1062	555	44	12.23	0.07	0.25
C20:4 CoA	1054	547	44	9.66	0.10	0.33

a Amount in a single injection.

2.4 Cell Culture

Human prostate cell lines (PNT2 and DU145) and hepatic cell lines (HepG2 and Hep3B) were purchased from American Type Culture Collection (ATCC). Cells were maintained in a humidified incubator under 5% CO_2 at 37℃ and grown in the recommended media supplemented with 5% fetal bovine serum (FBS) and 1% penicillin/streptomycin. When cells reached ~90% confluence, bovine serum albumin (BSA)-conjugated fatty acids including decanoic acid (C10:0), lauric acid (C12:0), myristic acid (C14:0), palmitic acid (C16:0), stearic acid (C18:0), oleic acid (*cis*-9-C18:1), elaidic acid (*trans*-9-C18:1) and arachidic acid (C20:0), were individually introduced to each cell line (n = 3) at a concentration of 400 μM and incubated for 24 h.

2.5 Sample Preparation

Cell culture media were removed and the cells were washed with phosphate-buffered saline (PBS) twice, incubated with 2 mL of methanol and 15 μL of 10 μM 15:0 CoA (internal standard, ISTD) at -80 ℃ for 15 min. The cells lysate was scraped from the culture plate and centrifuged at 15000 × g at 5 ℃ for 5 min. The supernatant was transferred to a glass tube, mixed with 1 mL of acetonitrile and evaporated in a vacuum concentrator at 55 ℃ for 1.5h. The

sample was reconstituted with 150 µL of methanol, vortexed and centrifuged at 15000 × g at 5 °C for 10 min. 100 µL supernatant was transferred into an autosampler vial for LC-MS/MS analysis.

2.6 Determination of Total Cellular Protein.

Precipitated protein was solubilized using a RIPA lysis buffer containing 50 mM Tris-HCl pH 7.4, 150 mM NaCl, 5 mM EDTA, 10% glycerol, 1% Triton X-100, 0.1% SDS, 0.5% sodium deoxycholate and protease inhibitor cocktail. Protein concentration was determined using the Bio-Rad DC protein assay kit.

2.7 Determination of mRNAs for Long-chain Acyl-CoA Synthetase Isoforms.

The total RNA was isolated from different cell lines using the Qiagen RNeasy Mini Kit (Valencia, CA). 1 µg of the total RNA was used for first-strand cDNA synthesis as recommended by the manufacturer Quanta Biosciences (Beverly, MA). Real time PCR was performed using SYBR Green as an indicator on the ABI StepOne Plus Real Time PCR system. The final reaction mixture contained 10 ng of cDNA, 100 nM of each primer, 5 µL of 2×SYBR Green PCR Master Mix (from Quanta Biosciences) and RNase-free water, to complete the reaction at a volume of 12.5 µL. PCR was carried out for 40 cycles at 95 °C for 15 s and 60 °C for 1 min. Fluorescence was read during the reaction, allowing a continuous monitoring of the amount of PCR product. The data were normalized to internal control glyceralde hyde-3-phosphate dehydrogenase (GAPDH) mRNA. The sequences of primers are as shown in Table S1.

2.8 Quantitation of Acyl-CoAs in Cells.

For each cell line, calibration samples (n = 3) were prepared by mixing 2.4, 6, 12, 24, 60, 120, 240 and 600 pmol acyl-CoAs with 8×10^5 cells prior to sample preparation. 11 acyl-CoA

compounds were included in the calibration samples, and a calibration curve for each analyte was plotted using the peak area versus the amount of supplemented acyl-CoA, with 1/x weighted linear regression. Slopes (k) of the linear regression of the analyte's calibration curve and the internal standard (ISTD) calibration curve were calculated, and the ratio of slopes (R) = $k_{analyte}$ / k_{ISTD} were calculated. In a real sample spiked with 150 pmol ISTD, the amount (pmol) of an analyte was calculated when its signal-to-noise ratio > 10, using the formula:

Analyte (pmol) = 150 (pmol) × Response ratio × (1/R), where response ratio = Peak area $_{analyte}$ / Peak area $_{ISTD}$

To correct for potential differences in the cell number among samples, the analyte amount was normalized to per mg of total cellular protein, and the final unit for quantitation of acyl-CoAs in cells is pmol/mg (about 3×10^6 cells).

2.9 Statistical Analysis.

For an analyte with a signal-to-noise ratio > 10, the level is regarded as above the limit of quantitation and is included for further data analysis. Calculation of peak areas and the linear regression were performed with Masslynx 4.0 software. Data were presented as mean ± SD. Significant differences are based on a student's t-test (two tailed) with P < 0.05. Heat map and hierarchical clustering were done using the software Gene-e (Broad Institue, http://www.broadinstitute.org/cancer/software/GENE-E/download.html).

3. Results and discussion

3.1 Method development.
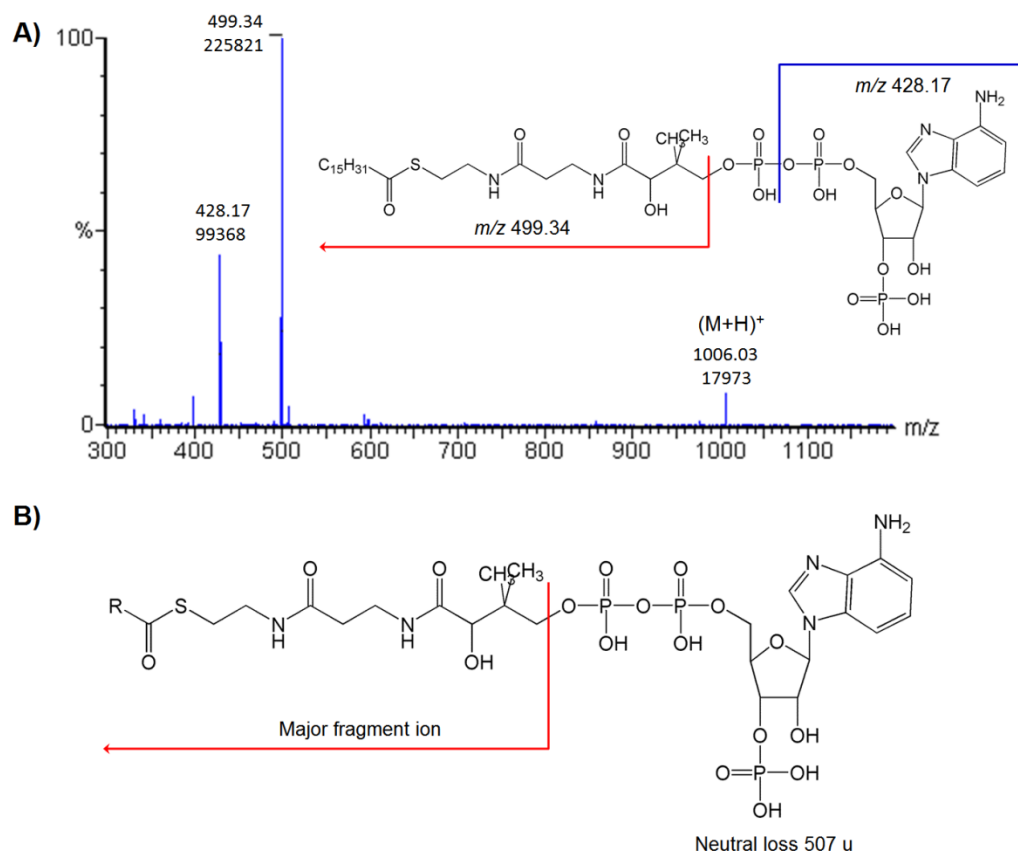
Figure 1. Fragment ions of acyl-CoAs. (A) Fragment ions of C16:0 CoA. (B) The major fragmentation mechanism for acyl-CoAs: a neutral loss of 507.

C15:0 CoA (pentadecanoyl CoA) is an odd-chain acyl-CoA undetectable in human cells. C15:0 CoA and other odd-chain acyl-CoAs have been reported to work as an ISTD for acyl-CoAs in other analytical assays.13, C15:0 CoA is selected as the ISTD for this assay because it has a median length of carbon chain among all acyl-CoAs to be determined.

The autotune mode imbedded in Masslynx 4.0 software by Waters was utilized to optimize MS parameters to increase signal response, accompanied by a direct infusion of a

standard solution containing all acyl-CoAs (5 µM in 50% acetonitrile) at 30 µL/min into the instrument. Product ion mass spectra for acyl-CoA were acquired to determine the precursor and product ion pairs to monitor. For all acyl-CoAs, the most abundant fragment ion was the one formed by a neutral loss of the phosphorylate ADP moiety (M-507) from the precursor ion (Figure 1). Ion transitions for detection of acyl-CoAs are listed in Table 2.

Various acyl-CoAs share similar physicochemical properties, allowing one sample preparation method to extract all of them. Acyl-CoAs are soluble in water and methanol. 2 mL methanol and 2 mL 80% methanol/20% water were tested to lyse cells and extract acyl-CoAs. The former was finally selected as the extraction solvent because it took 1.5 h to completely evaporate the methanol extract at 55 ℃ in the vacuum concentrator, while it took the latter 4 h under the same conditions and presented a poorer signal for analytes. This is probably because of a higher level of water in the latter extract, which likely increased during evaporation, facilitated the hydrolysis of acyl-CoAs. 1 mL of acetonitrile was mixed with the extract before evaporation, to decrease the ratio of water derived from cell lysis and to facilitate evaporation.

Acyl-CoAs are prone to hydrolysis, and are unstable in aqueous, especially alkaline and strongly acidic solutions. The stability of acyl-CoAs was tested in a series of solutions, to determine the reconstitution solution for dry samples after evaporation. Tested solutions include methanol, 50% methanol/50% 50 mM ammonium acetate (pH 7), water, 50 mM ammonium acetate (pH 7) and 50% methanol/50% 50 mM ammonium acetate (pH 3.5, adjusted with acetic acid). 500 nM acyl-CoAs in the above solutions were placed on the autosampler, and each sample was analyzed at time-zero, 4 h and 24h. The stability of each acyl-CoA was demonstrated as the percentage relative to the time-zero sample (Figure 2). Methanol was selected to reconstitute samples, because it provided the best stability for analytes over the tested periods of

time. Another interesting observation was the instability of acyl-CoAs in aqueous solutions, except for 50% methanol/50% 50 mM ammonium acetate (pH 7), which caused deterioration that increased with the length of fatty acid chain especially from 10:0 CoA to 16:0 CoA. This is possibility due to a longer fatty acid chain facilitating the hydrolysis of acyl-CoAs.
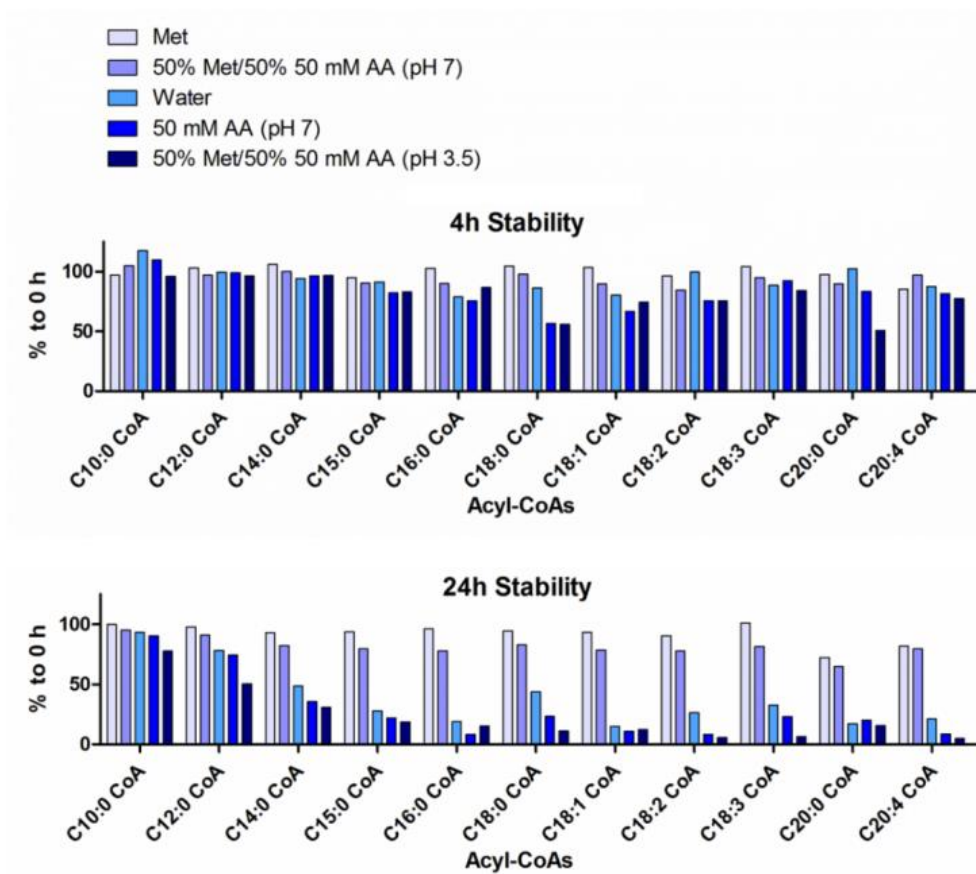
Figure 2. Stability of acyl-CoAs in solutions for reconstitution.

3.2 Separation of acyl-CoAs.

Chromatographic separation is important for analyzing acyl-CoAs when using LC-MS/MS, to reduce the competition for ionization between co-eluting analytes and other endogenous species, which would otherwise lead to serious ion suppression. A good separation

was achieved with the LC method, with little co-elution of analytes. As shown in Figure 3, 11 acyl-CoA standard compounds, 150 pmol each, was retained on the column and yielded retention times between 7 and 13 min. The retention time increases with the length of fatty acid chain of the analyte, and decreases with the number of double bonds in the fatty acid chain.
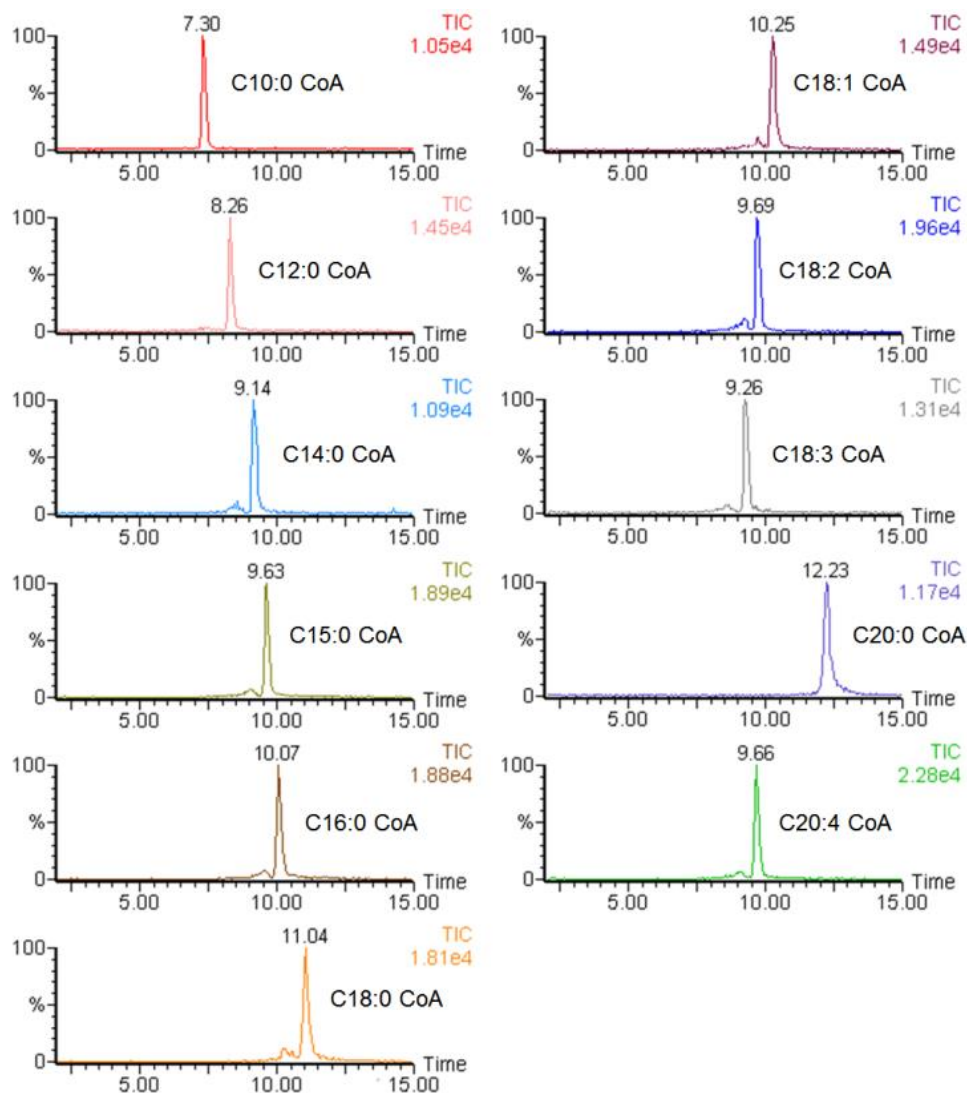
Figure 3. Extracted ion chromatograms of 150 pmol acyl-CoA standards.

3.3 Detection of acyl-CoAs in cells.

Calibration curves (n = 3) for acyl-CoAs in PNT2, DU145, HepG2 and Hep3B cell lines were prepared as described above. The coefficient of determination is over 0.98 for either analyte in either cell line, suggesting a strong linear relationship between the amount of the supplemented acyl-CoA and the response. Slopes (k) of the linear regression of the analyte's calibration curves and the ISTD calibration curve were calculated, and the ratio of slopes (R) = k analyte / k ISTD are shown in Table 3. The ratios are all between 0.6 and 1.6, but are slightly different for the same analyte in different cell lines, suggesting similar but different matrix effects from different cells.

The limit of detection (LOD) and the limit of quantitation (LOQ) are two key parameters for evaluating the sensitivity of an analytical assay. They were defined at a signal-to-noise (S/N) of 3, and at an S/N of 10, respectively. All analytes demonstrated a signal-to-noise ratio above 10 except C18:3 CoA in PNT2 and DU145 cells. The values for the ISTD were calculated from cells (n=3) spiked with 2.4 pmol 15:0 CoA standard, for a single injection (30 μL of the 150 μL final reconstituted sample) into the system. The LOD and LOQ for all analytes in each cell line were calculated using the values of the ISTD and their response ratio to the ISTD in Table 3, and the average values among tested cell lines are listed in Table 2.

3.4 Differential levels of endogenous acyl-CoA metabolites

The levels of acyl-CoAs including C10, C12, C14, C16, C18:0, C18:1, C18:2, and C18:3 CoA were higher in HepG2 cells (normal hepatic cells) than PNT2 cells (normal prostate cells) (Figure 4A and Table S2). Inter-estingly, the levels of acyl-CoAs were correlated with the mRNA levels of ACSL genes (Figure 4B and 4C), indicating a higher activity of fatty acid metabolism in hepatic cells.

Acyl-CoAs including C14, C16, C18:0 CoA and 18:1 CoA were predominant in the tested cells. The levels of these acyl-CoAs together with 12:0 CoA and 20:0 CoA were less expressed in Hep3B cells in comparison with HepG2 cells (P = 0.001, 0.001, 0.01, 0.0003, 0.0001, 0.00008, respectively), suggesting a loss of function for fatty acid metabolism in tumorigenic cells. The decreased levels of these acyl-CoAs were also correlated with the lower mRNA levels of ACSLs in Hep3B cells in comparison with HepG2 cells (Figure 4A and B). In two prostate cells lines, DU145 cells (prostate tumorigenic cells) had significantly lower levels of C12:0 CoA and C20:4 CoA (P = 0.04, 0.03, respectively), and significantly higher levels of C14:0 CoA and C16:0 CoA (P = 0.0002, 0.01, respectively) than PNT2 cells (nontumorigenic prostate cells). Collectively, the acyl-CoA profiles reflect the specificity in hepatic function and its alteration in fatty acid metabolism after tumorigenic change.

Table 3. Ratio of slopes between the analyte and the ISTD in the cell line from the calibration curve (n = 3).

	PNT2	DU145	HepG2	Hep3B
C10:0 CoA	0.66 ±0.03	0.61 ±0.00	0.69 ±0.00	0.74 ±0.03
C12:0 CoA	0.77 ±0.05	0.86 ±0.06	0.98 ±0.02	1.09 ±0.05
C14:0 CoA	1.16 ±0.07	0.64 ±0.02	0.77 ±0.01	0.70 ±0.05
C16:0 CoA	1.60 ±0.08	1.05 ±0.02	1.28 ±0.08	1.17 ±0.07
C18:0 CoA	1.45 ±0.05	1.51 ±0.07	1.01 ±0.05	1.37 ±0.14
C18:1 CoA	0.78 ±0.03	0.84 ±0.12	1.02 ±0.18	0.80 ±0.06
C18:2 CoA	0.67 ±0.02	0.84 ±0.05	0.91 ±0.03	0.92 ±0.06
C18:3 CoA	0.57 ±0.03	0.67 ±0.05	0.77 ±0.00	0.78 ±0.06
C20:0 CoA	1.48 ±0.04	1.40 ±0.11	0.98 ±0.08	1.36 ±0.06

| C20:4 CoA | 0.79 ±0.05 | 0.92 ±0.02 | 1.11 ±0.04 | 1.03 ±0.07 |

Figure 4. The Acyl-CoA levels and the mRNA expression of ACSL genes in prostate and hepatic cells. The prostate cells, PNT2 (normal prostate cells) and DU145 (prostate cancer cells), and hepatic cells, HepG2 (normal hepatic cells) and Hep3B (hepatic tumorigenic cells) were grown in the media recommended by ATCC. A) Cellular levels of acyl-CoAs measured by LC-MS/MS. "*" represents significant differences between nontumorigenic and tumorigenic cells ($P < 0.05$). B) Expression levels of ACSL1, 3, 4, 5 and 6 measured by RT-PCR. C) The spearman correlation between the level of individual acyl-CoA and the levels of each ACSL gene.
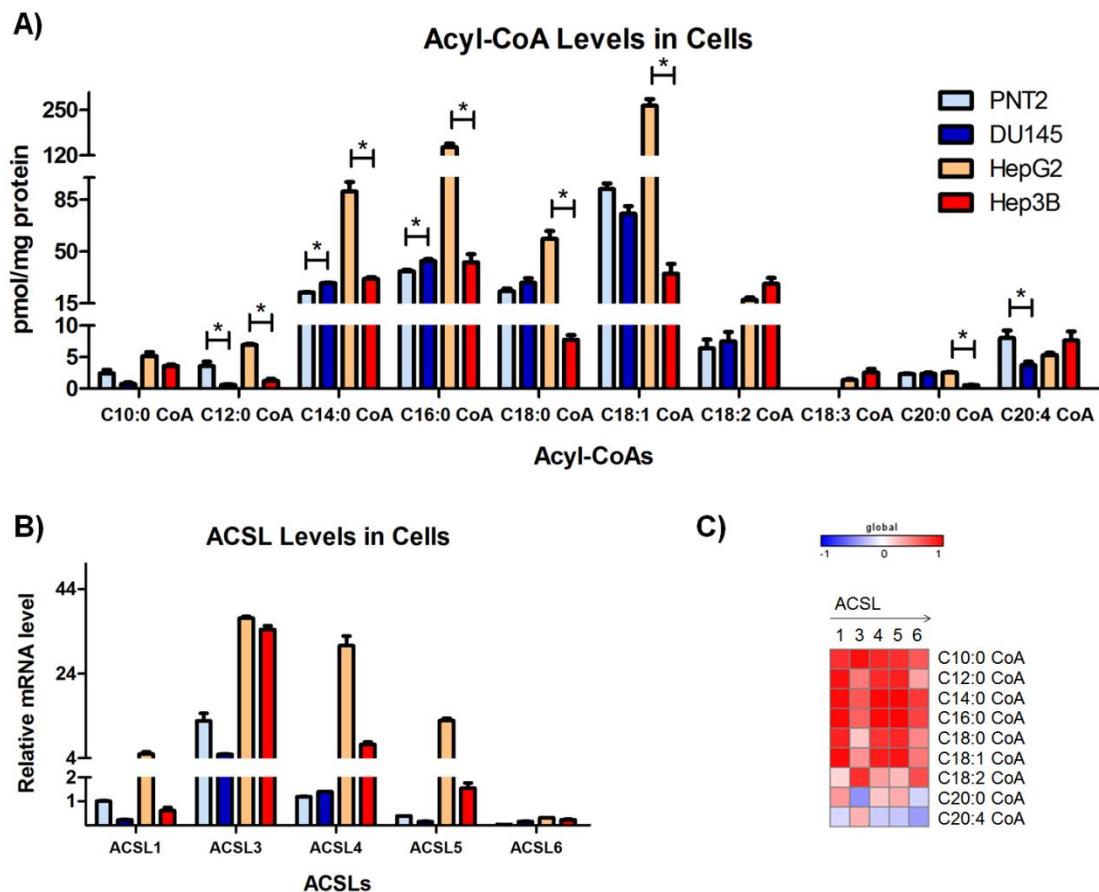
3.5 Acyl-CoA synthesis from exogenous fatty acids

The fatty acids decanoic acid (C10:0), lauric acid (C12:0), myristic acid (C14:0), palmitic acid (C16:0), stearic acid (C18:0), oleic acid (*cis*-9-C18:1), elaidic acid (*trans*-9-C18:1) and aracidic acid (C20:0) are typical dietary fatty acids in high fat diets for animals and humans. Heat maps were generated to provide a graphical representation of acyl-CoA levels, particularly to reflect deviations from baseline levels when under the stress of exogenous fatty acids (Figure 5 and Table S2). The alteration of intracellular acyl-CoAs reflected fatty acid metabolism during the biosynthesis, degradation, elongation, and desaturation of acyl-CoAs, and different metabolic rates for the C18:1 isomers.

While the heat map for each cell line was unique, some general rules are identifiable:

1) Biosynthesis of acyl-CoAs: The most noticeable elevation of an acyl-CoA always occurred after cells were treated with the fatty acid of the same length and degree of saturation, which corresponds to the process of fatty acid activation by acyl-CoA synthetases.

2) Degradation of acyl-CoAs: Treatment with an n-carbon saturated fatty acid (Cn:0) commonly resulted in a great increase of the C(n-2):0 CoA and smaller increases of other shorter acyl-CoAs, especially when n = 10~16. For example, palmitic acid (C16:0) significantly/very significantly increased the levels of C14:0 CoA, C12:0 CoA and C10:0 CoA in PNT2 cells, C14:0 CoA and C10:0 CoA in DU145 cells, C12:0 CoA in HepG2 cells, and C14:0 CoA and C12:0 CoA in Hep3B cells. The increases are possibly due to β-oxidation of the synthesized acyl-CoA inside the mitochondria, which yields an acetyl-CoA and a fatty acyl-CoA two carbons shorter after each cycle.
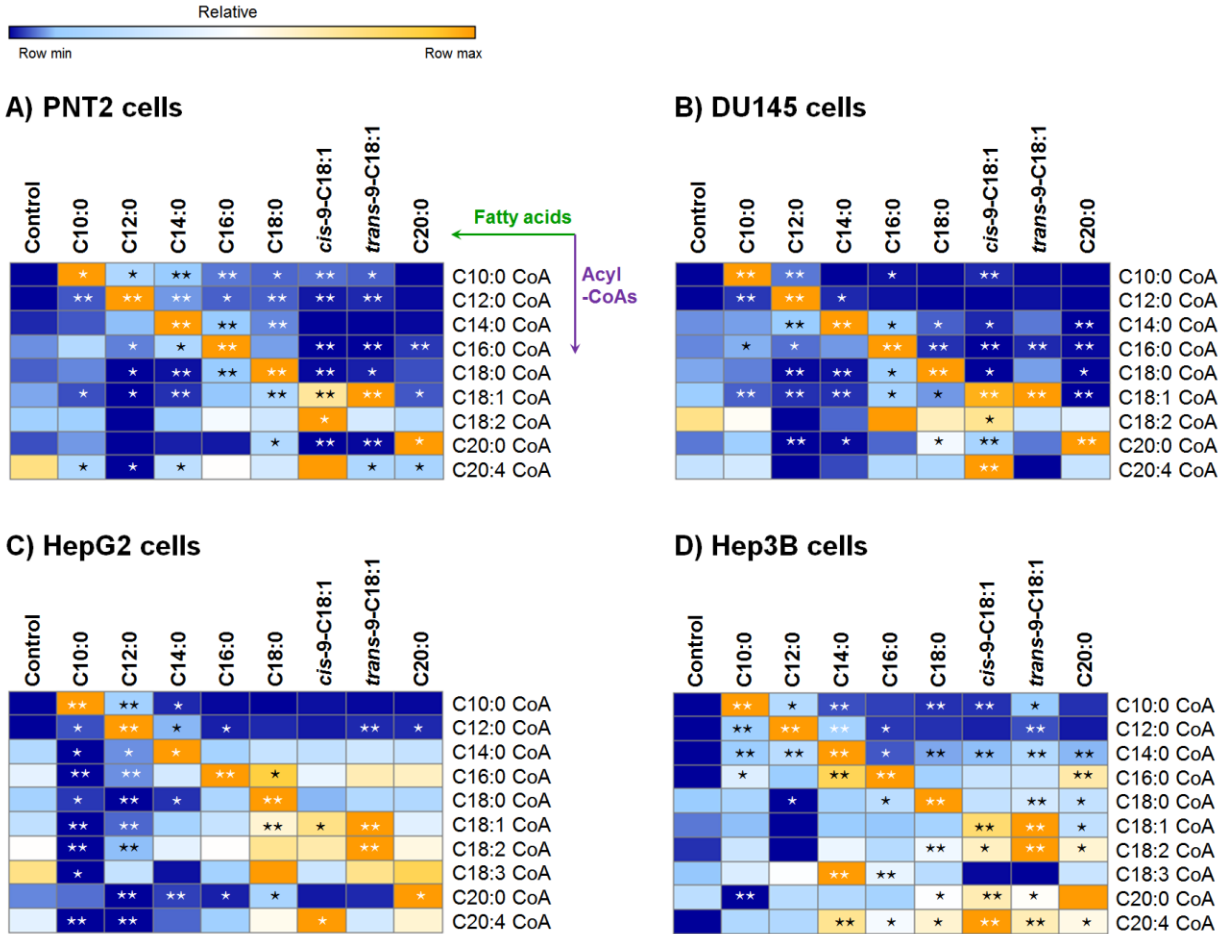
Figure 5. The acyl-CoA profile in prostate and hepatic cells. PNT2 (A), DU145 (B), HepG2 (C) and Hep3B (D) cells were cultured in media with and without 400 μM of individual fatty acids including decanoic acid (C10:0), lauric acid (C12:0), myristic acid (C14:0), palmitic acid (C16:0), stearic acid (C18:0), oleic acid (cis-9-C18:1), elaidic acid (trans-9-C18:1) and arachidic acid (C20:0) for 24 hours (n =3). Significant changes for each acyl-CoA between the control (the baseline level) and the treatment of individual fatty acid in respective group were labeled. ★: $p < 0.05$, ★★: $p < 0.01$.

3) Elongation of acyl-CoAs: Likewise, treatment with an Cn:0 resulted in increases of the C(n+2):0 CoA in most cell lines. For example, treatment of C10:0 significantly increased the

levels of C12:0 CoA in all cell lines; C12:0 increased C14:0 CoA in DU145, HepG2, and Hep3B cells; and C16:0 increased C18:0 CoA in PNT2, DU145, and Hep3B cells. The increase of C18:0 CoA in the presence of C16:0 is a reflection of fatty acid elongation in the endoplasmic reticulum, catalyzed by the very long chain fatty acid synthase complex, where C16:0 CoA is the substrate[20]. Increases of shorter acyl-CoAs can be mediated by the fatty acid synthase complex in the cytoplasm, through the addition of two carbons from malonyl-CoA. This process is initiated by the sequential transfer of an acyl-CoA to the acyltransferase domain, to an acyl carrier protein (ACP) domain, and finally to the β-ketoacyl synthase domain. Multiple enzymes involved in fatty acid synthesis have broad specificity which ensures efficient elongation all the way up to C16:0 CoA[21,22].

4) Competitive inhibition of ACSL: Decreases of C(n+m):0 CoA (m > 2) after the treatment with Cn:0 were also observed, such as significant decreases of C18:0 CoA in almost all cell lines following the metabolism of lauric acid (C12:0) and myristic acid (C14:0). The observation can be interpreted as the exogenous fatty acid inhibiting the synthesis of other acyl-CoAs from endogenous fatty acids, by competing for the same binding site on ACSLs. In addition, the decreases were frequently observed in Hep G2 cells, including C14:0 CoA and C16:0 CoA in the the presence of lauric acid (C12:0). This might be due to the higher abundance of ACSLs in HepG2 cells, which the ACSL-mediated bio-synthesis is more active for the generation of acyl-CoAs (Figure 4B). The decreases observed for C(n+m):0 CoA (m > 2) in cells cultured with Cn:0, suggest that the contribution from elongation would decline after multiple cycles, therefore being insufficient to offset other factors which may decrease C(n+m):0 CoA.

5) Desaturation of acyl-CoAs: C18:1 CoA and C18:2 CoA were significantly increased in some cells cultured with C18:0, cis-9-C18:1 or trans-9-C18:1. The desaturation process can be

mediated either by fatty acid desaturases, a major pathway for unsaturated fatty acid synthesis. , or by acyl-CoA dehydrogenase, which catalyzes the dehydrogenation process of acyl-CoAs in fatty acid β-oxidation.

6) Different metabolic rates for C18:1 fatty acid isomers: The metabolism of *trans*-9-C18:1 was similar to *cis*-9-C18:1 in terms of intracellular alterations of acyl-CoAs, however the levels of C18:1 CoA were slightly higher in the presence of *trans*-9-C18:1 than *cis*-9-C18:1. The difference is in agreement with previous reports indicating a slower degradation of *trans*-9-C18:1 CoA than *cis*-9-C18:1 CoA in rat heart mitochondria[23]. Trans-unsaturated fatty acids mainly originate from the food industry. It was reported that the degradation of the *trans*-fatty acid (elaidic acid, *trans*-9-C18:1) was effective but compromised when compared to its *cis* isomer (oleic acid, *cis*-9-C18:1) or its saturated form (stearic acid, C18:0), because the β-oxidation intermediate 5-*trans*-tetradecenoyl-CoA (*trans*-5-C14:1CoA) is a poorer substrate for long-chain acyl-CoA dehydrogenase (LCAD)[24]. As a result, the difference could lead to alterations in its accumulation, hydrolysis and conversion into an acylcarnitine, and subsequently a deviation from the metabolic process in the mitochondria[24].

Next, exogenous *cis*-9-C18:1 led to higher levels of C10:0 CoA than *trans*-9-C18:1. The increases could be explained by the β-oxidation process. Because of the location of the double bond, after three cycles of β-oxidation, elaidoyl CoA and oleoyl CoA would respectively generate *trans*-Δ^3-dodecenoyl-CoA and *cis*-Δ^3-dodecenoyl-CoA, which can be catalyzed by enoyl CoA isomerase to *trans*-Δ^2-dodecenoyl-CoA, a substrate of β-oxidation and subsequently be degraded to C10:0 CoA[25,26]. Additionally, the increase of C12:0 CoA was possibly due to elongation from C10:0 CoA, and changes of C14:0 CoA, 16:0 CoA and 18:0 CoA resulted from a mixture of competition for ACSLs (decreases) and elongation from 10:0 CoA (increases).

**3.6 Unique signature of individual fatty acid metabolism**

To analyze if the metabolism of individual fatty acids has a metabolic signature, hierarchical clustering on the levels of acyl-CoA metabolites was applied to the tested cell lines under the stress of a variety of fatty acids. The analysis was conducted based on the log ratio values due to a wide range of acyl-CoA abundance (0.5 pmol/mg ~ over 500 pmol/mg) in different cell lines and treatments. Clearly, cells cultured with the same saturated fatty acid were clustered despite the difference of cell types (Figure 6A), demonstrating that the metabolism of individual fatty acids has its signature from remodeling the intracellular acyl-CoA profile. This finding allows for a prediction on the alterations of the acyl-CoA profiles in other cells under the stress of the same saturated fatty acids. In addition, C18:1 *trans* and *cis* fatty acid isomers were clustered together (except *cis*-9-C18:1 in DU145 cells), demonstrating a similar impact on acyl-CoA remodeling from C18:1 isomers. Conversely, a different remodeling by *cis*-9-C18:1 in DU145 cells suggested a distinct alteration of the metabolic pathways for this unsaturated fatty acid in this prostate cell line.

3.7 Tumorigenesis-associated fatty acid metabolism

To discover tumorigenesis-associated abnormalities in acyl-CoA synthesis and metabolism, we merged the changes (log ratio) of acyl-CoAs in tumorigenic and nontumorigenic cells from the cell type. Hierarchical clustering was performed to cluster cellular acyl-CoAs with similar changes under a panel of fatty acids (Fig 6 B and C). This analysis revealed four groups (A1, A2, B1 and B2) in prostate cells, and four groups (C, D1, D2 and D3) in hepatic cells. The same length acyl-CoAs were clustered in the same group, despite the disparity in tumorigenecity, such as C10:0 CoA, C12:0 CoA, C14:0 CoA, C16:0 CoA and 20:0 CoA in prostate cells. However, C18:0 CoA and 18:2 CoA were segregated into different groups between normal and

tumorigenic prostate cells. C16:0 CoA, C18:3 CoA and C20:0 CoA were also clustered into different groups in normal or tumorigenic hepatic cells. The segregations suggest metabolic alterations between tumorigenic and normal cells under the challenge of exogenous fatty acids in acyl-CoA synthesis. The mechanisms for the alterations are not yet clear, but could be a result of dysregulation of multiple enzymes in the neoplasm, including ACSLs[27, 28], acyltransferases[29], desaturases[27], or fatty acid synthases[29].

Figure 6. Remodeling of the acyl-CoA profile across cell lines after treatment with various fatty acids. A) Hierarchical clustering of cells with a variety of fatty acid treatments based on remodeling of the acyl-CoA profile. B-C) Hierarchical clustering of acyl-CoA changes (log ratio) in B) prostate cells and C) hepatic cells in response to fatty acids. The log ratio of the measure is defined as the average amount of an acyl-CoA in a treatment group over the amount in a control group. The color code for log ratio 0.08 indicates a log ratio $\geqslant$ 0.08 (log 1.2) and for -0.08 indicates log ratio $\leqslant$ -0.08. (P: PNT2 cells, D: DU145 cells, G2: HepG2 cells and 3B: Hep3B cells)
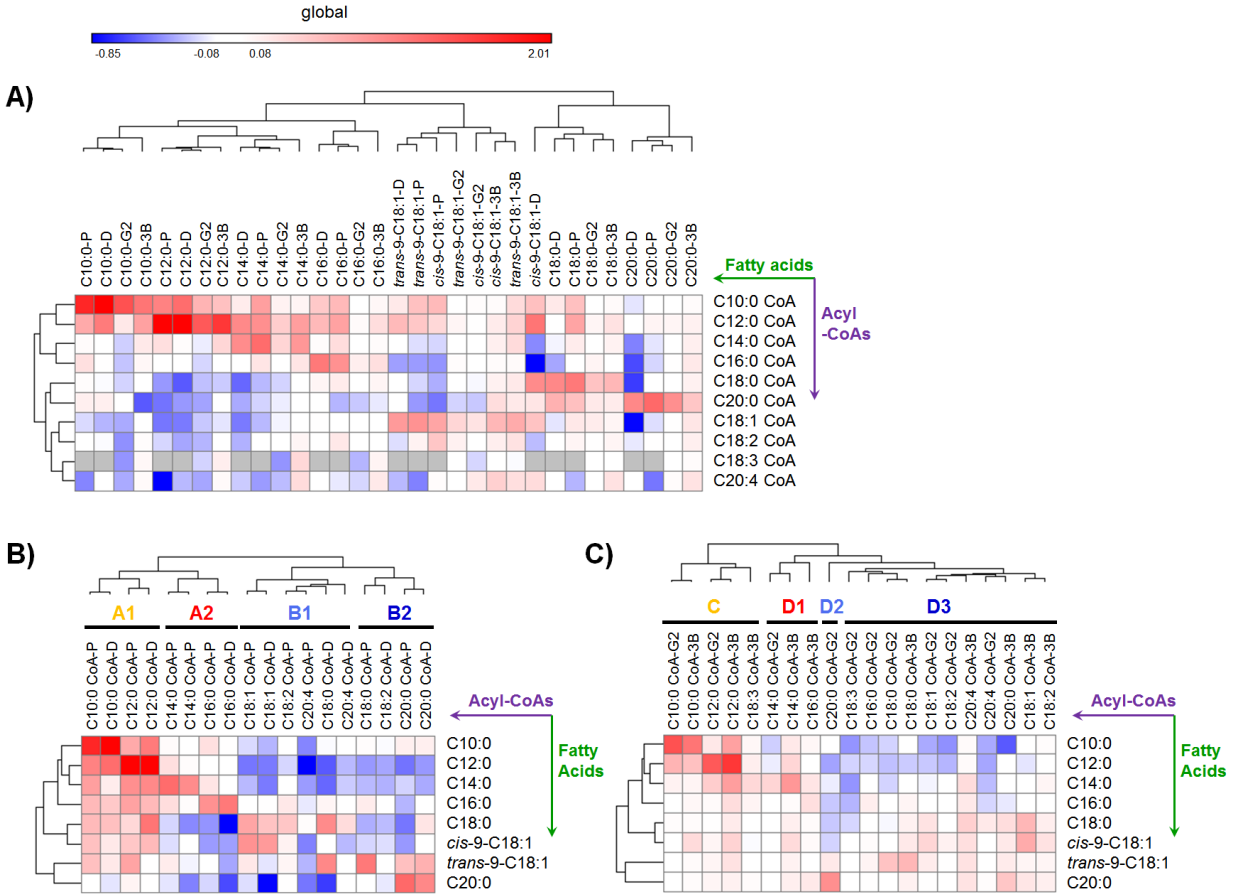
4. CONCLUSION

We developed a sensitive LC-MS/MS analytical method to quantitate acyl-CoAs in prostate and hepatic cell lines. Calibration curves were made from serially supplemented acyl-CoAs, and pentadecanoyl CoA (C15:0 CoA) was used as the internal standard. For the first time, how a variety of dietary fatty acids affect the pool of cellular acyl-CoAs was determined quantitatively, and interpretation of data reflected the involvement of multiple pathways and enzymes in acyl-CoA synthesis and metabolism. Hierarchical clustering in the remodeling of acyl-CoA profiles revealed a fatty acid-specific pattern across all cell lines. Individual acyl-CoAs which corresponded differently to fatty acids in cells at divergent states of tumorigenicity were

identified. Altogether, we believe this method provides a valuable tool for studying the role of fatty acids and subsequent remodeling of the acyl-CoA profile, in the progression of tumors and other diseases associated with nutrition and/or metabolic abnormalities.

References

1. Nomura, D. K.; Long, J. Z.; Niessen, S.; Hoover, H. S.; Ng, S. W.; Cravatt, B. F. Cell 2010, 140, 49-61.

2. Allott, E. H.; Hursting, S. D. Endocr.-Relat. Cancer 2015, 22, R365-R386.

3. Currie, E.; Schulze, A.; Zechner, R.; Walther, T. C.; Farese, R. V. Cell Metab. 2013, 18, 153-161.

4. Grevengoed, T. J.; Klett, E. L.; Coleman, R. A. In Annual Review of Nutrition, Vol 34, Cousins, R. J., Ed.; Annual Reviews: Palo Alto, 2014, pp 1-30.

5. Selvakumar, P.; Lakshmikuttyamma, A.; Shrivastav, A.; Das, S. B.; Dimmock, J. R.; Sharma, R. K. Prog. Lipid Res. 2007, 46, 1-36.

6. Yeste-Velasco, M.; Linder, M. E.; Lu, Y. J. Biochim. Biophys. Acta-Rev. Cancer 2015, 1856, 107-120.

7. Schmick, M.; Kraemer, A.; Bastiaens, P. I. H. Trends Cell Biol. 2015, 25, 190-197.

8. Chakrabandhu, K.; Herincs, Z.; Huault, S.; Dost, B.; Peng, L.; Conchonaud, F.; Marguet, D.; He, H. T.; Hueber, A. O. Embo J. 2007, 26, 209-220.

9. Zhou, B.; Liu, L.; Reddivari, M.; Zhang, X. A. Cancer Res. 2004, 64, 7455-7463.

10. Hemler, M. E. Nat. Rev. Cancer 2014, 14, 49-60.

11. Chow, A.; Zhou, W. Y.; Liu, L.; Fong, M. Y.; Champer, J.; Van Haute, D.; Chin, A. R.; Ren, X. B.; Gugiu, B. G.; Meng, Z. P.; Huang, W. D.; Ngo, V.; Kortylewski, M.; Wang, S. E. Sci Rep 2014, 4, 11.

12. Zimmermann, M.; Thormann, V.; Sauer, U.; Zamboni, N. Anal. Chem. 2013, 85, 8284-8290.

13. Haynes, C. A.; Allegood, J. C.; Sims, K.; Wang, E. W.; Sullards, M. C.; Merrill, A. H. J. Lipid Res. 2008, 49, 1113-1125.

14. Liu, X. J.; Sadhukhan, S.; Sun, S. Y.; Wagner, G. R.; Hirschey, M. D.; Qi, L.; Lin, H. N.; Locasale, J. W. Mol. Cell. Proteomics 2015, 14, 1489-1500.

15. Gao, L.; Chiou, W.; Tang, H.; Cheng, X. H.; Camp, H. S.; Burns, D. J. J. Chromatogr. B 2007, 853, 303-313.

16. Crowe, F. L.; Allen, N. E.; Appleby, P. N.; Overvad, K.; Aardestrup, I. V.; Johnsen, N. F.; Tjonneland, A.; Linseisen, J.; Kaaks, R.; Boeing, H.; Kroger, J.; Trichopoulou, A.; Zavitsanou, A.; Trichopoulos, D.; Sacerdote, C.; Palli, D.; Tumino, R.; Agnoli, C.; Kiemeney, L. A.; Bueno-de-Mesquita, H. B.; Chirlaque, M. D.; Ardanaz, E.; Larranaga, N.; Quiros, J. R.; Sanchez, M. J.; Gonzalez, C. A.; Stattin, P.; Hallmans, G.; Bingham, S.; Khaw, K. T.; Rinaldi, S.; Slimani, N.; Jenab, M.; Riboli, E.; Key, T. J. Am. J. Clin. Nutr. 2008, 88, 1353-1363.

17. Strom, S. S.; Yamamura, Y.; Forman, M. R.; Pettaway, C. A.; Barrera, S. L.; DiGiovanni, J. Int. J. Cancer 2008, 122, 2581-2585.

18. Epstein, M. M.; Kasperzyk, J. L.; Mucci, L. A.; Giovannucci, E.; Price, A.; Wolk, A.; Hakansson, N.; Fall, K.; Andersson, S. O.; Andren, O. Am. J. Epidemiol. 2012, 176, 240-252.

19. Iordanescu, G.; Brendler, C.; Crawford, S. E.; Wyrwicz, A. M.; Venkatasubramanian, P. N.; Doll, J. A. J. Magn. Reson. Imaging 2015, 42, 651-657.

20. Riezman, H. Cell 2007, 130, 587-588.

21. Jakobsson, A.; Westerberg, R.; Jacobsson, A. Prog. Lipid Res. 2006, 45, 237-249.

22. Smith, S.; Witkowski, A.; Joshi, A. K. Prog. Lipid Res. 2003, 42, 289-317.

23. Lawson, L. D.; Kummerow, F. A. Biochimica et biophysica acta 1979, 573, 245-254.

24. Yu, W. F.; Liang, X. Q.; Ensenauer, R. E.; Vockley, J.; Sweetman, L.; Schulz, H. J. Biol. Chem. 2004, 279, 52160-52167.

25. Mursula, A. M.; van Aalten, D. M. F.; Hiltunen, J. K.; Wierenga, R. K. J. Mol. Biol. 2001, 309, 845-853.

26. Janssen, U.; Fink, T.; Lichter, P.; Stoffel, W. Genomics 1994, 23, 223-228.

27. Sanchez-Martinez, R.; Cruz-Gil, S.; de Cedron, M. G.; Alvarez-Fernandez, M.; Vargas, T.; Molina, S.; Garcia, B.; Herranz, J.; Moreno-Rubio, J.; Reglero, G.; Perez-Moreno, M.; Feliu, J.; Malumbres, M.; de Molina, A. R. Oncotarget 2015, 6, 38719-38736.

28. Gaisa, N. T.; Reinartz, A.; Schneider, U.; Klaus, C.; Heidenreich, A.; Jakse, G.; Kaemmerer, E.; Klinkhammer, B. M.; Knuechel, R.; Gassler, N. Histol. Histopath. 2013, 28, 353-364.

29. Wakamiya, T.; Suzuki, S. O.; Hamasaki, H.; Honda, H.; Mizoguchi, M.; Yoshimoto, K.; Iwaki, T. Neuropathology 2014, 34, 465-474.

Supplemental Data

Figure S1. Representative chromatograms of acyl-CoA analytes in HepG2 cells. Retention times (min) and peak areas are labeled.
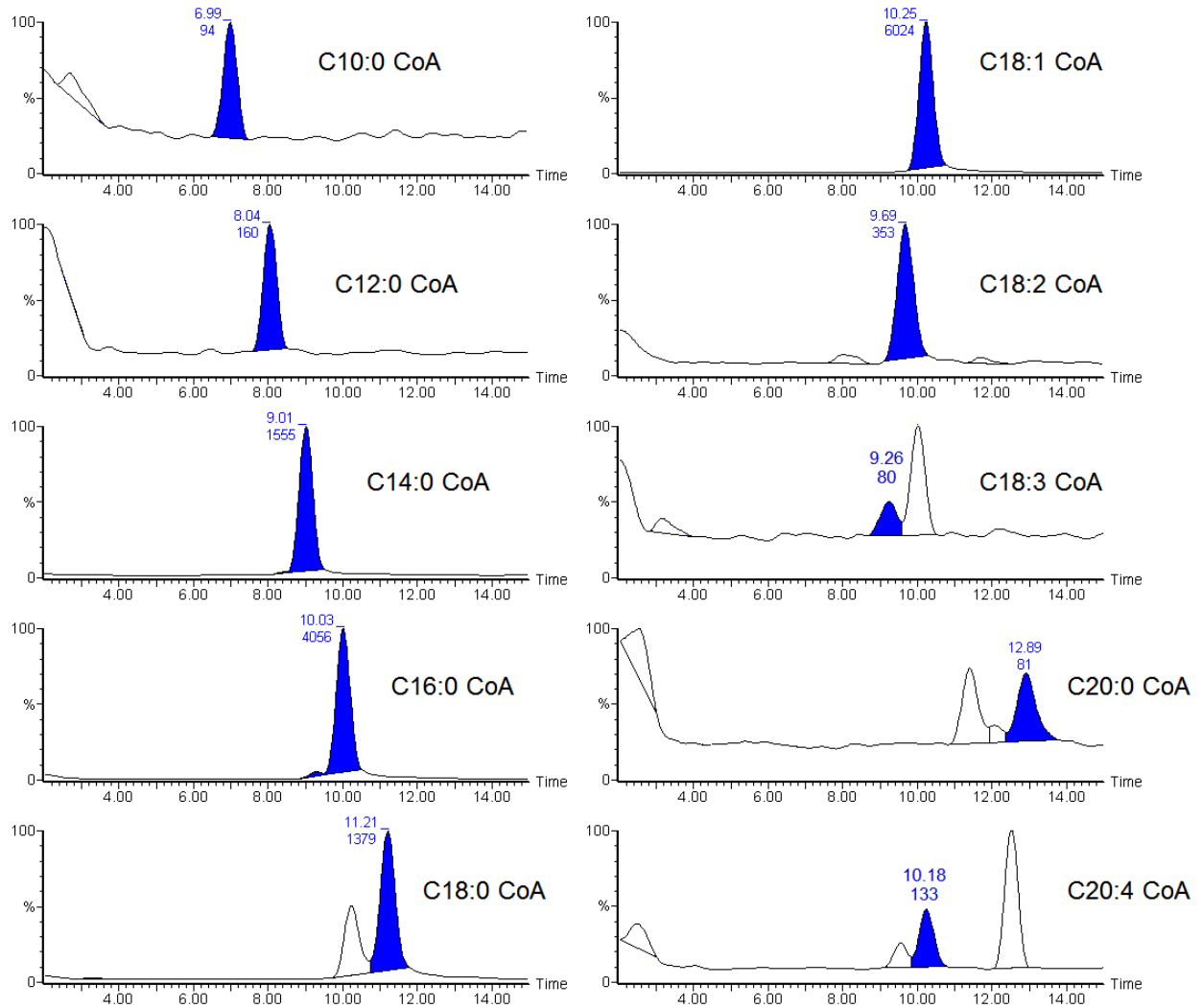
Table S1. Primer sets for real-time RT-PCR analysis of expression of ACSL genes.

Name	Forward Sequence	Reverse Sequence
ACSL1	TCTTCCCCGTGGTTCCAA	TGGTGTTTGCTTGTCCGAAA
ACSL3	ACTCCACTGTGCGACAGCTTT	CACCACACAACAGGAGACGAA
ACSL4	ACTGGCCGACCTAAGGGAG	GCCAAAGGCAAGTAGCCAATA
ACSL5	TGGCTATCTTACAAACAGGTGTC	TCCACTCTGGCCTATTCTGAG
ACSL6	CGCTACATCATCAATACAGCGG	GCATGGACTTAATGACCACCC
GAPDH	CCACATCGCTCAGACACCAT	ACCAGGCGCCCAATACG

Table S2. Amounts of acyl-CoAs (pmol/mg protein) in PNT2, DU145, HepG2 and Hep3B cells (n = 3) incubated with 400 μM fatty acids for 24 h.

PNT2	Control	C10:0	C12:0	C14:0	C16:0	C18:0	C18:1	C18:1 EA	C20:0
10:0 CoA	2.40 ± 0.99	129.88 ± 35.13	26.61 ± 1.44	15.44 ± 0.80	10.27 ± 1.00	9.00 ± 2.99	9.74 ± 1.35	8.66 ± 2.42	2.81 ± 1.81
12:0 CoA	3.55 ± 1.22	19.66 ± 4.95	365.17 ± 44.89	31.28 ± 6.62	21.75 ± 7.12	21.61 ± 1.80	8.76 ± 1.42	11.42 ± 1.16	5.34 ± 1.66
14:0 CoA	22.49 ± 0.41	29.67 ± 6.21	48.38 ± 1.37	363.56 ± 55.25	50.23 ± 3.23	37.97 ± 2.32	14.47 ± 1.68	15.35 ± 3.20	16.02 ± 3.81
16:0 CoA	36.81 ± 1.56	77.10 ± 17.15	34.70 ± 4.57	72.05 ± 13.08	316.58 ± 17.96	39.31 ± 8.12	14.75 ± 0.58	15.83 ± 1.50	23.71 ± 2.12
18:0 CoA	23.33 ± 3.15	29.87 ± 7.66	9.65 ± 1.73	12.22 ± 1.89	39.95 ± 2.97	298.33 ± 27.36	11.19 ± 1.83	15.14 ± 2.03	21.53 ± 1.63
18:1 CoA	92.25 ± 6.74	60.85 ± 16.74	30.55 ± 2.97	47.97 ± 11.38	103.78 ± 8.36	172.85 ± 9.33	545.17 ± 46.29	762.97 ± 24.58	63.04 ± 11.62
18:2 CoA	4.38 ±4.48	4.37 ±	2.84 ±	4.23 ±	8.14 ±	6.47 ±	14.34 ±	6.73 ±	5.45 ±

		0.71	0.67	1.25	1.38	1.69	1.61	1.17	2.55
20:0 CoA	2.28 ±0.18	3.66 ± 1.05	0.72 ± 0.76	1.39 ± 1.14	1.17 ± 0.68	8.43 ± 2.15	0.74 ± 0.32	0.92 ± 0.43	38.94 ± 11.49
20:4 CoA	8.03 ±2.09	2.92 ± 0.27	1.14 ± 0.66	3.41 ± 1.66	5.77 ± 2.28	4.16 ± 1.33	10.29 ± 2.81	2.84 ± 0.92	2.65 ± 1.57

DU145	Control	C10:0	C12:0	C14:0	C16:0	C18:0	C18:1	C18:1 EA	C20:0
10:0 CoA	0.73 ± 0.38	184.82 ± 32.23	11.74 ± 0.81	1.23 ± 0.45	2.32 ± 0.58	1.31 ± 0.37	4.67 ± 1.15	1.34 ± 0.74	0.52 ± 0.10
12:0 CoA	0.58 ± 0.15	7.39 ± 0.72	233.04 ± 5.58	5.59 ± 1.76	2.47 ± 0.53	0.62 ± 0.59	0.78 ± 0.70	2.36 ± 1.68	0.56 ± 0.26
14:0 CoA	28.78 ± 0.67	30.37 ± 2.56	36.67 ± 1.65	260.33 ± 30.37	36.66 ± 3.52	22.86 ± 2.84	15.34 ± 4.29	25.75 ± 7.58	10.16 ± 0.62
16:0 CoA	43.61 ± 2.17	54.59 ± 6.13	37.48 ± 1.30	48.69 ± 4.42	555.89 ± 24.79	20.00 ± 2.45	6.28 ± 1.43	18.90 ± 2.81	10.57 ± 2.60
18:0 CoA	28.96 ± 5.28	24.15 ± 3.67	7.62 ± 1.73	8.59 ± 0.98	42.07 ± 2.33	281.53 ± 13.10	5.97 ± 0.71	28.18 ± 8.73	6.27 ± 0.36

18:1 CoA	75.54 ± 8.97	37.48 ± 6.31	25.37 ± 0.17	25.85 ± 2.44	94.76 ± 6.47	53.20 ± 1.25	532.53 ± 31.64	552.21 ± 85.21	11.19 ± 1.48
18:2 CoA	7.49 ± 2.63	6.28 ± 0.41	3.41 ± 0.85	3.71 ± 0.99	8.89 ± 1.93	6.92 ± 1.21	7.37± 2.30	5.06 ± 1.40	5.49 ± 1.67
20:0 CoA	2.34 ± 0.36	3.80 ± 1.49	0.95 ± 0.23	1.08 ± 0.56	2.14 ± 0.85	11.17 ± 2.80	0.75 ± 0.47	2.29 ± 0.91	23.24 ± 1.47
20:4 CoA	3.70 ± 0.97	4.04 ± 0.38	1.94 ± 0.53	2.17 ± 0.45	3.23 ± 0.97	3.12 ± 0.74	8.39 ± 0.51	1.92 ± 0.22	3.78 ± 0.99

HepG2	Control	C10:0	C12:0	C14:0	C16:0	C18:0	C18:1	C18:1 EA	C20:0
10:0 CoA	5.16 ± 1.07	132.57 ± 18.76	23.51 ± 1.69	7.92 ± 0.17	5.84 ± 0.49	5.61 ± 2.86	6.65 ± 1.34	5.97 ± 1.00	6.13 ± 1.67
12:0 CoA	6.90 ± 0.35	12.87 ± 2.36	155.32 ± 9.00	20.51 ± 3.52	9.32 ± 1.23	10.16 ± 3.19	8.70 ± 1.63	9.95 ± 0.28	10.04 ± 1.75
14:0 CoA	90.62 ± 11.26	54.91 ± 9.23	67.8 ± 2.29	232.91 ± 58.40	82.33 ± 5.63	104.6 ± 21.37	101.23 ± 7.87	110.71 ± 18.00	104.31 ± 10.77
16:0 CoA	143.89 ±	81.25 ±	92.46 ±	132.75 ±	237.55 ±	219.25 ±	147.12 ±	183.35 ±	179.17 ±

	17.40	8.43	4.42	5.73	10.31	42.27	7.24	19.71	22.09
18:0 CoA	58.59 ± 9.10	36.84 ± 2.70	31.98 ± 2.64	36.81 ± 2.81	64.05 ± 7.14	208.47 ± 37.44	47.93 ± 4.61	67.40 ± 14.92	66.7 ± 12.69
18:1 CoA	262.57 ± 31.98	123.24 ± 7.97	151.9 ± 12.23	206.88 ± 17.71	275.4 ± 16.33	445.83 ± 86.15	526.67 ± 22.31	664.62 ± 99.36	332.83 ± 47.03
18:2 CoA	17.47 ± 2.84	6.82 ± 0.99	8.83 ± 0.92	15.24 ± 3.17	17.49 ± 1.74	21.99 ± 5.13	20.93 ± 3.40	27.84 ± 2.32	18.67 ± 3.34
18:3 CoA	1.35 ± 0.26	0.53 ± 0.30	0.83 ± 0.52	0.54 ± 0.47	0.69 ± 0.66	1.63 ± 1.01	0.86 ± 0.78	1.34 ± 0.74	1.46 ± 0.41
20:0 CoA	2.51 ± 0.20	2.29 ± 0.42	1.12 ± 0.07	1.85 ± 0.06	1.46 ± 0.39	4.56 ± 1.01	1.43 ± 1.26	1.56 ± 0.61	21.83 ± 2.24
20:4 CoA	5.32 ± 0.59	2.46 ± 0.45	2.45 ± 0.39	2.85 ± 1.78	3.43 ± 1.39	6.40 ± 2.87	9.75 ± 2.16	4.84 ± 4.10	6.78 ± 0.70

Hep3B	Control	C10:0	C12:0	C14:0	C16:0	C18:0	C18:1	C18:1 EA	C20:0
10:0 CoA	3.61 ±0.38	49.26 ± 6.96	13.12 ± 2.56	5.51 ± 0.66	5.14 ± 1.03	4.83 ± 0.30	4.73 ± 0.18	8.39 ± 2.36	4.74 ± 0.67

12:0 CoA	1.20 ±0.57	7.51 ± 0.85	48.95 ± 1.88	8.19 ± 1.07	2.61 ± 0.60	2.44 ± 0.63	2.10 ± 0.22	3.14 ± 0.48	1.92 ± 0.82
14:0 CoA	31.51 ± 2.26	56.12 ± 2.81	78.95 ± 4.26	238.85 ± 12.68	41.08 ± 4.25	49.08 ± 2.10	51.32 ± 6.90	73.51 ± 6.54	50.61 ± 6.49
16:0 CoA	42.79 ± 9.33	61.11 ± 3.01	48.52 ± 1.03	84.26 ± 4.18	92.00 ± 9.78	49.87 ± 7.90	56.82 ± 10.20	57.57 ± 7.06	76.09 ± 5.33
18:0 CoA	7.73 ±1.31	9.32 ± 3.34	4.51 ± 0.53	8.93 ± 0.45	11.43 ± 1.37	33.53 ± 2.86	12.25 ± 3.41	14.11 ± 0.72	12.25 ± 1.71
18:1 CoA	35.01 ± 11.58	40.64 ± 1.80	24.98 ± 1.93	43.22 ± 4.61	41.44 ± 4.39	50.35 ± 3.45	153.16 ± 22.16	187.26 ± 25.99	67.40 ± 8.07
18:2 CoA	28.29 ± 6.72	36.71 ± 0.83	27.51 ± 2.72	40.80 ± 6.42	34.27 ± 3.23	41.27 ± 3.96	46.86 ± 5.39	58.37 ± 10.08	45.90 ± 8.59
18:3 CoA	2.52 ±1.03	3.58 ± 1.05	4.13 ± 0.20	6.19 ± 0.45	3.80 ± 0.58	3.06 ± 0.86	2.14 ± 0.61	2.12 ± 0.25	3.31 ± 0.50
20:0 CoA	0.53 ±0.08	0.14 ± 0.02	0.50 ± 0.33	0.47 ± 0.22	0.39 ± 0.07	0.94 ± 0.45	1.20 ± 0.11	0.97 ± 0.23	1.75 ± 0.55

| 20:4 CoA | 7.63 ±2.53 | 10.26 ± 0.29 | 10.34 ± 1.12 | 17.44 ± 2.02 | 13.96 ± 1.67 | 15.75 ± 3.34 | 21.21 ± 2.54 | 16.44 ± 2.45 | 15.17 ± 3.75 |

CHAPTER 6

SIMULTANEOUS QUANTITATION OF QUETIAPINE AND ITS ACTIVE METABOLITE

NORQUETIAPINE IN RAT PLASMA AND BRAIN TISSUE BY HIGH PERFORMANCE

LIQUID CHROMATOGRAPHY/ELECTROSPRAY IONIZATION TANDEM MASS

SPECTROMETRY (LC-MS/MS)

Xiangkun Yang, Indrani Poddar, Caterina M. Hernandez, Alvin V. Terry Jr. and Michael G. Bartlett

Abstract

A sensitive method to simultaneously quantitate quetiapine and norquetiapine in rat plasma and brain tissue was developed using a one-step liquid-liquid extraction for sample preparation and LC-MS/MS for detection. The method provided a linear range of 1.0–500.0 ng/mL for each analyte in plasma and 3.0-1500.0 ng/g in brain tissue. The method was validated with precision within 15% relative standard deviation (RSD), accuracy within 15% relative error (RE), matrix effects within 10% and a consistent recovery. This method has been successfully applied in a preclinical study of quetiapine and norquetiapine to simultaneously determine their concentrations in rat plasma and brain tissue.

Key words

Quetiapine, norquetiapine, plasma, brain, LC-MS/MS

1. Introduction

Quetiapine (commercially available as quetiapine fumarate) is a second generation antipsychotic that has been approved by the United States Food and Drug Administration (USFDA) for indications including schizophrenia, bipolar mania and bipolar depression (mono/adjunct therapy)[1]. It has been demonstrated to be effective in clinical trials for generalized anxiety disorders, major depressive disorders[2,3], and is the only drug without the associated risk of veering into mania[4,5]. Quetiapine is a multifunctional molecule acting as an antagonist against multiple types of receptors. *In vitro* radioligand binding studies showed that quetiapine has a high affinity for serotonin $5\text{-}HT_2$ receptors, histamine H_1 receptors and adrenergic α_1 receptors, a low affinity for dopamine D_2 receptors, and a negligible affinity for muscarinic receptors[6].

Quetiapine is mainly metabolized by cytochrome P450 (CYP) 3A4 in the liver, and the major metabolites are quetiapine sulfoxide, N-desalkylquetiapine (norquetiapine), 7-hydroxyquetiapine and O-desalkylquetiapine[7]. Of all the metabolites, norquetiapine is active in mediating the antidepressant activity of quetiapine[8], by selectively inhibiting norepinephrine transporter (NET) reuptake. Norquetiapine is a partial $5\text{-}HT_{1A}$ receptor agonist and an antagonist against histamine H_1 receptors, presynaptic adrenergic α_2 receptors, serotonin $5\text{-}HT_{2C}$ and $5\text{-}HT_7$ receptors[8].

To investigate pharmacokinetics of quetiapine and its metabolites, a sensitive and accurate bioanalytical method is necessary. Traditional LC-UV methods were simple in operation, validated and can provide reliable data for quetiapine quantification in plasma, but lacked good sensitivity (lower limit of quantification, LLOQ = 2.5-15 ng/mL)[9,10]. GC-MS methods required compound derivatization and method sensitivity was not satisfactory (LLOQ in

plasma = 20 ng/mL)[11]. LC-MS technology provides methods with high sensitivity and accuracy for measuring small molecules in plasma, some early LC-MS/MS methods were sensitive for quetiapine, but did not measure any quetiapine metabolites[12,13]. A more recent LC-MS/MS method was validated to simultaneously determine quetiapine and four metabolites in human plasma[14]. The linear range was 5-800 ng/mL for quetiapine and norquetiapine, 100-15000 ng/mL for quetiapine sulfoxide and 2-100 ng/mL for O-desalkylquetiapine and 7-hydroxyquetiapine. However, it may not be sufficiently sensitive to support low-dose studies, and the necessity of monitoring the inactive metabolites of quetiapine has not been justified. Another method was validated to measure quetiapine and the only active metabolite norquetipine in human plasma, with higher sensitivity achieved (LLOQ for quetiapine = 0.5 ng/mL, LLOQ for norquetiapine = 0.6 ng/mL)[15], however, this method has not been extended to the brain which is the main organ effected by quetiapine.

Quetiapine and norquetiapine act on neurobiological processes in the central nervous system. Like some other second generation antipsychotics[16,17,18], both cognitive impairment and improvement were observed in different preclinical and clinical studies for quetiapine, which may be attributable to differences in dose, duration of treatment and the type of cognitive domain assessed[19,20,21,22]. To better establish a causal connection between quetiapine or its active metabolite and (positive or negative) alterations in cognitive function, it is important to be able to accurately measure concentrations of these compounds in the brain. However, it is more difficult to determine quetiapine and norquetiapine in brain tissue than in plasma, due to the abundant phospholipids and other endogenous lipophilic substances in brain, which can be co-extracted with the lipophilic analytes and lead to ion-suppression in MS analysis[23]. Until now, no method has been reported to simultaneously measure quetiapine and norquetiapine in brain tissue. There

is only one method developed for quantification of quetiapine in human brain tissue[24], but it required a complicated sample preparation (hybrid solid phase extraction-precipitation), the lower end of the linear range was 20 ng/mL and only a partial validation was performed.

In this paper, we have established and validated a new method, with a one-step liquid-liquid extraction for sample preparation and LC-MS/MS for detection, which simultaneously quantitates quetiapine and norquetiapine in rat plasma and brain tissue. After validation, this method was used to analyze plasma and brain samples from rats chronically treated with quetiapine in drinking water for the purpose of facilitating future studies to investigate the pharmacokinetics and impact of quetiapine and norquetiapine on cognition.

2. Experimental

2.1. Chemicals and reagents

Quetiapine fumarate and norquetiapine HCl were purchased from Cerilliant (Round Rock, TX), midazolam was purchased from Hoffmann-La Roche (Nutley, NJ). Sodium phosphate, dibasic (Na_2HPO_4) was purchased from J.T.Baker (Center Valley, PA). Sodium hydroxide, ammonium formate, diisopropyl ether, LC-MS grade acetonitrile, LC-MS grade methanol and LC-MS grade water were purchased from Sigma–Aldrich (St. Louis, MO). Male rat plasma was purchased from BioreclamationIVT (Westbury, NY).

Figure 1. Chemical structures and physicochemical properties of quetiapine, norquetiapine and midazolam. pKa values were obtained from PubChem database, XLogP3 values were predicted by XLOGP3 v 3.2.0. software.
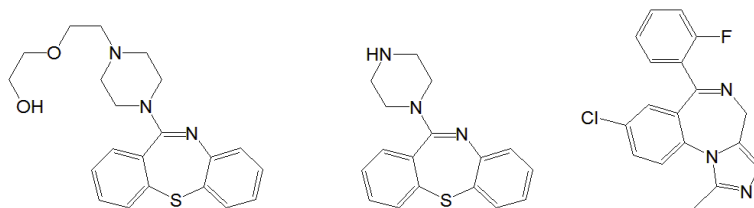
	Quetiapine	Norquetiapine	Midazolam
Mass	383.51	295.41	325.78
XLogP3	2.14	2.51	2.48
pKa	5.80	8.10	6.57

2.2. Instrumentation

An Agilent 1100 binary pump HPLC system (Santa Clara, CA) interfaced to a Waters Micromass Quattro Micro triple quadrupole mass spectrometer with an ESI (+) source (Milford, MA) was operated for LC–MS/MS analysis. Masslynx 4.0 software by Waters (Beverly, MA) was used for instrument control and data processing. A Labconco CentriVap Complete Vacuum Concentrator (Kansas City, MO) was utilized to evaporate samples.

2.3. LC-MS/MS conditions

A Waters Atlantis dC-18 (2.1×30 mm, 3 μm) column coupled with a Phenomenex SecurityGuard C-18 guard column (4.0 mm×2.0 mm) was used to separate the analytes. The column temperature was controlled at 25 ℃. The mobile phase A was 5 mM ammonium formate in water, mobile phase B was acetonitrile (ACN). The injection volume was 15 μL. Analytes were separated using a gradient method, with a 0.3 mL/min flow rate, (time/minute, % mobile phase B): (0, 20), (5, 100), (10, 100), (10.01, 20), (15, 20). The LC system was interfaced by a six-port divert valve to the mass spectrometer, introducing eluents from 1.0 to 6.0 min to the ion source. The autosampler injection needle was washed with methanol after each injection.

Samples were analyzed by the mass spectrometer in positive ion ESI mode. The capillary voltage was 3.50 kV and the cone voltage was 30 V. Nitrogen was used as the desolvation gas at a flow rate of 500 L/h. The desolvation temperature was 500 ℃ and the source temperature was 120 ℃. Argon was used as the collision gas, the collision cell pressure was 3.5×10^{-3} mbar and the collision energy was 23 eV. A multiple reaction monitoring (MRM) function was applied for quantification of analytes, the ion transitions monitored were 384→253 for quetiapine, 296→210 for norquetiapine and 326→291 for midazolam.

2.4. Solutions and standards

The primary stock solutions were prepared at 0.5 mg/mL in 50% methanol for quetiapine and norquetiapine, individually, and 0.2 mg/mL for midazolam (ISTD). All dilutions were made with 50% methanol. The secondary stock solution containing quetiapine and norquetiapine was diluted to 20 μg/mL, and the secondary ISTD stock solution was diluted to 10 μg/mL. Standard working solutions containing quetiapine and norquetiapine were obtained by serial dilutions to concentrations of 10.0, 20.0, 50.0, 100.0, 200.0, 500.0, 1000.0, 2000.0 and 5000.0 ng/mL. Quality control (QC) working solutions were prepared at concentrations of 10.0, 30.0, 300.0 and 4000.0 ng/mL. The ISTD working solution was prepared at 500.0 ng/mL. All solutions were stored in the refrigerator (-5 ℃) when not in use.

2.5. Spiked samples and real samples

Blank rat plasma with sodium EDTA was purchased from Bioreclamation (Westbury, NY). Blank brain was acquired from drug-free control rats. Brain homogenate was made with 2 weight units of water and 1 weight unit of brain tissue, and prepared in a glass tissue grinder homogenizer. 10 μL standard or QC working solution was spiked with 90 μL blank plasma or blank brain homogenate to make the corresponding standard or QC samples. The final

concentrations for calibration standard samples are 1.0, 2.0, 5.0, 10.0, 20.0, 50.0, 100.0, 200.0 and 500.0 ng/mL, and for QC samples are 1.0, 3.0, 30.0 and 400.0 ng/mL.

Real samples were collected from rats dosed with quetiapine in drinking water (25 mg/kg) for 60 days. Plasma was collected via cardiac puncture in sodium heparin. Brain samples were homogenized in the same way as blank brain.

All biological samples were stored at −20 °C until use. Fresh calibration standard samples and QC samples were prepared each day for method validation.

2.6. Sample preparation

A one-step liquid-liquid extraction was carried out to prepare samples. To each 100 μL rat plasma or brain homogenate sample, 10 μL ISTD working solution (500.0 ng/mL midazolam), 100 μL 0.5 M Na_2HPO_4 (pH = 11.5) and 1.7 mL diisopropyl ether were added. The mixture was vortexed for 10 min, then centrifuged at 10000×g at 5 °C for 10 min. 1.0 mL (for plasma samples) or 1.3 mL (for brain homogenate samples) organic supernatant was transferred and evaporated to complete dryness in the vacuum concentrator at 55 °C for 10 min. The sample was reconstituted with 150 μL methanol: 20 mM ammonium formate (70:30, pH = 3.9), sonicated, vortexed, and centrifuged at 15,000×g at 5 °C for 10 min. 100 μL supernatant was transferred for injection.

2.7. Method validation

To validate the method, selectivity, linearity, intra- and inter-day precision and accuracy, recovery, stability and dilution tests were conducted.

Selectivity (n = 6) was tested by comparing the chromatograms of analytes in blank plasma, or in blank brain homogenate, with analytes in the same matrix at 1.0 ng/mL, respectively. Linearity was validated with calibration standard samples over the range of 1.0-500.0 ng/mL. Calibration curves were made from peak area ratios between analytes and ISTD,

with 1/x weighted linear regression. The intra-day (n = 5) and inter-day (n = 15) precision and accuracy were tested by QC samples at 1.0, 3.0, 30.0 and 400.0 ng/mL.

Recovery (n = 3), including matrix effect, relative recovery and absolute recovery in plasma and brain homogenate, was tested by calculating from peak areas of spiked samples, post-preparation spiked samples and standard solutions at 3.0, 30.0 and 400.0 ng/mL.

Autosampler stability (25 ℃, 12 h), bench-top stability (25 ℃, 18 h) and freeze-thaw stability (3 freeze–thaw cycles, −20 °C, 72 h) of analytes in plasma and brain homogenate were tested at low (3.0 ng/mL) and high (400.0 ng/mL) concentrations.

Dilution test (n = 5) was conducted by diluting spiked plasma and brain homogenate samples at 2000.0 ng/mL to ULOQ (500.0 ng/mL) with corresponding blank matrix. Precision and accuracy (n = 5) were calculated.

2.8. Animal study

Male albino Wistar rats from Harlan Sprague-Dawley, Inc. (Indianapolis, IN) approximately 2 months old were housed singly in a temperature controlled room (25 ℃), maintained on a 12:12 h normal light–dark cycle with free access to water and food until used for plasma and brain studies (see below). All procedures employed in this study were reviewed and approved by the Georgia Regents University Institutional Animal Care and Use Committee and are consistent with AAALAC guidelines. Measures were taken to minimize pain and discomfort in accordance with the National Institutes of Health Guide for the Care and Use of Laboratory Animals (NIH Publications No. 80-23) revised in 1996. At the beginning of the animal treatment studies, normal drinking water was replaced with a solution containing quetiapine dissolved in distilled, deionized water for daily drug administration. Drug dosing (25.0 mg/kg/day) was based on the average daily fluid consumption and the weight of the animals.

Plasma samples were collected after 60 days of treatment. Rats were anesthetized with isoflurane and 3.0 mL of blood was collected via cardiac puncture in sodium heparin. The blood was centrifuged for 15 min at $2500 \times g$ at 4-5 ℃ and the resulting plasma was frozen until analyzed. Whole brains of sacrificed animals were removed, washed in phosphate buffered saline, and kept frozen at −70 °C until analysis.

3. Results and discussion

3.1. Method development

Midazolam is a central nervous system (CNS) depressant of the benzodiazepine class. It shares similar structure and physicochemical properties with quetiapine and norquetipine (See Figure 1). Midazolam is only available to in-hospital patients, thus it is easy to track and interference from blank samples is unlikely. Midazolam has been successfully used as the ISTD for several other LC-MS/MS assays for antipsychotics[25,26,27,28].

The autotune mode imbedded in Masslynx 4.0 software by Waters was utilized to optimize MS parameters to increase signal response, accompanied by direct infusion of standard solutions for quetiapine, norquetiapine and midazolam (each at 500.0 ng/mL) at 30 μL/min into the instrument.

Product ion mass spectra for quetiapine, norquetiapine and midazolam were acquired, using injections of standard solutions for quetiapine, norquetiapine and midazolam (each at 500.0 ng/mL) to determine precursor and product ion pairs to monitor. The most abundant fragment ion for each compound was selected for the monitored ion-transition in multiple reaction monitoring (MRM) mode. The determined ion transitions were 384→253 for quetiapine, 296→210 for norquetiapine and 326→291 for midazolam.

Both quetiapine and norquetipine are weakly basic and hydrophobic compounds (See Figure 1), thus a higher pH facilitates the neutralization in the aqueous phase and promotes distribution to the organic phase, increasing the extraction efficiency. However, the pH cannot be extremely high, since the analytes and ISTD may be unstable in a strongly basic environment. A series of solutions were tried to monitor the pH in the aqueous phase and 100 μL 0.5 M Na_2HPO_4 (pH = 11.5) was selected, which provided good extraction efficiency at a moderately basic pH.

A heating oven at 80-90 ℃ with negative pressure was initially used to evaporate the organic supernatant transferred from the liquid-liquid extraction. However, the evaporation was slow and MS signal intensities were weak and negatively correlated with the time in the oven. This data suggested the instability of quetiapine and norquetiapine at high temperatures. Finally we utilized a vacuum concentrator, which was able to speed sample evaporation with a combination of centrifugal force, vacuum and heat. Heating temperature was controlled to 55 ℃ and the evaporation was completed in 10 min. The MS response was increased by about 10 times compared to the case with the heating oven (data not shown).

3.2. Selectivity

Selectivity (n = 6) was validated by analyzing blank plasma samples, spiked plasma standard samples (1.0 ng/mL) with ISTD (50.0 ng/mL), blank brain homogenate samples, and spiked brain homogenate standard samples (1.0 ng/mL) with ISTD (50.0 ng/mL). The chromatograms were compared between the same type of matrix, to make sure there was no significant interference from endogenous substances or other components in the matrix. No significant interference was observed in either blank plasma or blank brain homogenate (see

Figure 2), demonstrating that the LC-MS/MS method has good selectivity to differentiate and quantify the analytes at 1.0 ng/mL in plasma and brain homogenate.
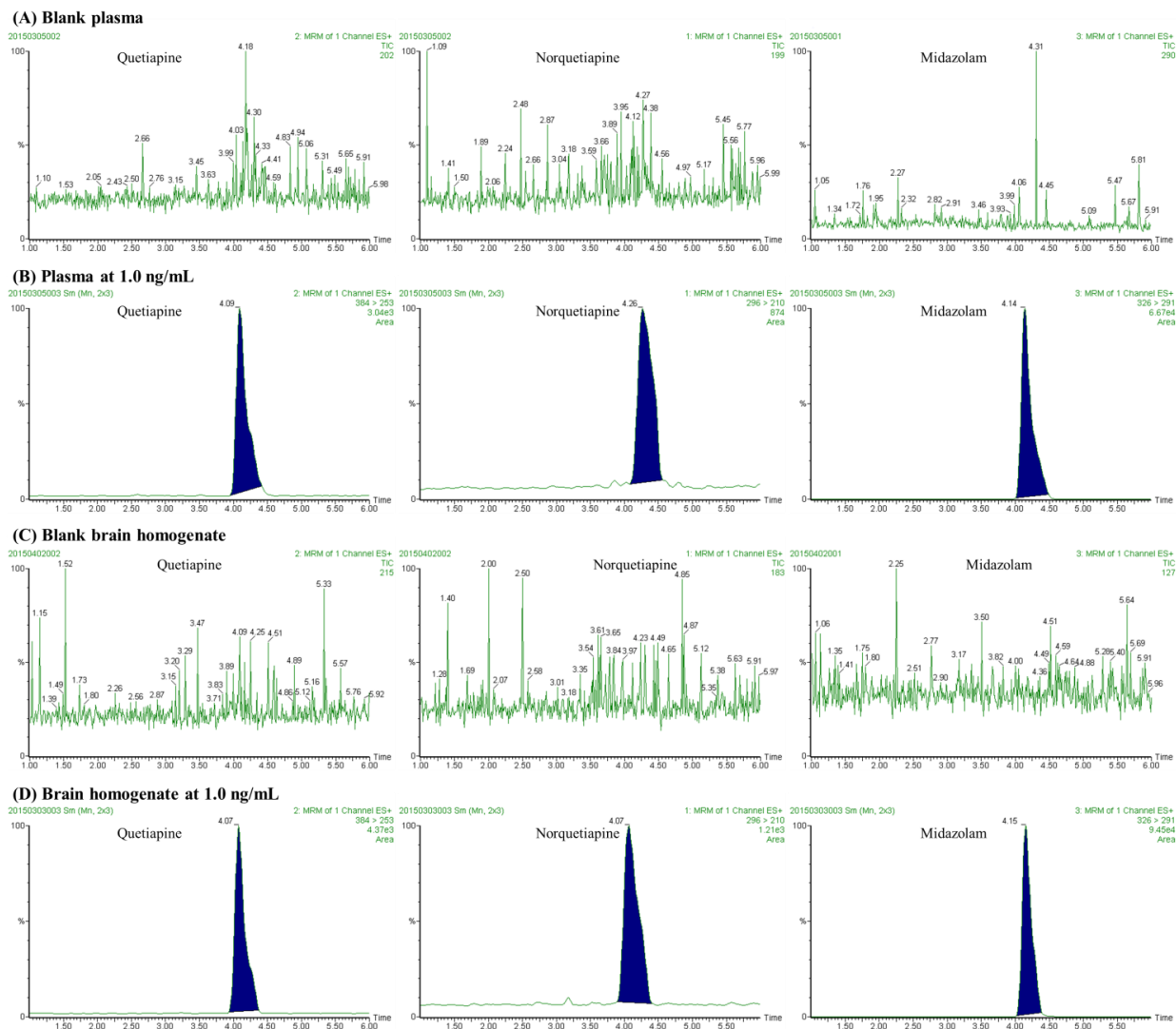
Figure 2. Representative chromatograms of quetiapine, norquetiapine and midazolam in blank plasma (A), plasma at 1.0 ng/mL (B), blank brain homogenate (C) and brain homogenate at 1.0 ng/mL (D). Retention times for analytes are shown in minutes.

3.3. Linearity

Linearity of method was validated within the range from 1.0-500.0 ng/mL for plasma and brain homogenate (3.0-1500.0 ng/g for brain tissue). Calibration curves were made from peak area ratios between analytes and ISTD, with 1/x weighted linear regressions. Slopes, intercepts and R^2 from the calibration curves are shown in Table 1. The R^2 values are over 0.99 for either analyte in either matrix, demonstrating the good linearity of the method when determining quetiapine and norquetiapine in plasma and brain homogenate within the tested range. Besides, the intercept of each calibration curve is within 20% of LLOQ, suggesting a low endogenous level of quetiapine and norquetiapine in blank plasma and brain homogenate, which is unlikely to significantly interfere with accurate quantification of analytes at low concentrations in these two types of biological matrices.

3.4. Precision and accuracy

The intra-day (n = 5) and inter-day (n = 15) precision and accuracy for both analytes were tested using QC samples at 1.0, 3.0, 30.0 and 400.0 ng/mL in both matrices. Precision, the closeness of a series of measurements from multiple sampling, was represented by relative standard deviation (RSD); accuracy, the closeness of measured value to the true value, was represented by relative error (RE). Table 2 shows RSD and RE values of analytes in all QC plasma samples and QC brain homogenate samples, which are all below 15% and meet the requirements from Guidance for Industry (Bioanalytical Method Validation) by FDA. In addition, according to the requirements of the same guidance, we have also validated that 1.0 ng/mL can serve as the LLOQ for both analytes in plasma and brain homogenate (3.0 ng/g in brain tissue): at 1.0 ng/mL, the RSD and RE for either analyte in either matrix are within 20%, and the

response of either analyte in either matrix is over 5 times the response from blank samples (data not shown).

3.5. Recovery

Absolute recovery, relative recovery and matrix effects (n = 3) were tested in plasma and brain homogenate, with spiked samples, post-preparation spiked samples and standard solutions at 3.0, 30.0 and 400.0 ng/mL in triplicate. The absolute recovery was represented by the ratio of peak areas between spiked samples and the average of standard solutions at the same concentration. Relative recovery was represented by the ratio of peak areas between spiked samples and the average of corresponding post-preparation spiked samples. Matrix effects, the interference in response by substances in the matrix, were represented by the ratio of peak areas between post-preparation spiked samples and the average of corresponding standard solutions. A ratio over 100% demonstrates an enhancing matrix effect, a ratio below 100% demonstrates a suppressing matrix effect, and the percentage of enhancement or suppression is calculated as the absolute difference from 100%. Table 3 shows the absolute recovery (AR), relative recovery (RR), matrix effect and its type in both matrices at 3 concentrations. Although the absolute recovery and relative recovery vary for different analytes in different matrices, the absolute and relative recoveries are validated, because the values for the same analyte in the same matrix are consistent, precise and reproducible at 3 concentrations.

A lower absolute recovery and relative recovery was observed in plasma, compared to brain homogenate, for each analyte at each concentration. This is mainly due to the difference in volumes of supernatant transferred after liquid-liquid extraction, which was 1 mL for plasma and 1.3 mL for brain homogenate. A smaller volume was transferred from plasma samples, because

there was a significant emulsification in plasma after liquid-liquid extraction, which increased the volume of interphase, and decreased the volume of supernatant.

Ion suppression was observed for both analytes, at all concentrations in both matrices. But the suppression was not evident (<10%), suggesting that sample preparation was effective in eliminating potentially interfering substances in plasma and brain homogenate, such as phospholipids and other endogenous lipophilic substances found in brain tissue.

3.6. Stability

To validate autosampler stability (25 ℃, 12 h), bench-top stability (25 ℃, 18 h) and freeze-thaw stability (3 freeze–thaw cycles, −20 °C, 72 h), three sets (n = 3) of spiked plasma and brain homogenate samples at 3.0 ng/mL and 400.0 ng/mL were prepared. The first set was analyzed immediately and used as a time zero control, then used for autosampler stability testing. The second set was placed on bench for 18h and then analyzed. The last set was stored at −20 °C for 24 h and then completely thawed at 25 ℃. This process was continued for an additional 2 freeze-thaw cycles. For each stability test, the ratio between concentrations in tested samples and the time-zero control was calculated. Data are shown in Table 4. A difference below 10% from time-zero control was observed for all stability tests, which validated the chemical stability of analytes in both matrices under common sample processing and storage conditions.

3.7. Dilution

Concentrations of quetiapine and norquetipine in real plasma and brain homogenate samples are dependent on dose, dosing route, intervariability of experiment subjects and numerous other factors. A dilution test (n = 5) was conducted to validate the need to accommodate analytes in real samples at concentrations higher than upper limit of quantitation (ULOQ, 500.0 ng/mL). Spiked plasma samples and brain homogenate samples at 2000.0 ng/mL

143

were diluted to the ULOQ with corresponding blank matrix. Measured concentrations, precision and accuracy (n = 5) are shown in Table 5. All RSD and RE values for both analytes in both matrices are within 15%, which validated that a 4-fold dilution can be applied in real samples over the ULOQ.

3.8. Application

The validated method was applied to analyze plasma and brain homogenate samples collected from rats (n = 3) dosed with quetiapine (25 mg/kg/day) in drinking water for 60 days. Plasma and brain homogenate samples from each rat were prepared and analyzed in duplicate, and the average concentration was recorded. Because brain homogenate was prepared with 1 weight unit of brain tissue and 2 weight units of water, the concentrations of analytes in brain tissue are 3 times the concentrations in brain homogenate. Both analytes were detected in plasma and brain homogenate samples from each rat, and the determined concentrations were within the validated linear range (data shown in Table 6). Quetiapine showed a much higher concentration (> 10 times) than norquetiapine in both types of biological samples. Assuming 1 g brain tissue is equivalent to 1 mL of plasma, the brain-to-plasma ratio of each analyte was calculated as the average concentration in the plasma over the average concentration in the brain tissue, to represent the ability of the analyte to cross the blood-brain barrier (BBB) and distribute into brain tissue. The brain-to-plasma ratio for quetiapine is 2.90 and for norquetiapine is 3.14. The ratios are higher than the ratio of cotinine (0.70)[29], an active metabolite of nicotine for anti-Alzheimer's disease; and are close to the antipsychotic drug aripiprazole[30]. The high brain-to-plasma ratios of quetiapine and norquetiapine suggest a high BBB permeability, which will facilitate the performance of both molecules on multiple neurobiological processes in the central nervous system.

4. Conclusion

A sensitive and robust LC-MS/MS method for simultaneous quantitation of quetiapine and norquetiapine in rat plasma and brain homogenate, has been developed and validated for the first time. The method showed good precision, accuracy and linearity for determining analytes within the range 1.0-500.0 ng/mL in plasma and 3.0-1500.0 ng/g in brain tissue. The LLOQ is 1.0 ng/mL in plasma and 3.0 ng/g in brain tissue. The method required a small sample volume (100 μL) of plasma or brain homogenate, and a one-step liquid-liquid extraction was used to prepare samples. This method has been successfully applied in preclinical studies of quetiapine and norquetiapine in rats, to allow concentrations in the target organ (brain) to be correlated with alterations in cognition and memory.

References

1. FDA Advisory Comitee Documentation: Seroquel XR (quetiapine fumarate) for Major Depressive Disorder (MDD) or Generalized Anxiety Disorder (GAD), 2009.

2. B. Bandelow, G. Chouinard, J. Bobes, A. Ahokas, I. Eggens, S. Liu, H. Eriksson, Int. J. Neuropsychopharmacol. 13 (2010) 305.

3. N. Maneeton, B. Maneeton, M. Srisurapanont, S.D. Martin, BMC Psychiatry 12 (2012).

4. M. Bauer, H.W. Pretorius, E.L. Constant, W.R. Earley, J. Szamosi, M. Brecher, J. Clin. Psychiatry 70 (2009) 540.

5. R.C. Shelton, G.I. Papakostas, Acta Psychiatr. Scand. 117 (2008) 253.

6. S.M. Cheer, A.J. Wagstaff, CNS Drugs 18 (2004) 173.

7. G. V Bakken, I. Rudberg, H. Christensen, E. Molden, H. Refsum, M. Hermann, Drug Metab. Dispos. 37 (2009) 254.

8. F. Lopez-Munoz, C. Alamo, Front. Psychiatry 4 (2013) 102.

9. M.A. Saracino, L. Mercolini, G. Flotta, L.J. Albers, R. Merli, M.A. Raggi, J. Chromatogr. B-Analytical Technol. Biomed. Life Sci. 843 (2006) 227.

10. D. Prakash, K. Bhat, R. Shetty, P. Chaudhary, S.R. Pathak, A. Ghosh, Arzneimittel-Forschung-Drug Res. 60 (2010) 654.

11. O. Lopez-Guarnido, M.J. Tabernero, A.F. Hernandez, L. Rodrigo, A.M. Bermejo, J. Appl. Toxicol. 34 (2014) 1104.

12. M.L. Kundlik, S. Kambli, V. Shah, Y. Patel, S. Gupta, R. Sharma, B. Zaware, S.R. Kuchekar, Chromatographia 70 (2009) 1587.

13. R. Nirogi, G. Bhyrapuneni, V. Kandikere, K. Mudigonda, D. Ajjala, K. Mukkanti, Biomed. Chromatogr. 22 (2008) 1043.

14. D.S. Fisher, S.A. Handley, D. Taylor, R.J. Flanagan, Biomed. Chromatogr. 26 (2012) 1125.

15. X. Xiong, L. Yang, J.L. Duan, Clin. Chim. Acta 423 (2013) 69.

16. A. V Terry, D.A. Gearhart, S.P. Mahadik, S. Warsi, J.L. Waller, Neuroscience 140 (2006) 1277.

17. A. V Terry, D.A. Gearhart, S.P. Mahadik, S. Warsi, L.W. Davis, J.L. Waller, Neuroscience 136 (2005) 519.

18. A. V Terry, S.P. Mahadik, J. Pharmacol. Exp. Ther. 320 (2007) 961.

19. E.J. Hutchings, J.L. Waller, A. V Terry, J. Pharmacol. Exp. Ther. 347 (2013) 547.

20. N. Hashimoto, A. Toyomaki, M. Honda, S. Miyano, N. Nitta, H. Sawayama, Y. Sugawara, K. Uemura, N. Tsukamoto, T. Koyama, I. Kusumi, Ann. Gen. Psychiatry 14 (2015) 8.

21. K.P. Singh, N. Tripathi, Int. J. Dev. Neurosci. 42 (2015) 59.

22. M.G. Soeiro-De-Souza, V. V Dias, G. Missio, V. Balanza-Martinez, L. Valiengo, A.F. Carvalho, R.A. Moreno, Exp. Ther. Med. 9 (2015) 643.

23. P. Li, M.G. Bartlett, Anal. Methods 6 (2014) 6183.

24. M.C. Sampedro, N. Unceta, A. Gomez-Caballero, L.F. Callado, B. Morentin, M.A. Goicolea, J.J. Meana, R.J. Barrio, Forensic Sci. Int. 219 (2012) 7.

25. G. Zhang, A. V Terry, M.G. Bartlett, Rapid Commun. Mass Spectrom. 21 (2007) 920.

26. G. Zhang, A. V Terry, M.G. Bartlett, J. Chromatogr. B-Analytical Technol. Biomed. Life Sci. 854 (2007) 68.

27. G. Zhang, A. V Terry, M.G. Bartlett, J. Chromatogr. B-Analytical Technol. Biomed. Life Sci. 856 (2007) 20.

28. G. Zhang, A. V Terry, M.G. Bartlett, Biomed. Chromatogr. 22 (2008) 671.

29. P. Li, W.D. Beck, P.M. Callahan, A. V Terry, M.G. Bartlett, J. Chromatogr. B-Analytical

Technol. Biomed. Life Sci. 907 (2012) 117.

30. F. Liang, A. V Terry, M.G. Bartlett, Biomed. Chromatogr. 26 (2012) 1325.

Table 1. Calibration curves for quetiapine and norquetiapine in plasma and brain homogenate (n = 3).

Analyte	Plasma			Brain homogenate		
	Slope	Intercept	R^2	Slope	Intercept	R^2
Quetiapine	2.3840	0.1977	0.9982	2.1214	0.1851	0.9993
	±0.2094	±0.1415	±0.0025	±0.0940	±0.0787	±0.0009
Norquetiapine	1.0653	0.0288	0.9967	0.9195	0.0420	0.9992
	±0.0912	±0.1276	±0.0040	±0.0549	±0.0353	±0.0007

Table 2. The intra-day (n = 5) and inter-day (n = 15) precision (RSD) and accuracy (RE) of the LC–MS/MS method used to quantitate quetiapine and norquetiapine in rat plasma and brain homogenate.

Matrix	Analyte	Nominal conc. (ng/mL)	Intra-day Measured conc. (ng/mL)	RSD (%)	RE (%)	Inter-day Measured conc. (ng/mL)	RSD (%)	RE (%)
Plasma	Quetiapine	1.0	0.96±0.04	4.17%	-4.00%	0.89±0.07	7.87%	-11.00%
		3.0	2.83±0.08	2.83%	-5.67%	2.69±0.14	5.20%	-10.33%
		30.0	25.85±0.06	0.23%	-13.83%	25.68±0.56	2.18%	-14.40%
		400.0	375.18±4.43	1.18%	-6.21%	359.85±14.41	4.00%	-10.04%
	Norquetiapine	1.0	0.99±0.09	9.26%	-1.00%	1.01±0.11	10.89%	1.00%
		3.0	2.62±0.09	3.30%	-12.67%	2.81±0.19	6.87%	-6.33%
		30.0	26.37±0.25	0.94%	-12.10%	26.77±0.66	2.46%	-10.77%
		400.0	354.50±11.28	3.18%	-11.38%	378.44±18.92	5.00%	-5.39%
Brain homogenate	Quetiapine	1.0	0.96±0.04	4.41%	-3.80%	0.93±0.04	4.39%	-6.60%
		3.0	2.83±0.14	4.93%	-5.62%	2.73±0.09	3.24%	-8.87%
		30.0	26.95±0.73	2.70%	-10.18%	26.46±0.64	2.40%	-11.81%

	400.0	388.97±17.50	4.50%	-2.76%	374.49±4.64	1.24%	-6.38%
Norquetiapine	1.0	1.05±0.04	3.40%	4.80%	1.09±0.08	7.04%	8.80%
	3.0	2.84±0.06	2.27%	-5.33%	2.94±0.13	4.29%	-2.00%
	30.0	27.36±0.60	2.19%	-8.80%	28.23±1.53	5.40%	-5.91%
	400.0	395.40±4.78	1.21%	-1.15%	411.57±28.23	6.86%	2.89%

Table 3. Absolute recovery (%AR, n = 3) , relative recovery (%RR, n = 3) and matrix effect (%ME, n = 3) of the method.

Matrix	Analyte	Conc. (ng/mL)	AR (%)	RR (%)	ME (%)		Type
Plasma	Quetiapine	3.0	34.41±1.80	37.88±1.98	90.84%	9.16%	Suppression
		30.0	31.52±0.47	33.22±0.50	94.89%	5.11%	Suppression
		400.0	32.42±0.14	34.38±0.15	94.29%	5.71%	Suppression
	Norquetiapine	3.0	21.97±1.13	23.82±1.23	92.27%	7.73%	Suppression
		30.0	24.56±0.33	24.00±0.32	95.66%	4.34%	Suppression
		400.0	24.14±0.31	25.86±0.33	93.35%	6.65%	Suppression
Brain homogenate	Quetiapine	3.0	47.55±1.27	50.08±1.34	94.95%	5.05%	Suppression
		30.0	42.86±0.74	44.59±0.77	96.12%	3.88%	Suppression
		400.0	45.62±0.37	47.37±0.39	96.31%	3.69%	Suppression
	Norquetiapine	3.0	42.68±0.78	42.85±0.76	99.58%	0.42%	Suppression
		30.0	40.61±0.30	43.57±0.32	93.20%	6.80%	Suppression
		400.0	43.48±0.11	46.52±0.12	93.46%	6.54%	Suppression

Table 4. Autosampler stability (n = 3), bench-top stability (n = 3) and freeze-thaw stability (n = 3) of quetiapine and norquetiapine at 3.0 and 400.0 ng/mL in plasma and brain homogenate. Stabilities are shown in forms of percentage of relative concentration to time zero control (mean ±SD).

Matrix	Analyte	Conc. (ng/mL)	Autosampler stability (%)	Bench-top stability (%)	Freeze-thaw stability (%)
Plasma	Quetiapine	3.0	101.57±4.10	99.88±4.32	99.59±6.10
		400.0	101.71±2.71	100.03±2.36	99.44±1.52
	Norquetiapine	3.0	100.92±9.00	106.62±5.77	100.70±5.13
		400.0	103.72±5.58	106.93±7.53	92.30±1.46
Brain homogenate	Quetiapine	3.0	99.64±6.55	103.02±2.41	99.40±2.00
		400.0	98.01±0.99	95.59±0.75	99.35±0.42
	Norquetiapine	3.0	97.45±5.19	96.58±3.79	103.46±3.84
		400.0	96.89±3.97	90.00±1.96	103.63±8.21

Table 5. Precision (RSD) and accuracy (RE) of spiked samples (n = 5) at 2000.0 ng/mL in plasma and brain homogenate diluted 4 folds to the ULOQ (500.0 ng/mL) concentration.

Analyte	Nominal conc. (ng/mL)	Plasma Measured conc. (ng/mL)	RSD (%)	RE (%)	Brain homogenate Measured conc. (ng/mL)	RSD (%)	RE (%)
Quetiapine	2000.0	1944.19±64.24	3.30%	-2.79%	1897.19±91.17	4.81%	-5.14%
Norquetiapine		1797.68±63.05	3.51%	-10.12%	2112.14±110.18	5.22%	5.61%

Table 6. Concentrations of quetiapine and norquetiapine in plasma and brain tissue obtained from rats (n = 3) dosed with quetiapine (25 mg/kg/day) in drinking water for 60 days.

Analyte	Plasma conc. (ng/mL)	Brain conc. (ng/g)	Brain-to-plasma ratio
Quetiapine	14.79±4.65	42.87±7.98	2.90
Norquetiapine	1.18±0.35	3.70±0.85	3.14

CHAPTER 7

CONCLUSIONS

In this dissertation, novel liquid chromatography-mass spectrometry (LC-MS) based analytical methods were developed to qualitatively and quantitatively study active xenobiotics and endogenous molecules, including chlorpyrifos, acyl-CoAs and quetiapine, to understand their mechanisms of actions including toxicity, metabolism and post-translational modification. Chapter 2 reviewed protein covalent modification by a wide variety of xenobiotics including organophosphates, polycyclic aromatic hydrocarbons, acetaminophen, alkylating agents and other related compounds, their toxicological target proteins were demonstrated and the application of protein adducts as potential biomarkers of exposure or toxic response were discussed. In Chapter 3, we have established and validated a method, with protein precipitation for cell sample preparation, liquid-liquid extraction for medium sample preparation and LC-MS/MS for detection, to simultaneously quantitate chloripyrifos, its active metabolite chlorpyrifos oxon and nontoxic metabolite TCP in neurons and culture medium. After validation, this method was applied to analyze neurons treated with chlorpyrifos to study the neurotoxicity. This method also facilitated investigating neuroprotective role of astrocytic cytochrome P450 enzymes against chlorpyrifos exposure in the astrocyte-neuron co-culture system. In Chapter 4, we developed the first analytical method to absolutely quantitate Lys-40 acetylated α-tubulin using immunoprecipitation-mass spectrometry, after the generation of a surrogate peptide using pepsin digestion. The method was validated with selectivity, specificity, accuracy and linearity within the range of 1-100 pmol/mg brain tissue. With this method, we have observed a

156

significant decrease of Lys-40 acetylated α-tubulin in the brains of rats chronically exposed to chlorpyrifos. In addition, the analytical method for this potential cognition relevant biomarker should facilitate neurodegenerative disease and other neurotoxicity studies, including the evaluation of pathological progression, the investigation of the mechanisms of actions, and the observation of therapeutic effects. In Chapter 5, we established a new method, with protein precipitation for sample preparation and reversed-phase chromatography for separation, followed by multiple reaction monitoring (MRM) mass spectrometry to simultaneously quantitate a variety of acyl-CoAs converted from dietary fatty acids in mammalian cells. This analytical approach reveals a signature for these cells in multiple fatty acid metabolic processes in addition to metabolic modification after tumorigenic alteration. In Chapter 6, we have established and validated a new method with a one-step liquid-liquid extraction for sample preparation and LC-MS/MS for detection, to simultaneously quantitate quetiapine and norquetiapine in rat plasma and brain tissue. After validation, this method was used to analyze plasma and brain samples from rats chronically treated with quetiapine in drinking water for the purpose of facilitating future studies to investigate the pharmacokinetics and impact of quetiapine and norquetiapine on cognition.